Royal Norwegian Council
for Scientific and Industrial Research
(NTNF)

# NORSAR

AD-A193 077

NORSAR Scientific Report No. 1-87/88

# Semiannual Technical Summary

## 1 April — 30 September 1987

L.B. Loughran (ed.)

Kjeller, December 1987

DTIC
ELECTE
MAR 2 8 1988
E

UNCLASSIFIED
SECURITY CLASSIFICATION OF THIS PAGE

ADA193077

# REPORT DOCUMENTATION PAGE

Form Approved
OMB No. 0704-0188

| 1a. REPORT SECURITY CLASSIFICATION UNCLASSIFIED | | 1b. RESTRICTIVE MARKINGS NOT APPLICABLE | | |
|---|---|---|---|---|
| 2a. SECURITY CLASSIFICATION AUTHORITY NOT APPLICABLE | | 3. DISTRIBUTION/AVAILABILITY OF REPORT APPROVED FOR PUBLIC RELEASE DISTRIBUTION UNLIMITED | | |
| 2b. DECLASSIFICATION/DOWNGRADING SCHEDULE NOT APPLICABLE | | | | |
| 4. PERFORMING ORGANIZATION REPORT NUMBER(S) Scientific Report 1-87/88 | | 5. MONITORING ORGANIZATION REPORT NUMBER(S) Scientific Report 1-87/88 | | |
| 6a. NAME OF PERFORMING ORGANIZATION NTNF/NORSAR | 6b. OFFICE SYMBOL (If applicable) GSD | 7a. NAME OF MONITORING ORGANIZATION HQ/AFTAC/TTS | | |
| 6c. ADDRESS (City, State, and ZIP Code) POST BOX 51 N-2007 KJELLER, NORWAY | | 7b. ADDRESS (City, State, and ZIP Code) PATRICK AFB, FL 32925-6001 | | |
| 8a. NAME OF FUNDING/SPONSORING ORGANIZATION DEFENCE ADVANCED RESEARCH PROJECTS AGENCY | 8b. OFFICE SYMBOL (If applicable) | 9. PROCUREMENT INSTRUMENT IDENTIFICATION NUMBER CONTRACT NO. F08606-86-C-0004 | | |
| 8c. ADDRESS (City, State, and ZIP Code) 1400 WILSON BLVD. ARLINGTON, VA 22209-2308 | | 10. SOURCE OF FUNDING NUMBERS | | |

| PROGRAM ELEMENT NO. | PROJECT NO. | TASK NO. | WORK UNIT ACCESSION NO. |
|---|---|---|---|
| R&D | NORSAR PHASE 3 | SOW TASK 5.0 | SEQUENCE NO. 003A2 |

11. TITLE (Include Security Classification)
SEMIANNUAL TECHNICAL SUMMARY 1 APR – 30 SEP 1987 (UNCLASSIFIED)

12. PERSONAL AUTHOR(S)
L.B. LOUGHRAN (ED.)

| 13a. TYPE OF REPORT SCIENTIFIC SUMMARY | 13b. TIME COVERED FROM 1 Apr TO 30 Sep 87 | 14. DATE OF REPORT (Year, Month, Day) Dec 1987 | 15. PAGE COUNT 129 |
|---|---|---|---|

16. SUPPLEMENTARY NOTATION
NOT APPLICABLE

| 17. | COSATI CODES | | 18. SUBJECT TERMS (Continue on reverse if necessary and identify by block number) |
|---|---|---|---|
| FIELD | GROUP | SUB-GROUP | NORSAR, NORWEGIAN SEISMIC ARRAY |
| 8 | 11 | | |

19. ABSTRACT (Continue on reverse if necessary and identify by block number)

This Semiannual Technical Summary describes the operation, maintenance and research activities at the Norwegian Seismic Array (NORSAR) for the period 1 Apr – 30 Sep 87.

to p. 11

| 20. DISTRIBUTION/AVAILABILITY OF ABSTRACT ☒ UNCLASSIFIED/UNLIMITED ☐ SAME AS RPT. ☐ DTIC USERS | 21. ABSTRACT SECURITY CLASSIFICATION UNCLASSIFIED | |
|---|---|---|
| 22a. NAME OF RESPONSIBLE INDIVIDUAL MAJOR JAMES A. ROBB | 22b. TELEPHONE (Include Area Code) (305) 494-7665 | 22c. OFFICE SYMBOL AFTAC/TTS |

DD Form 1473, JUN 86    Previous editions are obsolete.    SECURITY CLASSIFICATION OF THIS PAGE

UNCLASSIFIED

Abstract (cont.)

The NORSAR Detection Processing system has operated throughout the
reporting period with an average uptime of 98.9 per cent. A total of
1940 seismic events have been reported in the NORSAR monthly seismic
bulletin. The performance of the continuous alarm system and the auto-
matic bulletin transfer by telex to AFTAC have been satisfactory. Pro-
cessing of requests for full NORSAR/NORESS data on magnetic tapes has
progressed according to established schedules.

A new Detection Processing system has been implemented, providing
improvements especially in the data quality checking and reduction in
false detections caused by occasional data spikes. The NORSAR beam
table and event processing algorithms remain unchanged. Processing
code has been developed for on-line regional array analysis based on
SUN 3 computer systems.

Field maintenance activity has included regular preventive maintenance
at all subarrays and occasional corrective actions when required. No
special problems have been noted in the performance of field systems.
In addition, field maintenance personnel have participated in
establishing the new regional array in Finnmark, Northern Norway.

A study of Pn scattering has been conducted, using as a data base
NORESS recordings of six mining explosions in the Blåsjø area, at an
epicentral distance of about 300 km. Wideband f-k analysis of these
event recordings show a pronounced and consistent anomaly in the fre-
quency range 2-4 Hz, which is also the frequency band of maximum Pn
energy. This is found to be consistent with scattering by topographic
relief of the Moho discontinuity, and the inferred location of the
proposed topographic feature coincides with the border of the Oslo
Graben.

A study of the effect of lateral heterogeneities on short period sur-
face waves (T < 20 s), using numerical modelling with a coupled-mode
scheme, has been initiated. So far it has been found that the coupled-
local modes method can be applied to model wave propagation in
realistic structures, needing a reasonable amount of lateral zones and
local modes to achieve satisfactory precision in transmission and
reflection coefficients. The plan is now to apply this method to
laterally heterogeneous structures around Scandinavia, and compare the
results of the numerical modelling to surface wave data recorded at
NORSAR and NORESS.

The problem of threshold determination for regional event detection
has been investigated, addressing in particular the tradeoff between
detector sensitivity and false detections caused by noise fluctuations
or stochastic nature. It has been found that for the same false alarm
rate, thresholds of incoherent beams can be set at 4.5-7 dB lower than
for coherent beams. This implies that for Pn detection, coherent beams
will usually outperform incoherent beams, since the SNR gain is typi-
cally 8-15 dB. However, for secondary phase detection, the incoherent
beams will usually be the best, since the coherent beam gain in these
cases is much lower. A particularly promising result is that inco-
herent beamforming based on horizontal channels appears to provide
more effective noise variance reduction than is obtained using ver-
tical channels. Also a large number of noise detections can be iden-
tified as such using the slowness estimates provided by a small-
aperture array.

Initial data recorded at the new regional array in Finnmark, Northern
Norway, have been processed and compared to NORESS recordings. The
Finnmark array is found to provide the same excellent (better than $\sqrt{N}$)
noise suppression as NORESS in selected filter bands, using "optimum"
subgeometries for beamforming. The background noise level at Finnmark
is even lower than that of NORESS at high frequencies (greater than
2 Hz), but somewhat higher than for NORESS at the low frequency end,
due to closer distance from the coast. A feature of Finnmark recor-
dings not seen at NORESS is the presence of strong Rg phases for
mining explosions out to about 350 km epicentral distance. A two-week
test period of joint processing of the two arrays has shown that the
large majority of small events ($M_L < 2.0$) are detected by only one
array, whereas larger events ($M_L > 2.0$) detected by either array in most
cases have at least one confirming phase detection from the other
array.

Analysis of P coda and Lg phases recorded at NORSAR for a set of 72
large explosions from the Shagan River test area near Semipalatinsk,
USSR, has shown that such data can provide event magnitude estimates
comparable in stability to world-wide network $m_b$. A systematic dif-
ference in $m_b(P)-m_b(Lg)$ has been observed for the northeast and south-
west portion of the Shagan River test area. There are indications that
this is mainly due to a bias in $m_b(P)$ estimates, and if so, the $m_b(lg)$
values observed at NORSAR would be expected to give more reliable
relative yield estimates than can be obtained from P-wave data.

A large-scale study comprising NORESS recordings of 101 events from
the North Sea/western Norway region has been conducted with the aim to
determine optimum beam deployment for regional phase detection. The
study has reconfirmed that a number of narrow band filters applied in

88   3   25   078

parallel and in combination with array beams based on filter-dependent subgeometries produce the best detection performance. In particular, the study has demonstrated the usefulness of high-frequency (10-16 Hz) coherent beams for Pn phase detection. It has furthermore been shown that high frequency incoherent beams (10-16 Hz) formed from horizontal channels significantly enhance detectability of Sn phases. The best results in Lg phase detection are found for low frequency incoherent beams (1.5-4.5 Hz) combining both horizontal and vertical channels. Further work will in particular be directed toward analyzing events from other regions in order to determine a beam deployment that provides optimized detection in the entire regional distance range.

The local geology of the two regional array sites in Norway has been studied, with emphasis on compiling information that is considered relevant from a seismological viewpoint. At this stage, the main purpose has been to present results of various surveys conducted by the Norwegian Geological Survey and NORSAR scientists. In the future, this information is expected to become useful in explaining observed features in the recorded seismograms from the two arrays.

| Accession For | |
|---|---|
| NTIS GRA&I | ☒ |
| DTIC TAB | ☐ |
| Unannounced | ☐ |
| Justification | |

By_____
Distribution/
Availability Codes

| Dist | Avail and/or Special |
|---|---|

A-1

| AFTAC Project Authorization | : | T/6141/B/PMP |
|---|---|---|
| ARPA Order No. | : | 4138 |
| Program Code No. | : | OF10 |
| Name of Contractor | : | Royal Norwegian Council for Scientific and Industrial Research |
| Effective Date of Contract | : | 1 October 1985 |
| Contract Expiration Date | : | 30 September 1987 |
| Project Manager | : | Frode Ringdal (06) 81 71 21 |
| Title of Work | : | The Norwegian Seismic Array (NORSAR) Phase 3 |
| Amount of Contract | : | $ 1,509,253.00 |
| Contract Period Covered by the Report | : | 1 Apr - 30 Sep 1987 |

## TABLE OF CONTENTS

I.    SUMMARY

This Semiannual Technical Summary describes the operation, maintenance and research activities at the Norwegian Seismic Array (NORSAR) for the period 1 April - 30 September 1987.

The uptime of the NORSAR online detection processor system has averaged 98.9 per cent during the reporting period as compared to 99.6 for the previous period. 04C and 06C have been the most frequently affected systems due to cable damage (04C) and synchronization problems (06C). A total of 1940 seismic events were reported in the NORSAR monthly seismic bulletins in this period, giving a daily average of 10.6 events.

The new Detection Processor (DP) was put into routine operation on day 289. The detector program is executing on the IBM 4341/L01 computer for the NORSAR array. There are no changes in the beam table. From day 320, the MODCOMP processor has been doing data acquisition only, as the beamforming and filtering tasks have been moved to the IBM 4341. The new detection process has lead to a significant reduction in load on the event processor, due to a greatly reduced number of "spike" detections. There are no changes in the event processor code. There are also no changes in the 'online' RONAPP detection processing for the NORESS array, but the new detector package now being used for NORSAR has also been applied to NORESS data and is executing regularly on tapes with data from the new Finnmark regional array.

A new program, SEGPRO - Segmented processing, has been developed to do the onset determination as well as phase velocity and azimuth measurements on detections reported from the new detector package. on a

routine basis. A new event processor code is under development to pro-
cess NORESS and Finnmark array data.

The data acquisition and real-time processing systems for the new
Finnmark array will be based on three Sun 3 computers. The IBM/PC
currently used for controlling critical tasks in the NORSAR/NORESS
systems will also be used for the new array.

Much time and effort has been spent by the field maintenance personnel
on preparatory work in connection with the new array in Finnmark, and
the actual installation of the array required extensive field work
during the summer of 1987.

The research activity is summarized in section VII. Section VII.1
presents a scattering model of regional $P_n$ wave propagation. Section
VII.2 describes preliminary tests for surface waves in 2-D structures.
In Section VII.3 false alarm statistics and threshold determination
for regional event detection are presented. Section VII.4 gives ini-
tial results from analysis of data recorded at the new regional array
in Finnmark. In Section VII.5 the potential of using NORSAR recorded P
coda and Lg waves to obtain stable magnitude estimates of large Semi-
palatinsk explosions is investigated. Section VII.6 describes
investigations of optimum beam deployment for NORESS using a North Sea/
western Norway data base. In Section VII.7 the local geology of the
regional array sites in Norway is presented.

II.     OPERATION OF ALL SYSTEMS

II.1     Detection Processor (DP) Operation

There have been 88 breaks in the otherwise continuous operation of the
NORSAR online system within the current 6-month reporting interval.
The uptime percentage for the period is 98.9 as compared to 99.6 for
the previous period.

Fig. II.1.1 and the accompanying Table II.1.1 both show the daily DP
downtime for the days between 1 April and 30 September 1987. The
monthly recording times and percentages are given in Table II.1.2.

The breaks can be grouped as follows:

a)   Hardware failure                          4

b)   Stops related to program work or error    0

c)   Hardware maintenance stops                6

d)   Power jumps and breaks                     5

e)   TOD error correction                       6

f)   Communication lines                       67

The total downtime for the period was 50 hours and 26 minutes. The
mean-time-between-failures (MTBF) was 2.5 days, as compared to 2.0 for
the previous period.

J. Torstveit

| Month | DP uptime hours | DP uptime % | No. of DP breaks | No. of days with breaks | DP MTBF* (days) |
|-------|-----------------|-------------|------------------|-------------------------|-----------------|
| APR   | 713.60          | 99.1        | 37               | 13                      | 0.8             |
| MAY   | 718.35          | 96.5        | 7                | 6                       | 3.7             |
| JUN   | 714.27          | 99.2        | 14               | 8                       | 2.0             |
| JUL   | 743.75          | 99.9        | 8                | 6                       | 3.4             |
| AUG   | 738.40          | 99.3        | 13               | 8                       | 2.2             |
| SEP   | 713.20          | 99.1        | 9                | 8                       | 3.0             |
|       |                 | 98.9        | 88               | 49                      | 2.5             |

* Mean-time-between-failures = total uptime/no. of up intervals.
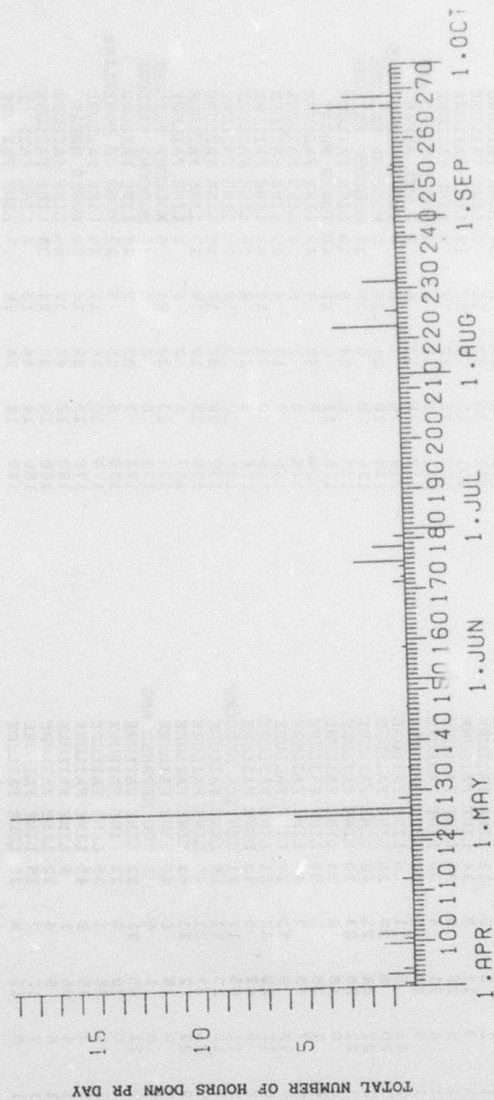
Table II.1.2  Online system performance, 1 April – 30 September 1987.

Fig. II.1.1   Detection Processor downtime in the period 1 Apr - 30 Sep 1987.

LIST OF BREAKS IN DP PROCESSING THE LAST HALF-YEAR

| DAY | START | | STOP | | COMMENTS |
|-----|-----|-----|-----|-----|----------|
| 91 | 0 | 59 | 1 | 3 | LINE FAILURE |
| 91 | 2 | 3 | 2 | 11 | LINE FAILURE |
| 91 | 3 | 11 | 3 | 14 | LINE FAILURE |
| 91 | 3 | 28 | 3 | 30 | LINE FAILURE |
| 91 | 4 | 31 | 4 | 39 | LINE FAILURE |
| 91 | 5 | 40 | 5 | 42 | LINE FAILURE |
| 92 | 11 | 5 | 6 | 6 | LINE FAILURE |
| 93 | 20 | 6 | 20 | 26 | LINE FAILURE |
| 93 | 21 | 34 | 21 | 48 | LINE FAILURE |
| 93 | 22 | 28 | 23 | 10 | LINE FAILURE |
| 94 | 20 | 18 | 0 | 35 | LINE FAILURE |
| 96 | 1 | 38 | 1 | 51 | LINE FAILURE |
| 97 | 13 | 9 | 7 | 44 | LINE FAILURE |
| 98 | 12 | 20 | 12 | 10 | LINE FAILURE |
| 99 | 6 | 42 | 6 | 21 | SERVICE NODCOMP |
| 99 | 12 | 55 | 12 | 28 | LINE FAILURE |
| 99 | 21 | 27 | 21 | 40 | LINE FAILURE |
| 99 | 23 | 2 | 23 | 43 | LINE FAILURE |
| 100 | 0 | 18 | 0 | 40 | LINE FAILURE |
| 100 | 6 | 1 | 6 | 2 | TOD RETARED 6MS |
| 100 | 21 | 49 | 21 | 52 | LINE FAILURE |
| 101 | 20 | 10 | 0 | 27 | LINE FAILURE |
| 101 | 1 | 28 | 1 | 35 | LINE FAILURE |
| 101 | 2 | 35 | 2 | 45 | LINE FAILURE |
| 101 | 4 | 56 | 5 | 9 | LINE FAILURE |
| 101 | 6 | 9 | 6 | 12 | LINE FAILURE |
| 101 | 7 | 12 | 7 | 15 | LINE FAILURE |
| 101 | 8 | 15 | 8 | 21 | LINE FAILURE |
| 101 | 9 | 26 | 9 | 57 | LINE FAILURE |
| 101 | 10 | 57 | 11 | 0 | LINE FAILURE |
| 101 | 12 | 7 | 12 | 10 | LINE FAILURE |
| 101 | 12 | 22 | 12 | 30 | LINE FAILURE |
| 111 | 6 | 1 | 6 | 2 | TOD RETARED 6MS |
| 112 | 5 | 32 | 5 | 6 | POWER BREAK |
| 118 | 6 | 3 | 6 | 4 | TOD RETARED 10MS |
| 125 | 18 | 20 | 24 | 0 | MODCOMP FAILURE |
| 126 | 0 | 0 | 19 | 17 | MODCOMP FAILURE |
| 127 | 6 | 14 | 6 | 15 | LINE FAILURE |
| 128 | 12 | 6 | 12 | 40 | POWER BREAK |
| 134 | 8 | 42 | 8 | 48 | LINE FAILURE |
| 146 | 6 | 1 | 6 | 2 | LINE FAILURE |
| 146 | 6 | 19 | 6 | 20 | LINE FAILURE |
| 146 | 10 | 44 | 10 | 47 | LINE FAILURE |
| 158 | 8 | 27 | 8 | 29 | LINE FAILURE |
| 158 | 12 | 33 | 12 | 35 | LINE FAILURE |
| 158 | 18 | 50 | 18 | 55 | LINE FAILURE |
| 158 | 19 | 10 | 19 | 13 | LINE FAILURE |
| 167 | 6 | 2 | 6 | 3 | LINE FAILURE |
| 171 | 23 | 24 | 24 | 0 | MODCOMP FAILURE |
| 172 | 0 | 0 | 0 | 11 | MODCOMP FAILURE |
| 174 | 7 | 33 | 7 | 48 | LINE FAILURE |
| 175 | 6 | 55 | 9 | 22 | WORK ON POWERLINE |
| 178 | 10 | 46 | 11 | 26 | LINE FAILURE |
| 178 | 13 | 28 | 14 | 20 | POWER BREAK |
| 180 | 12 | 44 | 12 | 45 | LINE FAILURE |
| 180 | 14 | 35 | 14 | 39 | LINE FAILURE |
| 180 | 14 | 46 | 15 | 8 | LINE FAILURE |
| 180 | 18 | 34 | 18 | 37 | LINE FAILURE |

Table II.1.1  Daily DP downtime in the period 1 Apr - 30 Sep 1987.

| LIST OF BREAKS IN DP PROCESSING THE LAST HALF-YEAR | | | |
|---|---|---|---|
| DAY | START | STOP | COMMENTS......... |
| 187 | 6 | 2 | 3 LINE FAILURE |
| 188 | 6 | 24 | 25 LINE FAILURE |
| 191 | 9 | 19 | 21 LINE FAILURE |
| 194 | 6 | 3 | 4 LINE FAILURE |
| 194 | 6 | 7 | 8 LINE FAILURE |
| 198 | 6 | 1 | 2 LINE FAILURE |
| 198 | 6 | 12 | 13 LINE FAILURE |
| 204 | 11 | 30 | 37 CE SERVICE |
| 204 | 11 | 0 | 16 MODCOMP FAILURE |
| 222 | 11 | 11 | 14 MODCOMP FAILURE |
| 222 | 11 | 20 | 45 TOD RETARED 10MS |
| 225 | 7 | 44 | 42 CE MAINTENANCE |
| 225 | 9 | 7 | 35 LINE FAILURE |
| 230 | 6 | 34 | 40 LINE FAILURE |
| 231 | 10 | 39 | 31 CE MAINTENANCE |
| 232 | 6 | 50 | 48 TOD RETARED 12MS |
| 232 | 6 | 47 | 8 TOD RETARED 12MS |
| 233 | 8 | 6 | 7 LINE FAILURE |
| 236 | 8 | 21 | 22 LINE FAILURE |
| 243 | 8 | 18 | 19 LINE FAILURE |
| 243 | 6 | 23 | 25 LINE FAILURE |
| 247 | 6 | 32 | 33 LINE FAILURE |
| 250 | 6 | 0 | 2 LINE FAILURE |
| 250 | 13 | 19 | 33 POWER BREAK |
| 253 | 15 | 15 | 25 LINE FAILURE |
| 254 | 15 | 56 | 2 TOD RETARED 14MS |
| 261 | 6 | 0 | 53 CE SERVICE MODCOMP |
| 266 | 11 | 14 | 22 CE SERVICE MODCOMP |
| 268 | 11 | 0 | 13 LINE FAILURE |
| 273 | 5 | 22 | 26 LINE FAILURE |

Table II.1.1 (cont.)

## II.2    Array communications

Table VII.2.1 reflects the systems performance in the reporting period.

04C and 06C have been the most frequently affected systems due to cable damage (04C) and synchronization problems (06C).

The communication machine (Modcomp) has failed two times, in May and September, a voltage and a "Floating point processor" failure, respectively. The latter failure caused problems during the restarting phase.

**Summary**

Apr    In April most systems were affected especially in connection with our attempts to localize the noise source common to all communication channels. Systems were switched off one by one, but also in groups of 2 and 3. Later NTA/Hamar and Lillestrøm did observations which revealed noise in the transmission channel equipment between Hamar and Oslo. NTA switched to a spare channel group which for a period gave us improved performance.

May    Apart from 06C which was affected weeks 19, 21 and 22 causing 0.5% outages, the systems were most reliable in May. The high error figures were caused by a Modcomp failure week 19, representing an outage of approx. 15.4% that week. Figures in brackets represent system performance/reliability exclusive Modcomp failure (see Table II.2.1).

Jun       In spite of varying line quality at 06C weeks 25 and 26 and
relatively high error figure (9.5%) this period may be
characterized as satisfactory for the remaining systems,
although a 0.21% error figure at 04C could have been better.

Jul       Defective cable between Berge Central and the 04C CTV was a
problem. Roadwork was going on in the 04C area, affecting the
communication cable which had to be cut/spliced at different
places along the path. NTA, who was responsible for the cable
work, assumed (by the end of the month) that it would take
another 2-3 weeks before the work could be finished.

02C (8.2% outages) was frequently affected, but NTA did not
localize the irregularity.

06C communication system had synchronization problems which
may have been a result of a "stressed" Modcomp, caused by
04C.

High performance by the remaining systems.

Aug       Week 35 NTA finished the cable work at 04C, and the error
figures decreased to 0.06% that week.

NTA was told to check the 06C communication line thoroughly.
Outages occurred frequently, but the station was back in
operation after restarting the Modcomp.

Most satisfactory performance of the other systems.

Sept     After the cable work finished week 34, 04C communication
system functioned most satisfactorily the three following
weeks (35, 36, 37), but 16 September data again disappeared.
After a temporary repair the system was back in operation 23
September. Between 24 and 28 September the performance was bad.

06C pattern did not change compared to July/August.
Resynchronization is possible and brings the system up again.

The NMC staff will as soon as they have finished the installa-
tion of the new array in Finnmark check relevant equipment
(power, modem, Loop Control, Logic, etc.), which may be
carried out in conjunction with NTA/Hamar and the NDPC staff.

O.A. Hansen

| Sub-array | APR 87 (5) (30.3-4.5) | MAY 87 (4) (4-31.5) | JUN 87 (4) (1-28.6) | JUL 87 (5) (29.6-2.8) | AUG 87 (4) (3.-30.8) | SEP 87 (4) (31.8-27.9) | Average ½ yr |
|---|---|---|---|---|---|---|---|
| 01A | 1.18 | *3.85 (0.004) | 0.05 | 0.01 | 0.05 | 0.05 | 0.86 (0.22) |
| 01B | 0.03 | *3.85 (0.002) | 0.10 | 0.01 | 0.04 | 0.05 | 0.68 (0.04) |
| 02B | 3.29 | *3.84 (0.005) | 0.05 | 0.02 | 0.05 | 0.05 | 1.21 (0.57) |
| 02C | *7.90 | *3.84 (0.002) | 0.05 | *8.22 | 0.04 | 0.04 | 3.35 (2.71) |
| 03C | 2.55 | *3.84 (0.004) | 0.04 | 0.02 | 0.04 | 0.03 | 1.08 (0.44) |
| 04C | *81.08 | *3.85 (0.003) | 0.21 | *51.91 | *49.59 | *33.50 | 36.69 (36.05) |
| 06C | *13.98 | *4.34 (0.50) | *9.49 | *22.99 | *30.75 | *27.36 | 18.15 (17.51) |
| | | | | | | | |
| AVER | 15.71 | 3.91 | 1.48 | 11.88 | 11.51 | 8.72 | 8.86 (8.22) |
| Less | 04C,06C 2.99 | Modcomp failures | 04C | 02C,04C 06C | 04C,06C | 04C,06C | 04C,06C 04C, 06C |
| | 02C,04C,06C 1.76 | 0.07 | 0.08 | 0.01 | 0.04 | 0.04 | 1.43 (0.80) |

* see item II.2 regarding figures preceded by an asterisk.

Table II.2.1  Communications performance. The numbers represent error rates in per cent based on total transmitted frames/week (1 Apr – 30 Sep 1987).

III.    ARRAY PERFORMANCE

Event Processor Operation

In Table III.1 some monthly statistics of the Event Processor opera-
tion are given:

|  | Teleseismic | Core Phases | Sum | Daily |
|---|---|---|---|---|
| APR 87 | 264 | 69 | 333 | 11.1 |
| MAY 87 | 254 | 62 | 316 | 10.2 |
| JUN 87 | 275 | 60 | 335 | 11.2 |
| JUL 87 | 332 | 85 | 417 | 13.5 |
| AUG 87 | 205 | 57 | 262 | 8.5 |
| SEP 87 | 210 | 67 | 277 | 9.2 |
|  | 1540 | 400 | 1940 | 10.6 |

Table III.1   Event Processor Statistics, April – September 1987.

B. Paulsen

## IV    IMPROVEMENTS AND MODIFICATIONS

### IV.1    NORSAR detection processing

The 'new' NORSAR detection processor was put into routine operation on day 289, after a long period of parallel processing for verification.

The change to the new detection processor was done under a period of bad data conditions. Three subarrays were temporarily out of order, and many communication errors were present. However, these bad data conditions were exploited to gain valuable experience with the data quality control part of the system. We now have a program system that controls all bad data conditions due to communication errors and resynchronizations. Moreover, the data quality control procedure is changed from treating only the special features of the NORSAR array to a more general parameterized control routine. This routine performs data control on the NORSAR, NORESS and new Finnmark arrays using the same program code for all arrays.

The output from the detector system is in the form of accumulated sequential files. One file gives a list of detections, another gives a list of 'events' from the data quality control part. Data quality control reporting includes time and length of data gaps for individual channels and for the array due to communication errors and/or recording gaps. Moreover, spikes are reported if detected, using max. amplitude comparison between one sensor and the average or median value of all sensors. (Other parameterized procedures may also be selected). Using this procedure, spikes of significant amplitudes are effectively removed.

The detector program is executing on the IBM 4341/L01 computer for the NORSAR array.  There are no changes in the beam table. Coherent

beams 1 - 180 and incoherent beams 1 - 64 are directed as before
(Beam tables 451 and 271, respectively).

To reduce computer power requirements, the band pass filtering is
done using a 20 Hz sample rate, whereas the array beamforming is done
using 10 Hz sampling. This reduction in sample rate has in practice
shown no degradation of the signal-to-noise ratio within the frequency
bands used. We even get a better performance relative to the 'old'
system where the beamforming was done using two steps: Firstly,
subarray beamforming was done using a small set of beams, and then
array beamforming was done using this set of subarray beams. The new
detector forms array beams using all sensors, with individual delays
for all beams, thus obtaining a better signal-to-noise ratio.

The 4341 computer executes MODCOMP communication, data recording task,
detection processing, event processing and AFTAC telex message
handling for the NORSAR array. For 60 seconds of data, the computer
spends on the average 50 seconds of elapsed time to execute all these
processes. The detection processor runs in a mode where it takes a
3-minute break every time it catches up with real time.

In this mode, close to real time, the program may execute for several
weeks without interruptions. For this reason, the detector system has
a built-in task which may communicate externally, and performs file
management without interrupting the continuity in the data or the exe-
cution of the program. However, the detector program has so far been
stopped every 7 days to do manual maintenance of output files and
backup. (The "old" online disk loop with data and detection lists is
maintained.)

## IV.2     MODCOMP subarray communication

From day 320, the MODCOMP processor has been doing data collection
only, as subarray beamforming and filtering was removed from the
code. The removing of subarray beamforming and filtering has relieved
the CPU comsumption on the MODCOMP, leading to a much better perfor-
mance on handling the SLEM communication.

## IV.3     NORSAR event processing

The new detection process has lead to a significant relief on the
event processor, as most of the 'bad data events' are removed.

There are no changes in the event processor code.

An actual improvement in automatic processing results requires a new
time delay correction data base.

## IV.4     NORESS detection processing

There are no changes in the 'online' RONAPP detection processing, but
the new detector package now being used for the NORSAR array pro-
cessing has also been applied to NORESS data and gives results inden-
tical to those of RONAPP. Potential gain in detection capabilities
using extended beam sets for NORESS are discussed elsewhere in this
report.

## IV.5     Finnmark regional array detection processing

The detector package now being used for the NORSAR array data is now
executing regularly on tapes with data from the new Finnmark regional
array. Results from this detection processing are given elsewhere in
this report.

## IV.6    NORESS/Finnmark array event processing

There are no changes in the event processing for NORESS data. The event
processing consists of phase identification, phase association and
event epicenter determination, and subsequent plotting of relevant
data and f-k spectra.

A new program, SEGPRO - Segmented processing, has been developed to do
the onset determination as well as phase velocity and azimuth measure-
ments on detections reported from the new detector package, on a
routine basis. The SEGPRO package is regularly processing Finnmark
array data. The detector and the SEGPRO package together perform all
RONAPP functions, and are using the same data interface routines. This
means that the programs may use data from disk loops, tape, disk files
or any other media or format that is supported.

A new event processor code is under development to process NORESS
and Finnmark array data using these routines. The processor will use
the SEGPRO output files for detection parameters and f-k matrices,
thus preparing for a complete replacement of RONAPP.

The NORSAR and NORESS/Finnmark array event processors differ too much
to have a common program, but much individual coding for subprocesses
is common to all packages. The main topic for event processor develop-
ment will be code structuring.

Processes involving file management, plotting and computations will be
separated to form smaller entities. This is done both in order to get
smaller general purpose routines and to identify and separate codes
that may be machine dependent.

IV.7    Hardware to be installed for processing of data from the new
        Finnmark, northern Norway, regional array

Fig. IV.7.1 shows how the data processing equipment proposed in con-
junction with the newly installed regional array in Finnmark, Norway,
will be integrated into and networked with already existing resources
at NORSAR's Data Processing Center at Kjeller. The data acquisition
systems for the NORSAR and NORESS arrays (not shown in this figure)
are integrated into the total system in similar ways.

The data acquisition and real-time processing systems (termed FRS
online in the figure) for the new Finnmark array are based on three
Sun 3 computers. The bottom Sun 3/260 is interfaced to a CIM
(Communication Interface Module) which receives data from the Finnmark
field system using a dedicated satellite link. The communication pro-
tocol used is SDLC, which is also used for the NORESS installation.
The CIM system can buffer up to 20 minutes of data. In normal opera-
tion, data are sent on to the Sun system without delays.

Recording of both high frequency (HF) and array data from the new
Finnmark site will utilize disk loops that can hold 84 hours of array
data and also 84 hours of HF data. One disk drive will be assigned to
each of the two data types. The Sun 3/260 computer that handles the
data acquisition task will also be running a state-of-health program
to verify data quality and generate statistics on uptime, com-
munication errors and calibration results. All data will be per-
manently archived on tapes, in the NORESS format.

Data contained in the disk loops will be generally accessible using
NFS. The data will also be accessible from the IBM system using
NORSAR's network software for reading files that are stored on com-
puters in the network.

The other Sun 3/260 system in the "FRS online"-box of Fig. IV.7.1 will be used for real-time processing and subsequent plotting of data. Relevant plots will be produced on the Versatec system. This Sun 3/260 computer is configured in exactly the same way as the acquisition computer, so it can act as a backup for the acquisition task.

The Sun 3/110 will be used for quality checking and array monitoring purposes.

The IBM/PC is the system currently being used for controlling critical tasks in the NORSAR/NORESS system. This system automatically calls the operator on duty in case of system failures. The FRS online system will be integrated into this alarm system. PC/NFS will be used to read current status directly from files stored in the Sun online system.

The third SUN 3/260 system will be used for data exchange, data analysis and program development.

In addition to these four Sun computers, our hardware proposal contains another two Sun 3/60 systems and a Sun 3/50 computer (only one of the Sun 3/60 systems is shown in the figure). These systems will be available in the network as general purpose work stations.

J. Fyen
T. Kværna
B. Paulsen
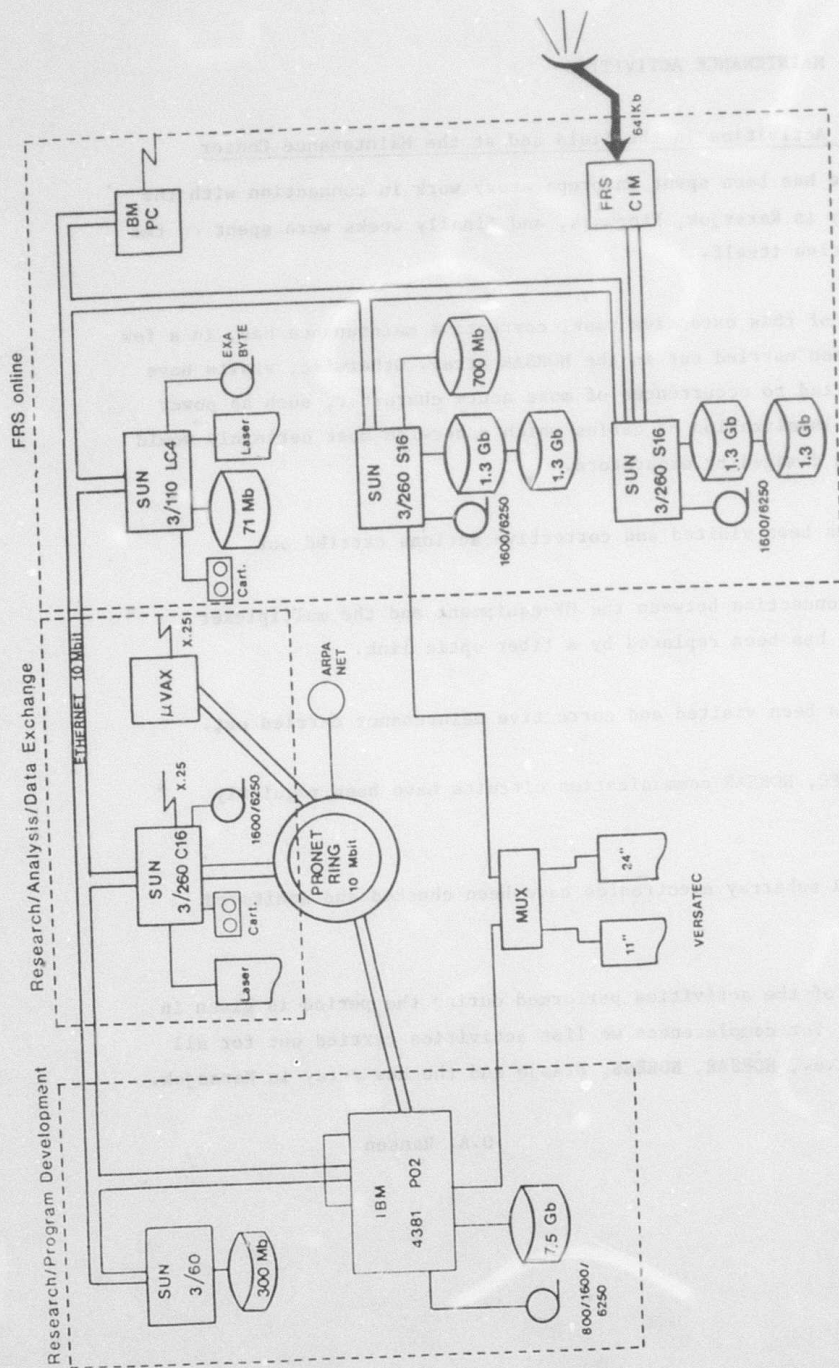R. Paulsen
S. Mykkeltveit

Fig. IV.7.1  The figure shows how the equipment for processing data from the new Finnmark regional array will be integrated into existing equipment at NORSAR's data processing center. Note that the current NORSAR/NORESS data acquisition system (based on IBM 4341 computers) come in addition to this figure.

V.        MAINTENANCE ACTIVITIES

V.1       Activities in the field and at the Maintenance Center

Much time has been spent on preparatory work in connection with the
new array in Karasjok, Finnmark, and finally weeks were spent on the
installation itself.

In spite of this extensive task, corrective maintenance has, in a few
cases, been carried out in the NORSAR array. Otherwise, visits have
been limited to occurrences of more acute character, such as power
failure, localization of cables which otherwise most certainly would
have been damaged by excavators.

NORESS has been visited and corrective actions carried out.

A cable connection between the HF-equipment and the multiplexer
(Megamux) has been replaced by a fiber optic link.

Blåsjø has been visited and corrective maintenance carried out.

At the NDPC, NORSAR communication circuits have been regularly
checked.

The NORSAR subarray electronics have been checked and monitored
regularly.

A summary of the activities performed during the period is given in
Table V.1. For completeness we list activities carried out for all
systems, i.e., NORSAR, NORESS, Blåsjø and the new array in Karasjok.

                                              O.A. Hansen

| Subarray/area | Task | Date |
|---|---|---|
| NORSAR | P.W. Larsen attended a project meeting with Sandia in connection with the new Finnmark array. | 14 Apr |
| Karasjok | P.W. Larsen participated in a survey in Karasjok together with representatives from Sandia. | 15,16 Apr |
| NORSAR | P.W. Larsen attended a meeting at NORSAR together with the project manager and Barlindhaug A/S, the consultants | 28 Apr |
| Oslo | NMC staff participated in a fiber optic course. | 27-30 Apr |
| NORESS | Repaired a DHL 70 card for site AO | 21 Apr |
| NDPC | Daily routine check of SP/LP data. Weekly calibration of SP/LP seismometers. Daily check of communication systems. | April |
| 04C | P.W. Larsen met representatives from NTA/Hamar and road administration 2 May in the 04C area to clarify responsibilities in connection with 04C communication cable rerouting. | 2 May |
| 06C | Replacement of the vertical long period centering device (RCD), incl. adjustments | 19,20,21 May |
| NORESS | NMC staff assisted representatives from Sandia Nat. Lab. (Dick Kromer) in connection with replacing the cable between HF-equipment and the Megamux with a fiber optic link connection. | 19,20,21 |
| NMC | Continued planning and preparation in connection with the Finnmark array. | May |
| NDPC | Daily check of SP/LP data. Weekly calibration of SP/LP seismometers. Daily checks of communication systems. | May |

| Subarray/<br>area | Task | Date |
|---|---|---|
| 01B (05) | Cable localized in connection with excavation damage. | 16 June |
| 01B (03) | In connection with trenching, cable pointed out. | 24 June |
| 02B (04) | Cable pointed out. | 17 June |
| 04C (02) | Cable pointed out. | 19 June |
| 06C (03) | Cable work. | 17,18,22 June |
| Karasjok | Survey in connection with the new array. | 11-15 June |
| Blåsjø | Various repair and maintenance work carried out. | 16-20 June |
| NORESS | A fiber connector repaired at site C2 | 27 June |
| NDPC | SP/LP daily checks. Calibration of SP/LP seismometers weekly. Daily control of communication systems. | June |
| 02B (tel.) | Corrective maintenance performed. | 21,23 July |
| 04C (03) | Cable localized. | 29 July |
| 06C (04) | Found damaged cable. | 30 July |
| Karasjok | P.W. Larsen attended a meeting in Alta regarding contractual relations. | 6 July |
| Karasjok | P.W. Larsen visited Karasjok in connection with start of the construction work (main building and cable trenching). | 14-17 July |
| FINE^A | Visited and expanded the array with 5 new C-points. | 29 July |
| NDPC | Daily check of SP/LP data. Weekly calibration of SP/LP seismometers. Daily control of the communication systems. | July |

| Subarray/ area | Task | Date |
|---|---|---|
| 06C | Visit in connection with damaged cable. | 7 Aug |
| 01B | Visit in connection with damaged cable. | 12 Aug |
| NDPC | Daily check of SP/LP data. LP seismometers continuously checked with regard to mass position (MP), and free period (FP). Adjustment carried out when outside specifications. Communication systems checked daily. | Aug |
| Karasjok | NMC staff engaged in the new Finnmark array throughout the period. | Sept |
| NDPC | In addition to ordinary daily/weekly checks/ tests, the A/D converters of all the data acquisition equipment (SLEMs) have been checked with respect to their ability to reproduce correct numbers. | Sept |

Table V.1   Activities in the field and at the NORSAR Maintenance
            Center, including NDPC activities related to the NORSAR
            array, 1 Apr - 30 Sep 1987.

V.2      Improvements and modifications (NORSAR array)

No changes since last reporting period.

V.3      Array status

As of 30 Sept 87 the following channels deviated from tolerances:

        01A 01    8 Hz filter
            02       -"-
            04    30 dB attenuation

```
01B   05
      08

04C   01
      08

06C   04
      05   Broadband filter installed.
      08
```

O.A. Hansen

VI.     DOCUMENTATION DEVELOPED

Bache, T.C., S.R. Bratt and H. Bungum (1986): High-frequency
    attenuation along 5 teleseismic paths from Central Asia,
    Geophys. J.R. astr. Soc., 85, 505-522.

Loughran, L.B. (ed.): Semiannual Technical Summary, 1 October 1986 -
    31 March 1987, NORSAR Sci. Rep. No. 2-86/87, Kjeller, Norway.

L.B. Loughran

VII    SUMMARY OF TECHNICAL REPORTS / PAPERS PREPARED

VII.1    A scattering model of regional $P_n$ wave propagation

The $P_n$ phase is crucial for the detection and location of regional
events. It is therefore important to determine its characteristic
properties. The properties of $P_n$ are well understood in one-
dimensional crust-mantle models:   $P_n$ is an ordinary head wave asso-
ciated with the Moho in models of uniform plane layers and $P_n$ can be
interpreted as a sum of whispering gallery waves forming a so-called
interference head wave in models of spherical layers and/or models
having a positive velocity gradient below the Moho (Menke and
Richards, 1980). The phenomenon of the whispering gallery can explain
the relatively long duration and high frequencies of $P_n$ at teleseismic
distances. However, it cannot explain the often observed relatively
large amplitudes in the later part of the signal. Similar charac-
teristics are observed at regional distances. To determine the cause
of these characteristics we have analyzed in some detail the NORESS
records of $P_n$ from a suite of 6 mining explosions in the Blåsjø area.
The explosion site is about 300 km from NORESS in an azimuth direction
of 240°. A typical record section of $P_n$ from these explosions is shown
in Fig. VII.1.1.

It can be seen that the first arrival is relatively weak. In fact,
this arrival is easily missed for small events, whence $P_n$ is often
associated with the dominant part of the wave train. We have applied
wide-band f-k analysis (Kværna and Doornbos, 1986) to the $P_n$ wave
trains from all 6 events. Slowness solutions as a function of fre-
quency are summarized in the velocity-azimuth spectrum of Fig.
VII.1.2. The solutions show a pronounced and consistent anomaly within
the range 2-4 Hz; this is also the range where the signal has its
maximum energy (Fig. VII.1.3). From an analysis of slowness as a func-
tion of time (Fig. VII.1.4 displays the results for one of the events)

we infer that the first arrival has a slowness and azimuth consistent
with $P_n$ in a one-dimensional crust-mantle model, and the anomaly is
related to wave energy being delayed by about 0.5-0.6 seconds. The
anomaly cannot be generated locally near the surface since this would
significantly perturb the wave front; the wavenumber solution shows
that the wave front is in fact very nearly plane. The observational
results suggest that these "$P_n$" waves are actually the result of scat-
tering at depth. Ray tracing backward in the direction given by the
measured slowness leads to the result that the 0.5-0.6 s time delay is
explained by a scattering source within the depth range 30-40 km. The
Moho here is usually taken to be at about 35 km depth. Hence the
observational results are consistent with scattering by topographic
relief of the Moho. An interesting geological aspect is that the
inferred location of the proposed topographic feature, 70 km from
NORESS in the southwest direction, coincides with the border of the
Oslo Graben.

Scattering will of course affect all waves interacting with a rough
Moho discontinuity. However, the scattered waves usually arrive in
the coda of a relatively strong primary wave. In contrast, the first
arriving $P_n$ is relatively weak due to the small coefficient of refrac-
tion through the Moho, and scattering due to topography of the boun-
dary may dominate the wave train.

To illustrate these concepts, we can apply a recently developed method
for modelling scattering by topographic relief (Doornbos, 1988). The
first applications of this method concerned the relatively complicated
case of a solid-liquid boundary. We have done some numerical experi-
ments with a liquid layer over a solid half space, letting velocities
and densities correspond to values in the crust and mantle. One of the
results is given in Fig. VII.1.5. Here we have assumed a boundary

topography characterized by a correlation length of 6 km and an average height of 1 km, and the wave field is taken monochromatic at 2 Hz. The figure shows energy flux of P transmitted upward through the boundary, as a function of slowness of incident P. Two modes of scattering are shown: (1) The specular flux $E^O$ in the direction defined by the plane wave-plane interface concept. The specular flux through a rough interface is reduced with respect to the flux through a plane. (2) The diffuse flux $E^{SC}$ due to multiple scattering in all (upward) directions. $E^{SC}$ does not exist for a plane interface. The figure illustrates well the sharp increase of the ratio $E^{SC}/E^O$ as the slowness approaches the critical value corresponding to $P_n$, thus supporting in a qualitative way the scattering model for propagation of this wave.

It should be noted that $E^O$ and $E^{SC}$ are not observable parameters. What can be inferred is the flux at a receiver location on the surface. To model this we need to know the areal extent of topography, and the decay factor accounting for attenuation of $P_n$ along the Moho. Clearly these parameters as well as those describing the topography needed to compute $E^{SC}$ and $E^O$ are presently not or only poorly constrained, and further experiments are needed to establish useful constraints. Our preliminary results nevertheless suggest that the scattering model of $P_n$ wave propagation is viable, and consequently that a careful calibration is needed before using this phase for event location and velocity determination purposes.

D.J. Doornbos, Univ. of Oslo
T. Kværna

## References

Doornbos, D.J. (1988): Multiple scattering by topographic relief
with application to the core-mantle boundary. Geophys. J.,
in press.

Kværna, T. and D.J. Doornbos (1986): An integrated approach to slow-
ness analysis with arrays and three-component stations. Semi-
annual Technical Summary, 1 Oct 1985 - 31 Mar 1986, NORSAR Sci.
Rep. No. 2-85/86, Kjeller, Norway.

Menke, W.H. and P.G. Richards (1980): Crust-mantle whispering gallery
phases: A deterministic model of teleseismic $P_n$ wave propagation.
J. Geophys. Res. 85, 5416-5422.
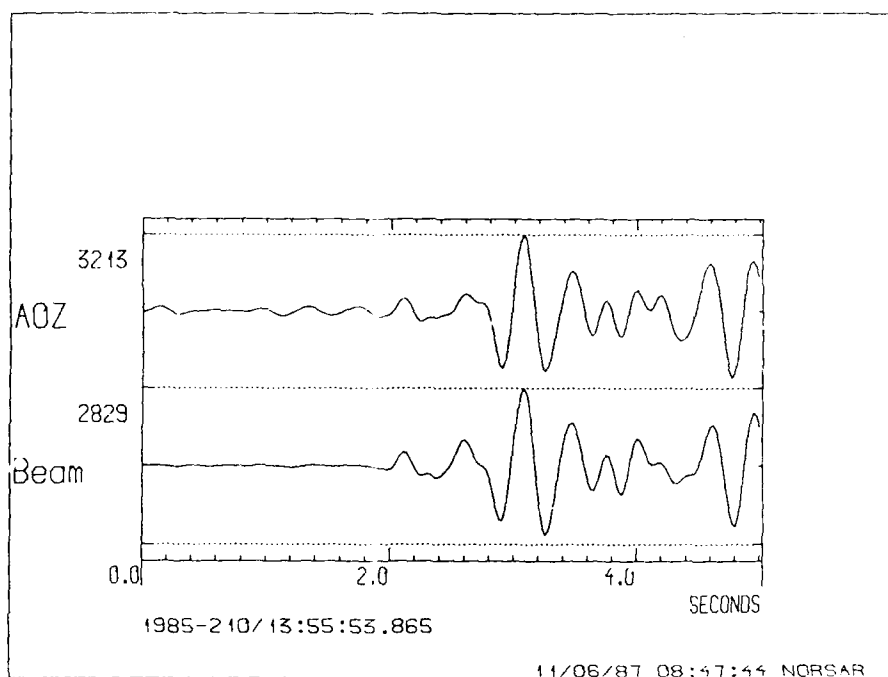
Fig. VII.1.1   Noress record of the $P_n$ phase from an explosion in the
               Blåsjø area. The top trace is the single channel obser-
               vation, and the lower trace is the steered beam, both
               bandpass filtered between 2.0 Hz and 4.0 Hz. Note the
               relatively weak first arrival at about 2.0 seconds com-
               pared to the stronger signal arriving 0.5-0.6 seconds
               later.

SLOWNESS ANALYSIS – BLÅSJØ EVENTS
MOVING FREQUENCY BANDS – PN PHASE
BAND: 0.8 HZ    STEP: 0.4 HZ
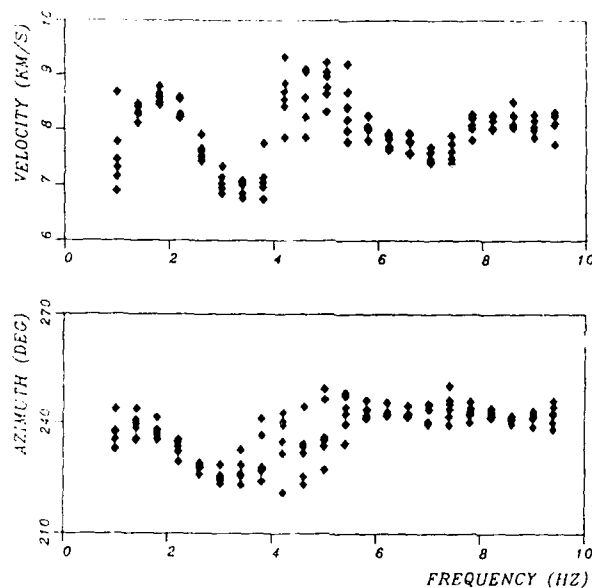
Fig. VII.1.2  Velocity and azimuth estimates for the $P_n$ phases as a
function of frequency. The six events were processed by
the wide-band method in 0.8 Hz wide frequency windows
with 0.4 Hz steps. Between 2 and 4 Hz the deviation from
theoretical azimuth is between 10 and 15 degrees, and
the apparent velocity is significantly lower than
expected for the $P_n$ phase.

BLAASJOE
MEAN UNCORRECTED SPECTRA
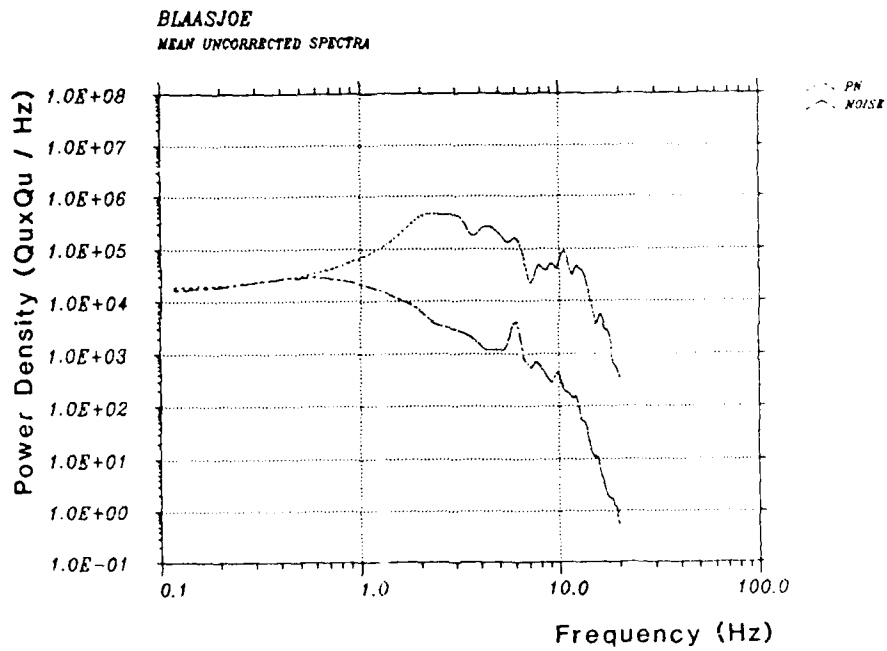


Fig. VII.1.3  This figures shows the uncorrected power density spectra
of both the $P_n$ phase and the preceding noise for a typi-
cal Blåsjø event.

SLOWNESS ANALYSIS - BLÅSJØ EVENTS
MOVING TIME WINDOWS - PN PHASE
WINDOW: 0.8 SEC    STEP: 0.2 SEC
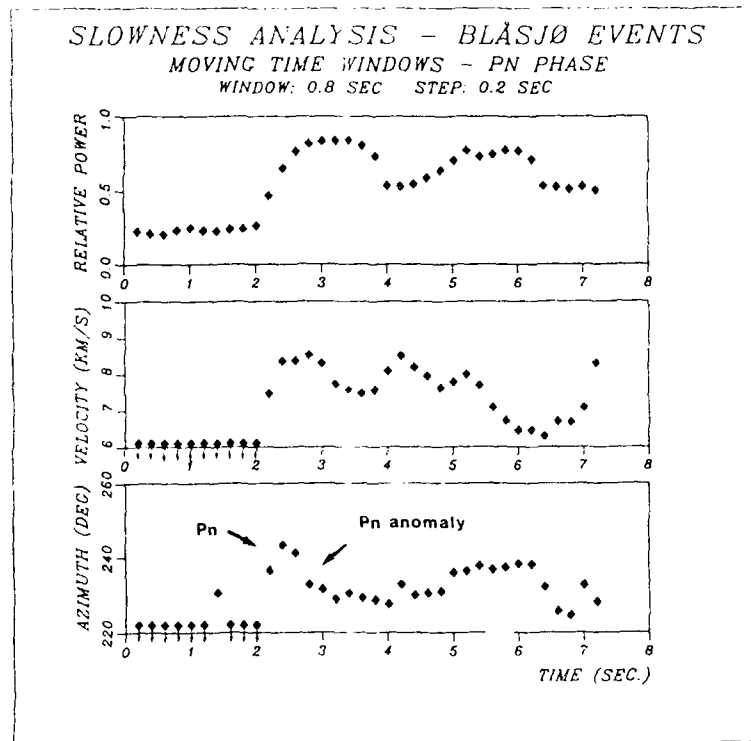
Fig. VII.1.4   Slowness estimates for one of the Blåsjø events as a
function of time. The data were processed by the wide-
band method in the frequency range 2.0-4.0 Hz. The
traced data were prealigned to compensate for offset
across the array.
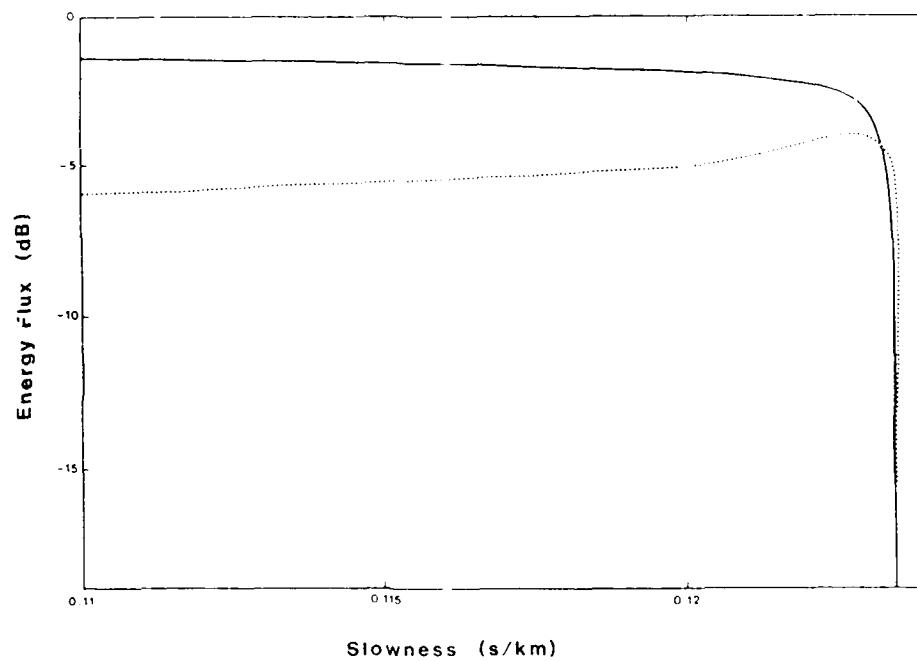
Fig. VII.1.5  Energy flux at 2 Hz through rough solid-liquid interface with the velocity-density structure $v_p^{+/-} = 6.8/8.1$ km/s, $v_s^{+/-} = 4.5/0$ km/s, $\rho^{+/-} = 2.9/3.4$ g/cm$^3$. The boundary roughness is characterized by an average height of 1 km and a correlation length of 6 km. The scattered flux is upward through the boundary. ————— : specular direction; ............... : integrated diffuse flux.

## VII.2    Preliminary tests for surface waves in 2-D structures

### Introduction

Surface waves at short periods (T < 20 s), and especially the Lg
crustal surface waves, usually exhibit complex wavetrains. For
example, relative amplitudes of the Lg to body-wave phases observed at
the NORSAR array were shown to be strongly path-dependent (Kennett et
al, 1985), and large transversal motion was observed on Lg-phases pro-
duced by explosive sources in the North Sea (Kennett and Mykkeltveit,
1984).

Lateral heterogeneities are thought to be responsible for this
complexity, but due to the lack of methods which are available to
model surface wave propagation in laterally heterogeneous structures,
little of the complex wavetrains has yet been explained. In order to
get some further insight into these surface wavetrains, we have ini-
tiated a research effort aiming at comparing surface wave recordings
at the NORSAR and NORESS arrays with results of numerical modelling,
using a coupled mode scheme. The preliminary results presented here do
not intend to model a realistic situation, but to check the applicabi-
lity of the method, and especially to analyze the influence of its two
main parameters.

### Method

We give here an outline of a coupled local mode method, the details of
which can be found in Maupin (1987). It is appropriate for propagation
across 2-D structures, the angle of incidence of the waves upon the
structure being possibly nonperpendicular to the symmetry direction y
of the structure. The wavefield is decomposed into a laterally varying
sum of the local modes:

$$\vec{u}(x,y,z,t) = \int\limits_{-\infty}^{+\infty} \int\limits_{-\infty}^{+\infty} (\sum_r c_r(x)\vec{u}_r(>,z;\omega,p)$$

$$\exp(-i \int\limits_0^x k^r(\zeta)d\zeta)\; e^{-ipy}\; e^{i\omega t}\; dp\; d\omega \tag{1}$$

where $\vec{u}$ is a displacement-stress vector of the elastic wavefield,
$\vec{u}_r$ are displacement-stress vectors of the local modes, and $(k^r,p,0)$ is
the local wave vector of the mode r in the cartesian coordinate system
$(x,y,z)$, at the frequency $\omega$.

The lateral heterogeneity introduces a lateral variation of the wave-
numbers $k^r$, as well as energy transfers between modes expressed by
lateral variations of the amplitude coefficients $c_r$. The lateral
variations of these two quantities satisfy the equations:

$$\frac{dk^r}{dx} = F_{rr}$$

$$\frac{dc_r}{dx} = \sum_{q \neq r} F_{qr} \frac{1}{(k^q - k^r)} \cdot \exp(i \int\limits_0^x (k^q - k^r)\, d\zeta)\, c_q \tag{2}$$

where $F_{qr}$ is an expression involving the local mode displacements and
tensions, combined with the elastic coefficients and density in inter-
face terms, and with their lateral derivatives in an integral over
depth.

The system (2) is transformed to yield a first-order equation in x for
reflection and transmission matrices, which is solved numerically in x
using a fourth-order Runge-Kutta scheme.

The method is tested on the continental margin model designed by
Badal and Serón (1987) (Fig. VII.2.1) to calculate Love wave
transmission by finite element method. We use an integration step in
x of 5 km and a variable integration step in z of the form $a^{(n-1)} dz_0$
for the n-th step, with $dz_0 = 0.5$ km and $a = 1.02$. In the following
two paragraphs, we investigate the influence on the coupling matrices
of the precision with which the local modes are calculated, and of the
number of modes used in the representation of the wavefield.

**Influence of the number of zones**

The local modes $\vec{u}^r$ appear free of lateral differentiation in the
expression $F_{qr}$ of equation (2). In order to facilitate their com-
putation, it is thus possible not to calculate them at each integra-
tion step in x, but to take them as constant inside zones where the
total lateral variation of the structure is small enough for their
shape not to vary significantly. The coarser a zoning we define across
the laterally heterogeneous structure, the less accurate local dis-
placement functions we use in the calculation of the expression $F_{qr}$,
which in turn result in less accurate coupling matrices and local
wavenumbers.

In order to determine how fine the zoning must be, we divide the con-
tinental margin of Fig. VII.2.1 into 2, 5 and 10 zones. The coupling
equation is integrated with the three different zonings, using the
local modes at a period of 20 s, calculated at the center of each zone
by a classical Haskell-Dunkin method. The resulting local phase velo-
cities of the Rayleigh wave fundamental mode are shown on Fig.
VII.2.2a as a function of x. The phase velocities calculated at the
center of each zone by the Haskell-Dunkin method, as well as the local
phase velocities calculated in each of the smaller zones using the
variational method, are shown on Fig. VII.2.2b for comparison.

The variational method is designed to calculate first-order variations
of the phase velocity associated with velocity and density variations
as a function of depth, preferably for flat layer boundaries. Equation
(2) treats separately the effect on phase velocities of sloping layer
boundaries and velocity variations inside the layers. It gives
obviously more accurate results than the variational method in this
continental margin model, where the slope of the layer boundaries is
important.

The accuracy of the phase velocity improves significantly when using 5
zones instead of 2, but remains stable between 5 and 10 zones. The
number of zones required to fit a given velocity curve can be foreseen
from the linear trend of the integrated phase velocity inside a zone.
The proper zoning for a given model and frequency depends on the cur-
vatures of the different mode phase velocity variations. The discre-
pancy observed between the integrated phase velocity and the zonal
phase velocities around $x = 30$ km may be related to a systematic
discrepancy between the vertically varying velocity profile and the
set of homogeneous layers required by the Haskell-Dunkin method to
calculate the zonal phase velocities.

The zoning must be designed to calculate accurately not only the phase
velocities, but also the transmission and reflection matrices. Fig.
VII.2.3 shows the transmission matrices for the 6 first modes of
Rayleigh and Love waves at right angle to the continental margin when
the modes are calculated at 20 s period for 2, 5 and 10 zones. The
zoning has a negligible influence on the transmission matrices. The
reflection matrices are zero whatever the zoning for this model.

When the propagation is not at right angle to the structure, Love and
Rayleigh waves are coupled. As the dispersion curves of Love and
Rayleigh modes of the same harmonic rank are usually very close and
may even cross each other, small relative errors in k produce large
errors in $(k^q-k^r)$, leading to a loss of accuracy in the Rayleigh-Love

coupling terms. The accuracy of the phase velocity has therefore a stronger influence on the coupling matrices in that case.


**Influence of the mode cut-off**

To be complete, the wavefield representation (1) should include all the surface wave modes and body-wave terms, or the infinite set of modes of a structure equivalent to the spherical Earth. For practical reasons, we need to restrict the set of modes to those which have somewhere along the structure a significant energy in the frequency range we are studying. Except in particular cases of well-defined waveguides, the coupling between modes usually decreases gradually with harmonic rank difference and the mode cut-off is often chosen somewhat arbitrarily. Therefore, it is important to know which elements in the coupling matrices are influenced by the drop-off of the higher modes.

Transmission matrices for Love waves crossing the continental margin at right angle were calculated for the 6, 8 and 10 first modes at a period of 10 s (Fig. VII.2.4). The influence of the mode cut-off can essentially be inferred from on the last row and column of the matrices. It is clear for example that the addition of modes 9 and 10 has no significant influence on the transmission matrix of the first 7 modes, including the 6th mode which is very strongly coupled to neighboring modes.

The important point to note here is that the energy of the higher modes not accounted for is mainly fed into the coupling terms of the higher modes of the representation, and not systematically into the diagonal terms. Therefore the cut-off does not produce an upper bias of the self-transmission terms.

## Conclusion

We have shown that the coupled-local modes method can be applied to model wave propagation in realistic structures, needing a reasonable amount of lateral zones and local modes to achieve a satisfactory precision in transmission and reflection coefficients. The method has acceptable computing times (typically 10 minutes of CPU time on the IBM 4381/P02 of NORSAR for the examples displayed in Figs. VII.2.3 and VII.2.4). Next, we intend to apply this method across laterally heterogeneous structures around Scandinavia, like the North Sea Graben and the Tornquist-Teisseyre lineament, and compare the results of the modelling with surface wave data recorded at the NORSAR and NORESS arrays.

V. Maupin, Postdoctorate Fellow

## References

Badal, J. and F.J. Serón (1987): Love wave normally incident at the Atlantic margin of the Iberian Peninsula. Annales Geophysicae, 5B, 273-280.

Kennett, B.L.N., S. Gregersen, S. Mykkeltveit and R. Newmark (1985): Mapping of crustal heterogeneity in the North Sea basin via the propagation of Lg-phases. Geophys. J.R. astr. Soc., 83, 299-306.

Kennett, B.L.N. and S. Mykkeltveit (1984): Guided wave propagation in laterally varying media. II: Lg waves in north-western Europe. Geophys. J.R. astr. Soc., 79, 257-267.

Maupin, V. (1987): Surface waves across 2-D structures: a method based on coupled local modes. Submitted to the Geophys. J.R. astr. Soc.
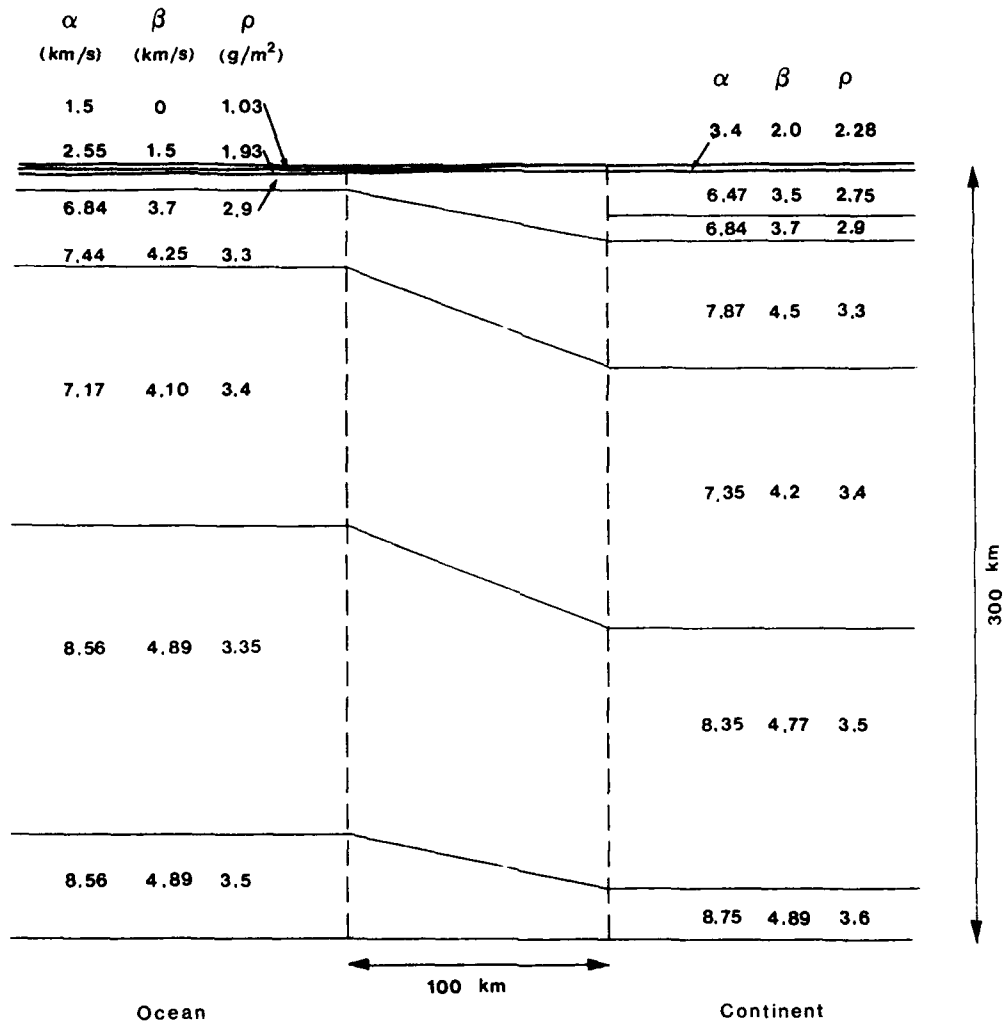
Fig. VII.2.1  Continental margin model after Badal & Serón (1987).
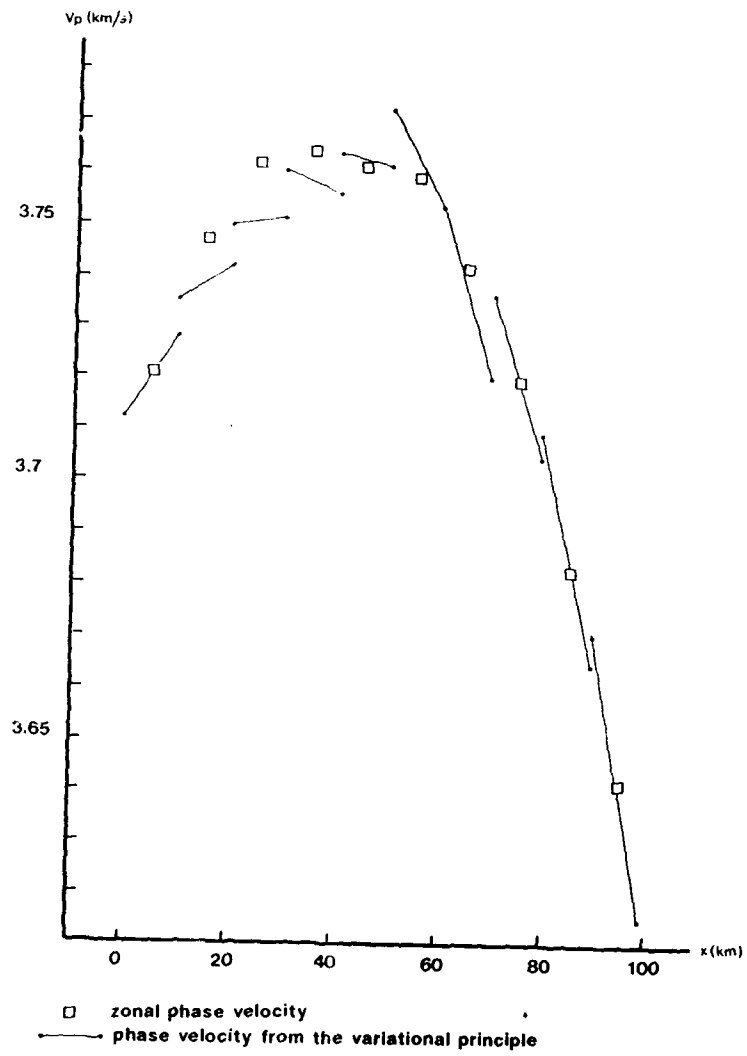
Fig. VII.2.2a
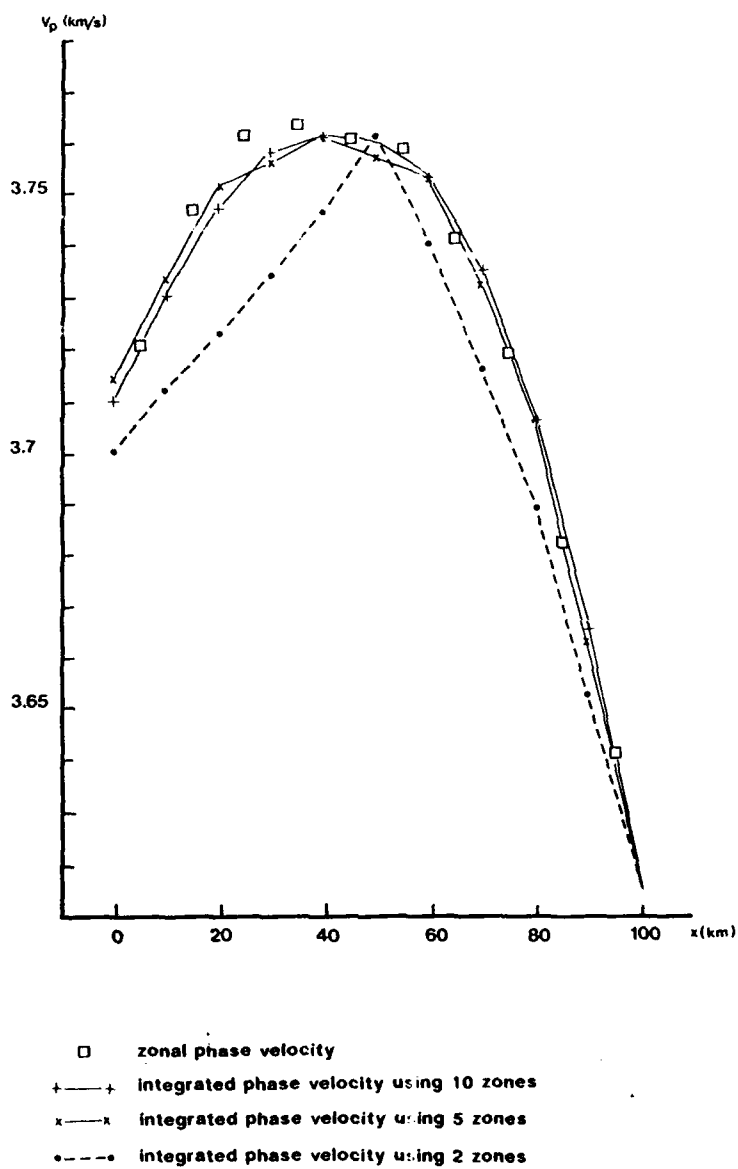
Fig. VII.2.2b

2 zones :

| | 1 | 2 | 3 | 4 | 5 | 6 | | 1 | 2 | 3 | 4 | 5 | 6 |
|---|---|---|---|---|---|---|---|---|---|---|---|---|---|
| 1 | 99 | 3 | 6 | 3 | 5 | 4 | | 86 | 39 | 27 | 7 | 9 | 6 |
| 2 | 6 | 94 | 29 | 9 | 9 | 6 | | 46 | 85 | 21 | 3 | 1 | 1 |
| 3 | 4 | 28 | 93 | 20 | 5 | 6 | | 9 | 26 | 79 | 53 | 4 | 4 |
| 4 | 2 | 13 | 18 | 95 | 17 | 0 | | 10 | 14 | 48 | 76 | 38 | 2 |
| 5 | 3 | 8 | 2 | 15 | 93 | 31 | | 11 | 8 | 14 | 31 | 89 | 25 |
| 6 | 5 | 7 | 8 | 6 | 29 | 94 | | 9 | 2 | 2 | 11 | 22 | 96 |

5 zones :

| | 1 | 2 | 3 | 4 | 5 | 6 | | 1 | 2 | 3 | 4 | 5 | 6 |
|---|---|---|---|---|---|---|---|---|---|---|---|---|---|
| 1 | 99 | 4 | 7 | 3 | 5 | 4 | | 83 | 43 | 28 | 6 | 9 | 7 |
| 2 | 6 | 94 | 28 | 8 | 6 | 6 | | 50 | 84 | 19 | 5 | 1 | 2 |
| 3 | 5 | 27 | 93 | 22 | 3 | 5 | | 8 | 26 | 78 | 55 | 4 | 4 |
| 4 | 3 | 13 | 19 | 94 | 20 | 0 | | 10 | 13 | 49 | 75 | 38 | 2 |
| 5 | 4 | 7 | 0 | 17 | 91 | 33 | | 11 | 8 | 14 | 31 | 88 | 26 |
| 6 | 5 | 7 | 7 | 7 | 31 | 93 | | 11 | 2 | 2 | 12 | 22 | 95 |

10 zones :

| | 1 | 2 | 3 | 4 | 5 | 6 | | 1 | 2 | 3 | 4 | 5 | 6 |
|---|---|---|---|---|---|---|---|---|---|---|---|---|---|
| 1 | 99 | 3 | 7 | 3 | 5 | 4 | | 84 | 42 | 28 | 6 | 9 | 7 |
| 2 | 0 | 94 | 28 | 8 | 8 | 6 | | 49 | 84 | 20 | 4 | 0 | 2 |
| 3 | 5 | 27 | 93 | 23 | 3 | 5 | | 3 | 27 | 77 | 55 | 4 | 4 |
| 4 | 3 | 13 | 20 | 94 | 20 | 0 | | 10 | 13 | 50 | 75 | 38 | 2 |
| 5 | 4 | 7 | 0 | 17 | 91 | 33 | | 11 | 8 | 14 | 31 | 89 | 26 |
| 6 | 5 | 7 | 7 | 7 | 32 | 93 | | 10 | 2 | 2 | 12 | 22 | 96 |

Rayleigh modes          Love modes

Fig. VII.2.3  Transmission matrices in % for the 6 first Rayleigh and
Love modes across a continental margin model, at 20 s of
period, using 2, 5 and 10 zones. The matrix elements are
amplitude transmission coefficients for modes which
carry a unit energy flux.

|   | 1 | 2 | 3 | 4 | 5 | 6 |
|---|----|----|----|----|----|----|
| 1 | 96 | 13 | 14 | 14 | 6 | 4 |
| 2 | 21 | 73 | 59 | 21 | 4 | 2 |
| 3 | 8 | 52 | 35 | 67 | 21 | 27 |
| 4 | 6 | 34 | 65 | 52 | 23 | 7 |
| 5 | 5 | 17 | 17 | 24 | 40 | 84 |
| 6 | 6 | 10 | 18 | 14 | 85 | 44 |

|   | 1 | 2 | 3 | 4 | 5 | 6 | 7 | 8 |
|---|----|----|----|----|----|----|----|----|
| 1 | 96 | 12 | 14 | 14 | 7 | 5 | 6 | 3 |
| 2 | 20 | 73 | 59 | 21 | 5 | 1 | 1 | 2 |
| 3 | 7 | 52 | 34 | 68 | 24 | 23 | 5 | 3 |
| 4 | 5 | 34 | 65 | 60 | 21 | 7 | 10 | 8 |
| 5 | 5 | 17 | 18 | 21 | 45 | 72 | 38 | 1 |
| 6 | 3 | 6 | 9 | 6 | 58 | 4 | 73 | 30 |
| 7 | 5 | 6 | 12 | 13 | 55 | 52 | 27 | 54 |
| 8 | 8 | 4 | 8 | 12 | 13 | 35 | 48 | 77 |

|   | 1 | 2 | 3 | 4 | 5 | 6 | 7 | 8 | 9 | 10 |
|---|----|----|----|----|----|----|----|----|----|----|
| 1 | 96 | 12 | 14 | 13 | 7 | 5 | 6 | 4 | 3 | 2 |
| 2 | 20 | 73 | 59 | 21 | 5 | 0 | 2 | 4 | 3 | 2 |
| 3 | 6 | 52 | 34 | 68 | 24 | 23 | 6 | 6 | 3 | 2 |
| 4 | 4 | 33 | 65 | 58 | 21 | 7 | 10 | 15 | 13 | 9 |
| 5 | 5 | 17 | 18 | 22 | 45 | 72 | 39 | 2 | 2 | 1 |
| 6 | 3 | 6 | 9 | 7 | 58 | 5 | 71 | 34 | 7 | 1 |
| 7 | 6 | 6 | 12 | 13 | 55 | 53 | 28 | 52 | 10 | 5 |
| 8 | 5 | 3 | 5 | 9 | 13 | 31 | 38 | 59 | 60 | 6 |
| 9 | 5 | 5 | 6 | 9 | 0 | 16 | 23 | 39 | 61 | 58 |
| 10 | 7 | 7 | 9 | 15 | 3 | 5 | 14 | 25 | 47 | 80 |

Fig. VII.2.4  Transmission matrices in % for the 6, 8 and 10 first
Love modes across a continental margin model, at 10 s of
period. The matrix elements are amplitude transmission
coefficients for modes which carry a unit energy flux.

### VII.3 False alarm statistics and threshold determination for regional event detection

In order to improve the event detection performance during automatic processing of regional array data, the detection thresholds for the different beams need to be closely examined. In this context, several factors should be considered:

i)  We wish to make the detection process as sensitive as possible with emphasis on small events, i.e., we want to operate on a low threshold.

ii) We need to specify how many false alarms per time unit can be accepted; e.g., operation of the NORSAR array has shown that false alarm rates of up to 50 % are acceptable.

iii) Too many false alarms will cause the phase association algorithm to produce fictitious events.

iv) The number of false alarms increases with the number of beams. In an extended beam set, we should only include the beams that improve the detectability without significantly increasing the number of false alarms.

In this study we have attempted to determine the thresholds for a large beam set from false alarm considerations. The procedure has been as follows:

1)  Based on previous studies (Kværna and Mykkeltveit, 1986) and the NORSAR staff's experience with processing of regional array data (RONAPP), define the filter bands that appear most appropriate for regional event detection. The resulting twelve filters are given in Table VII.3.1.

2)  For each filter band, find the best array sub-geometry and the
    corresponding steering delays for coherent beamforming. For
    detection of P-waves we have attempted to have maximum 3 deci-
    bels signal loss due to missteering. For coherent beam detec-
    tion of S-waves, we have also applied the 3 dB criterion. The
    resulting P-wave beam deployment spanned the velocity space
    from 6.0 km/s to infinity, whereas the velocity space from
    about 3.8 km/s to 5.3 km/s was spanned by the S-beams. This
    resulted in 72 P-beams and 132 S-beams.

3)  For each filter band, find the best array sub-geometry for
    incoherent beamforming of the vertical channels. The sub-
    geometries were chosen from the criterion that the noise should
    be uncorrelated between channels. Due to the wide response pat-
    tern of the incoherent beams (Ringdal et al, 1975), only one
    incoherent beam (with infinite velocity) was formed for each
    filter band.

4)  For each filter band, form an incoherent beam from the
    eight horizontal channels.

5)  Under the assumption that the SNR is lognormally distributed
    during noise conditions, it can be shown that the cumulative
    distribution of number of detections versus detection threshold,
    approximately follows a straight line when both are plotted
    with logarithmic axes (see Appendix 1). In this study, we have
    selected a time interval (1987/:072.04.30.0 -
    1987/072:16.00.00.0), and run all beams with a low threshold.
    From the cumulative distributions we have extrapolated the
    noise slopes down to a common level, in this case 10 detec-
    tions, and found the corresponding detection thresholds.

In addition to the obtained threshold values, a description of the
beam deployment is given in Table VII.3.2a and Table VII.3.2b.

Fig. VII.3.1 (a-l) show the cumula ive distributions for the coherent
P-beams and the incoherent beams made from the vertical channels.
The dashed tangent lines are the inferred noise slopes extrapolated
down to the 10 detections level. At this threshold we thus expect to
have 10 false alarms ("noise detections") in each filter band during
the examined time interval.

From Fig. VII.3.1 we can see that he threshold differences between
the coherent and incoherent beams ary between 4.5 and 7 decibels.
From this observation we can infer that for detection of phases where
we consistently can achieve coherent beam gain exceeding these
threshold differences, coherent be m detection is superior to inco-
herent detection. From NORESS expe ience (Kværna and Mykkeltveit,
1986), coherent beamforming of in phases will typically result in a
SNR gains between 8 and 15 dB, thus coherent beams are clearly
superior for P-phase detection. For secondary phases like Lg where we
may not achieve coherent beam gain exceeding the threshold differen-
ces, incoherent beamforming may outperform the coherent procedure.

Another interesting feature seen from Fig. VII.3.1i) and Fig.
VII.3.1j), is the large number of detections exceeding the obtained
thresholds for the two filters 8.0-16.0 Hz and 10.0-16.0 Hz. These
filter bands have been subjected to additional detection analysis
of a 24 hours time interval, where we found that the majority of
the detections exceeding the obtained thresholds occurred during
working hours.  A viable hypothesis is therefore that most of these
detections are due to nearby man-made activity.

Fig. VII.3.2 (a-d) show the cumulative distributions for the inco-
herent beams from both the vertical and horizontal channels. An
interesting feature is that the inferred thresholds from the inco-
herent  beams based on 8 horizontal channels, is not higher than the
thresholds inferred from the incoherent beams based on 22 vertical
channels.  This observation suggests that incoherent beamforming on
a mixture of horizontal channels more effectively reduces the
noise variance than using vertical channels alone.

The number of noise detections (10) chosen as a common limit for each
filter band in this study is of course rather arbitrary, and has been
made mainly for the purpose of achieving a common basis for com-
parison.  In practical operation, it may be desirable to operate at
different false alarm rates, and the corresponding thresholds may
easily be inferred, e.g., to reduce the number of detections in the
8.0-16.0 Hz filter band by a factor of two (Fig. VII.3.1i), the
thresholds have to be raised by about 3 decibels.

It should be emphasized that the false alarms discussed in this
paper are due to the stochastic nature of the noise, and
that intervals with different noise characteristics (Fycn, 1986)
may give deviations from these curves.  Noise bursts and close
events which may be considered as false alarms do not follow
the lognormal distribution.  To avoid detection of these signals,
the thresholds would have to be raised above the levels obtained
in this study. Fig. VII.3.3 shows a histogram of RONAPP detections
with apparent velocities less than 3.0 km/s for a period of 86 days.
These signals are mostly generated by local activity in the
northeastern direction from NORESS.  These detections can easily be
separated from the 'interesting' local and regional events on the
basis of their apparent velocities.  The incoherent beams that mostly

detect these local events, are also our best tool for detecting
regional Lg phases. So raising the threshold to avoid the low velocity
signals, would also imply missing a number of regional Lg detections.
This illustrates some of the conflicting interests that has to be
taken into account when determining thresholds and detection beams.

In conclusion, the thresholds obtained from the extrapolated noise
slopes, indicate the lowest operational level. If in the detection
process we want to exclude signals generated by nearby activity or
local noise bursts, the thresholds should be raised. But as outlined
earlier, many other factors have to be considered for a final beam
deployment and the corresponding thresholds.

T. Kværna
S. Kibsgaard
F. Ringdal

References

Fyen, J. (1986): NORESS noise spectral studies - noise level
    characteristics. Semiannual Technical Summary, 1 April -
    30 September 1986, NORSAR Sci. Rep. No. 1-86/87, Kjeller, Norway.

Kværna, T. and S. Mykkeltveit (1986) Optimum beam deployment for
    NORESS P-wave detection. Semiannual Technical Summary, 1 April -
    30 September 1986, NORSAR Sci. Rep. No. 1-86/87, Kjeller, Norway.

Ringdal. F., E.S. Husebye and A. Dahle (1975): P-wave envelope
    representation in event detection using array data, in
    Exploitation of Seismograph Networks, K. G. Beauchamp, Editor,

Appendix 1

We assume that the quantity STA/LTA (short-term to long-term average)
computed at regular intervals on a seismic trace (beam or single chan-
nel) follows a lognormal distribution during noise conditions (Ringdal
et al, 1975).

Setting U = log (STA/LTA) we thus get the following probability den-
sity of this variable

$$f(u) = \frac{1}{\sqrt{2\pi}\cdot\sigma} \cdot e^{-\frac{(u-\mu)^2}{2\sigma^2}} = \frac{1}{\sigma} \cdot \phi \left( \frac{u-\mu}{\sigma} \right) \qquad (1)$$

where $\phi(z)$ denotes the standard Gaussian density.

The probability of U exceeding a given threshold value becomes

$$F(u) = P(U > u) = \int_u^\infty f(t) \, dt = 1 - \Phi\left( \frac{u-\mu}{\sigma} \right) \qquad (2)$$

where $\Phi(z)$ denotes the standard Gaussian distribution function.

With a logarithmic frequency axis, we obtain from (2) the following
slope S(u) of the distribution function at a given threshold u

$$S(u) = \frac{d(\log F(u))}{du} = \frac{F'(u)}{F(u)} = \frac{-\frac{1}{3} \cdot \phi\left(\frac{u-\mu}{\sigma}\right)}{1 - \Phi\left(\frac{u-\mu}{\sigma}\right)} \qquad (3)$$

For values of $t > 3$, we may use the following approximation, with a relative error of less than 10 per cent:

$$1 - \Phi(t) \approx \frac{1}{t} \cdot \phi(t) \qquad (4)$$

Applying this approximation to (3), and also noting that $\mu \approx 0$, since STA/LTA fluctuates around 1 during noise conditions, we obtain

$$S(u) \approx - \frac{u}{\sigma^2} \qquad \text{for } \frac{u}{\sigma} > 3 \qquad (5)$$

In practical detector operation, we are only interested in thresholds corresponding to large values of $\frac{u}{\sigma}$, thus the approximation (5) is applicable. For example, a threshold value of $u = 3.5 \cdot \sigma$ corresponds to 1 false alarm in 4000 independent STA/LTA computations, whereas $u = 4\sigma$ gives 1 false alarm per 30,000 such computations. A practical operating threshold is likely to be somewhere between these values; thus the slope (5) will be approximately constant around the threshold value, for a given $\sigma$.

| Nr. | Prototype | Type | Low | High | Order |
|------|-----------|------|------|------|-------|
| BP01 | BU | BP | 1.0 | 3.0 | 3 |
| BP02 | BU | BP | 1.5 | 3.5 | 3 |
| BP03 | BU | BP | 2.0 | 4.0 | 3 |
| BP04 | BU | BP | 2.5 | 4.5 | 3 |
| BP05 | BU | BP | 3.0 | 5.0 | 3 |
| BP06 | BU | BP | 3.5 | 5.5 | 3 |
| BP07 | BU | BP | 5.0 | 7.0 | 3 |
| BP08 | BU | BP | 6.5 | 8.5 | 3 |
| BP09 | BU | BP | 8.0 | 16.0 | 3 |
| BP10 | BU | BP | 10.0 | 16.0 | 3 |
| BP11 | BU | BP | 1.0 | 2.0 | 2 |
| BP12 | BU | BP | 2.0 | 3.0 | 2 |

Table VII.3.1 This table show the filters applied in the experiment.
All were recursive Butterworth bandpass filters of
order 2 or order 3.

Coherent P-Beams
-----------------

| Filter | Configuration | # beams | Test(dB) | Threshold(dB) | # Detections |
|--------|---------------|---------|----------|---------------|--------------|
| 1.0- 3.0 Hz | AO CD | 1 | 6.0 | 12.0 | 28 |
| 1.5- 3.5 Hz | AO CD | 1 | 6.0 | 11.0 | 40 |
| 2.0- 4.0 Hz | AO CD | 10 | 6.0 | 12.7 | 51 |
| 2.5- 4.5 Hz | AO BCD | 10 | 6.0 | 12.4 | 50 |
| 3.0- 5.0 Hz | AO BC | 7 | 6.0 | 11.4 | 58 |
| 3.5- 5.5 Hz | AO BC | 9 | 6.0 | 10.9 | 64 |
| 5.0- 7.0 Hz | AO BC | 9 | 6.0 | 11.7 | 64 |
| 6.5- 8.5 Hz | AO BC | 9 | 6.0 | 11.5 | 70 |
| 8.0-16.0 Hz | AOAB | 8 | 4.0 | 8.4 | 100 |
| 10.0-16.0 Hz | AOAB | 8 | 4.0 | 8.5 | 114 |
| 1.0- 2.0 Hz | AO CD | 1 | 6.0 | 12.7 | 29 |
| 2.0- 3.0 Hz | AO CD | 1 | 6.0 | 12.7 | 28 |

Coherent S-Beams
----------------

| Filter | Configuration | # beams | Test(dB) | Threshold(dB) | # Detections |
|--------|---------------|---------|----------|---------------|--------------|
| 1.0- 3.0 Hz | AO CD | 6 | 6.0 | 12.7 | 40 |
| 1.5- 3.5 Hz | AO CD | 12 | 6.0 | 12.9 | 49 |
| 2.0- 4.0 Hz | AO CD | 12 | 6.0 | 12.9 | 58 |
| 2.5- 4.5 Hz | AO BCD | 12 | 6.0 | 12.5 | 66 |
| 3.0- 5.0 Hz | AO BC | 12 | 6.0 | 12.3 | 58 |
| 3.5- 5.5 Hz | AO BC | 12 | 6.0 | 12.0 | 61 |
| 5.0- 7.0 Hz | AO BC | 12 | 6.0 | 12.7 | 45 |
| 6.5- 8.5 Hz | AOABC | 12 | 6.0 | 11.8 | 72 |
| 8.0-16.0 Hz | AOAB | 12 | 6.0 | 9.0 | 93 |
| 10.0-16.0 Hz | AOAB | 12 | 6.0 | 9.0 | 114 |
| 1.0- 2.0 Hz | AO CD | 6 | 6.0 | 13.2 | 33 |
| 2.0- 3.0 Hz | AO CD | 12 | 6.0 | 13.7 | 49 |

Table VII.3.2a In addition to the inferred thresholds and the number
of detections exceeding these thresholds, a description
of the coherent beam deployment for detection of P and
S-phases is shown in this table. The respective coloums
describe the following parameters:

Filter : The investigated filter band.
Configuration: The array sub-geomery applied in the
beamforming. AO means AOZ, A means A-
ring, etc.
# beams : Number of coherent beams within the
filter band.
Test : The experimental threshold in dB.
Threshold : The threshold in dB inferred form the
slope of the cumulative distributions.
# Detections : Number of detections exceeding the
deduced thresholds.

Incoherent beams on vertical channels
----------------------------------------

| Filter | Configuration | # beams | Test(dB) | Threshold(dB) | # Detections |
|--------|---------------|---------|----------|---------------|--------------|
| 1.0- 3.0 Hz | AO  CD  | 1 | 1.9 | 6.4 | 48 |
| 1.5- 3.5 Hz | AO  CD  | 1 | 1.9 | 6.6 | 61 |
| 2.0- 4.0 Hz | AO  CD  | 1 | 1.9 | 6.9 | 44 |
| 2.5- 4.5 Hz | AO BCD  | 1 | 1.9 | 6.9 | 42 |
| 3.0- 5.0 Hz | AO BCD  | 1 | 1.9 | 7.2 | 33 |
| 3.5- 5.5 Hz | AO BCD  | 1 | 1.9 | 6.8 | 36 |
| 5.0- 7.0 Hz | AO BCD  | 1 | 1.2 | 4.7 | 72 |
| 6.5- 8.5 Hz | AO BCD  | 1 | 1.2 | 4.5 | 95 |
| 8.0-16.0 Hz | AO BCD  | 1 | 1.2 | 4.0 | 77 |
| 10.0-16.0 Hz | AO BCD | 1 | 1.2 | 4.0 | 80 |
| 1.0- 2.0 Hz | AO  CD  | 1 | 1.9 | 6.8 | 36 |
| 2.0- 3.0 Hz | AO  CD  | 1 | 1.9 | 7.9 | 45 |

Incoherent beams on horizontal channels
----------------------------------------

| Filter | Configuration | # beams | Test(dB) | Threshold(dB) | # Detections |
|--------|---------------|---------|----------|---------------|--------------|
| 1.0- 3.0 Hz | E-W N-S | 1 | 1.9 | 6.8 | 35 |
| 1.5- 3.5 Hz | E-W N-S | 1 | 1.9 | 7.0 | 50 |
| 2.0- 4.0 Hz | E-W N-S | 1 | 1.9 | 7.4 | 40 |
| 2.5- 4.5 Hz | E-W N-S | 1 | 1.9 | 6.8 | 48 |
| 3.0- 5.0 Hz | E-W N-S | 1 | 1.9 | 6.1 | 54 |
| 3.5- 5.5 Hz | E-W N-S | 1 | 1.9 | 5.3 | 52 |
| 5.0- 7.0 Hz | E-W N-S | 1 | 1.2 | 5.1 | 44 |
| 6.5- 8.5 Hz | E-W N-S | 1 | 1.2 | 4.8 | 81 |
| 8.0-16.0 Hz | E-W N-S | 1 | 1.2 | 3.7 | 81 |
| 10.0-16.0 Hz | E-W N-S | 1 | 1.2 | 3.7 | 92 |
| 1.0- 2.0 Hz | E-W N-S | 1 | 1.9 | 7.3 | 23 |
| 2.0- 3.0 Hz | E-W N-S | 1 | 1.9 | 8.6 | 29 |

Table VII.3.2b In this table we have shown the same parameters as in
               Table VII.3.2a, but now for the incoherent beams.
               E-W means the channels AOE, C2E, C4E and C7E.
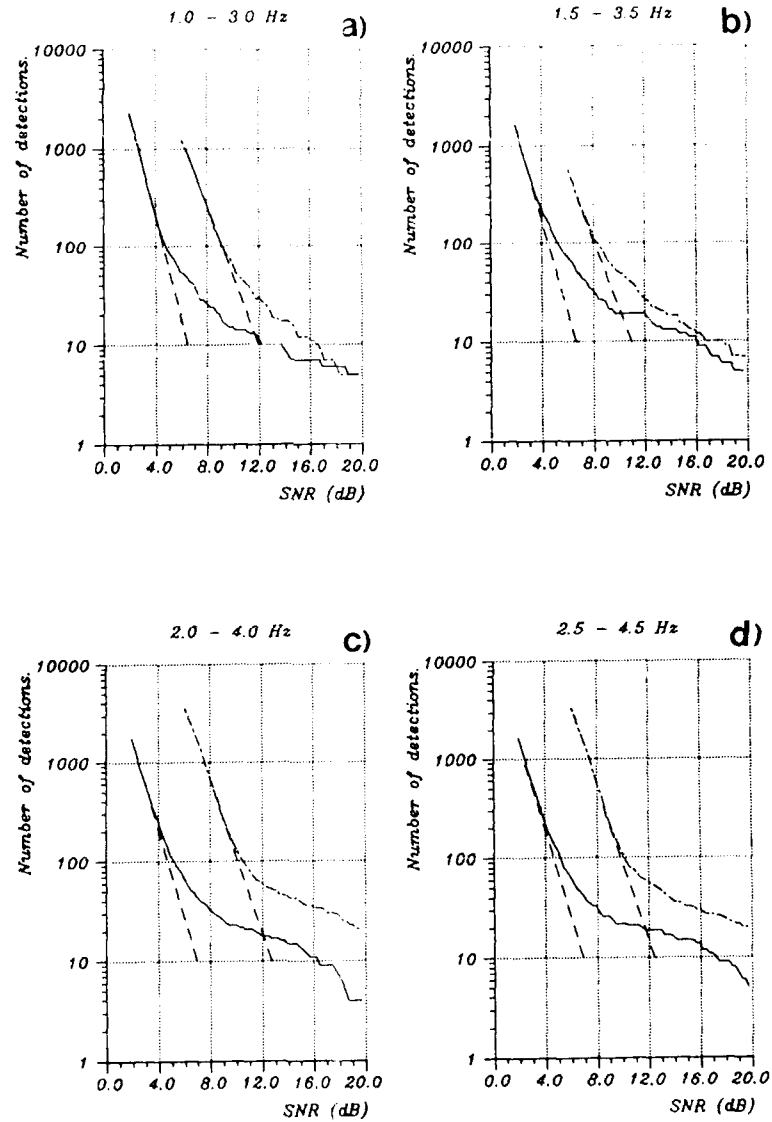               N-S means the channels AON, C2N, C4N and C7N.

Fig. VII.3.1  These figures (a-1) show the cumulative distributions
for the coherent P-beams (dashed-dotted curves) and for
the incoherent beams made from the vertical channels
(solid lines) in all filter bands investigated.  The
dashed lines indicate the slopes of the distribution of
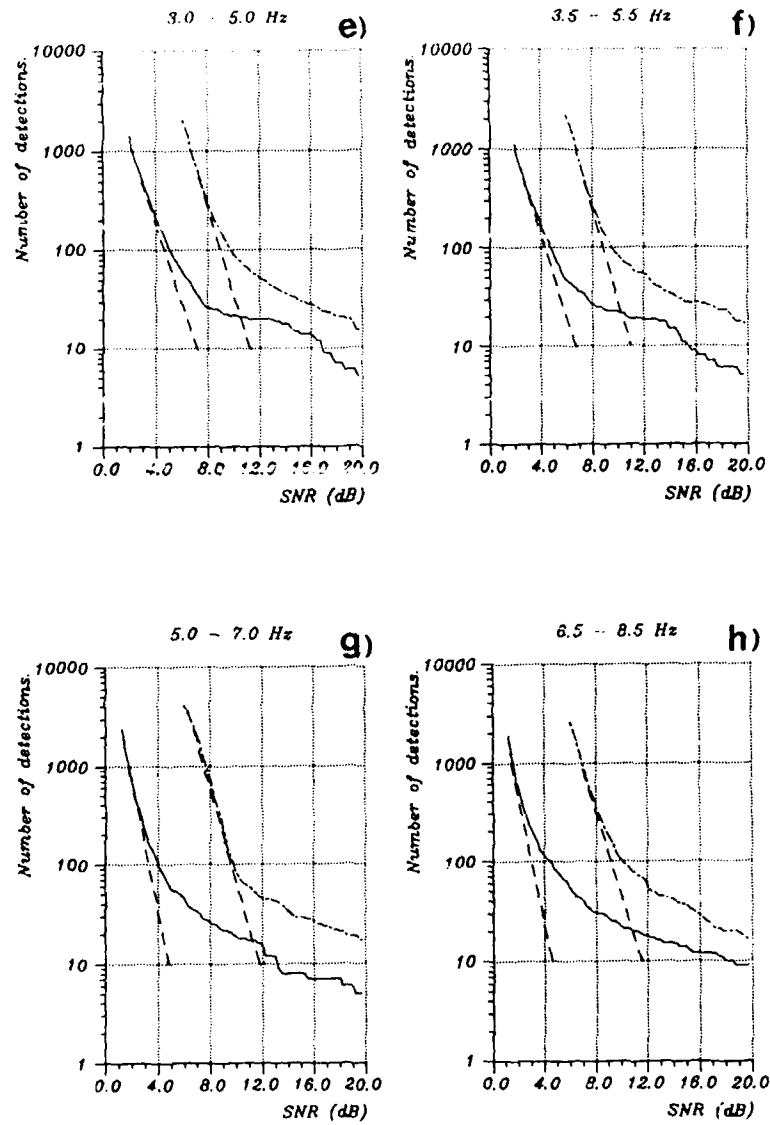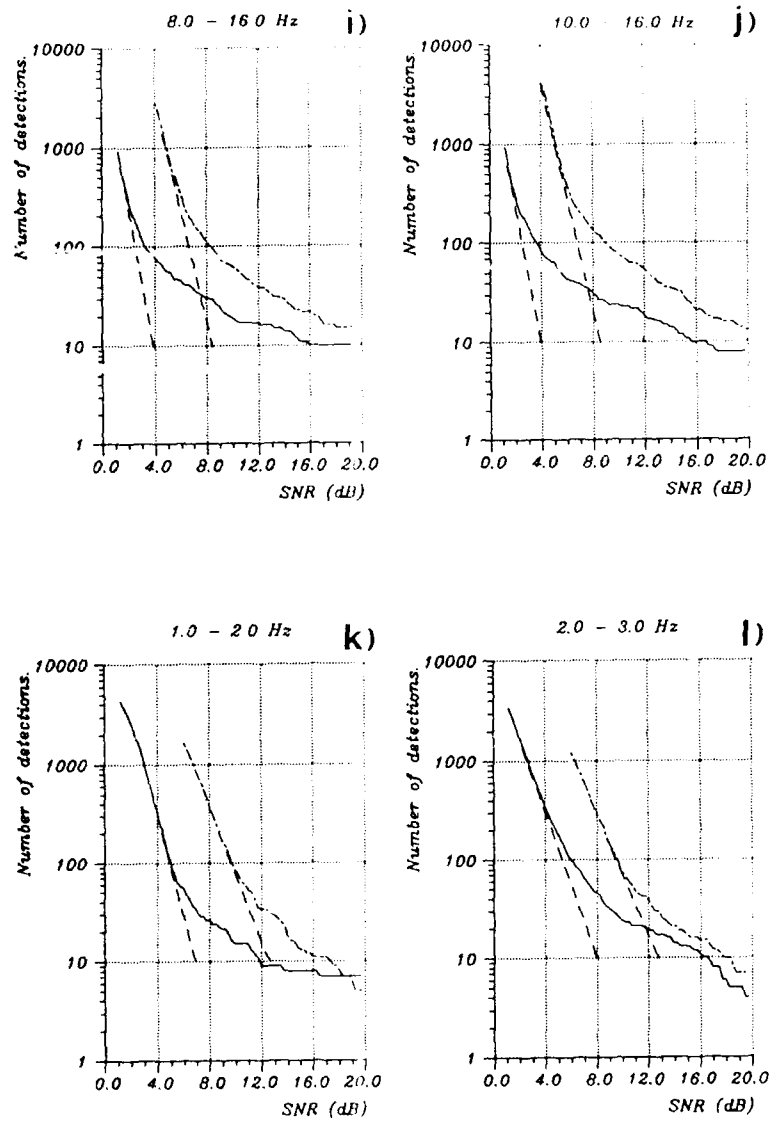'noise' detections.

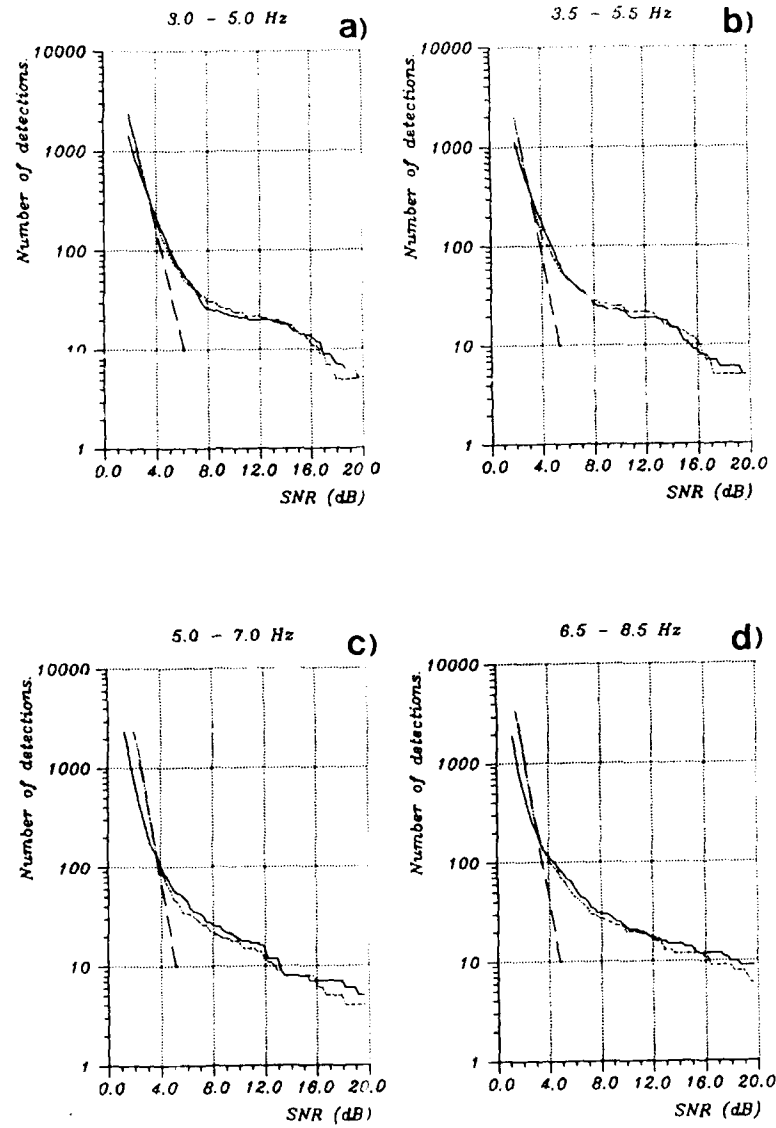Fig. VII.3.1  (cont.)

Fig. VII.3.1 (cont.)

Fig. VII.3.2  This figure (a-d) show the cumulative distributions for
the incoherent beams from the vertical channels (solid
lines) and from the horizontal channels (dotted lines)
for four different filter bands.  The dashed lines indi-
cate the noise slopes inferred from the 'noise' distri-
butions of the 'horizontal' beams.

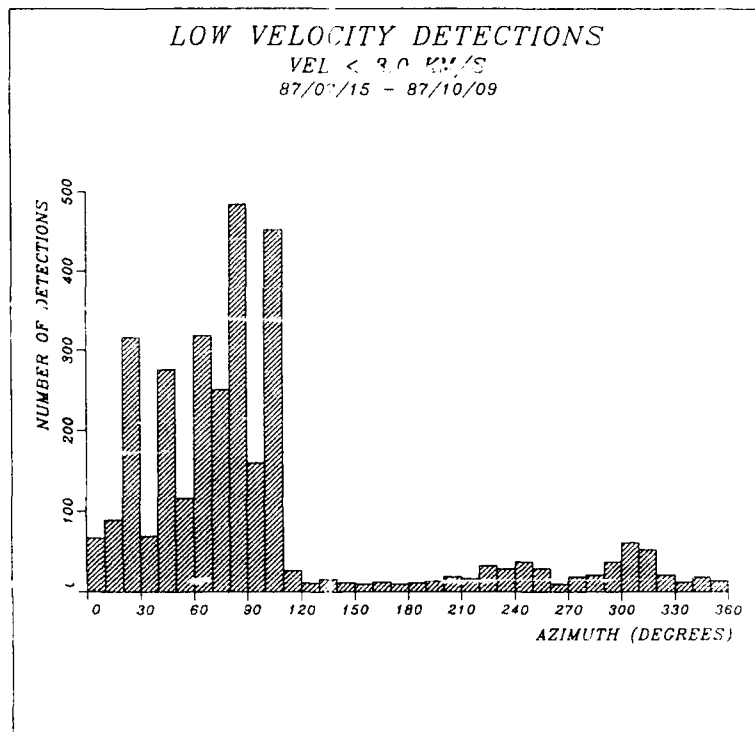**LOW VELOCITY DETECTIONS**
*VEL < 3.0 KM/S*
*87/0?/15 - 87/10/09*

Fig. VII.3.3  This histogram displays the azimuthal distribution of
RONAPP detections during the 86-day period indicated,
with apparent velocities less than 3.0 km/s. Within the
investigated time interval there were totally 10000
detections. 3140 of these detections had an apparent
velocity less than 3.0 km/s.

VII.4    Initial results from analysis of data recorded at the new
         regional array in Finnmark, Norway

During the summer and fall of 1987, a regional array was installed
near the town of Karasjok in the county of Finnmark in northern
Norway. The new Finnmark array was designed to be as closely as
possible a copy of the NORESS regional array, which was established in
southern Norway in 1984. The geometries of the two arrays are there-
fore practically identical (deviations between corresponding sensor
positions are of the order of a few tens of meters, due to local
terrain conditions), and the data outputs are the same for the two
arrays. Fig. VII.4.1 shows the location of the two regional arrays
in Norway, and also the location of the FINESA regional array in
Finland, which was described by Korhonen et al (1987). The geometry of
NORESS (and for most practical purposes, also the geometry of the
Finnmark array) is shown in Fig. VII.4.2.

Data from the new Finnmark array have been transmitted continuously
via satellite to the NORSAR data processing center at Kjeller since
November 1, 1987. The data are subjected to automatic detection
processing, with a beam deployment identical to the one used for
NORESS.

In the following, we report on some findings resulting from analysis
of data from the new Finnmark array. It should be emphasized at the
outset that the available data cover no more than a two-week period,
and that a comprehensive assessment of the capabilities of the new
array must await the collection of data covering a longer time span.

**Noise spectra**

Fig. VII.4.3a shows corrected noise spectra for altogether 17 elements
of the new Finnmark array (the vertical sensors at A0 and the C- and

D-rings, see Fig. VII.4.2), taken at 00.00 GMT on day 315. For com-
parison, NORESS noise spectra for the same number of channels and
taken at the same time, are shown in Fig. VII.4.3b. From these
figures, it is seen that below 2.0 Hz, the Finnmark array experiences
a higher noise level than NORESS, whereas above 2.0 Hz the Finnmark
site is clearly the quieter.

The high noise level at low frequencies at the Finnmark site has been
confirmed by other data and is typically even higher than shown in
Fig. VII.4.3a. At the time of these spectra, the nearby coast of Finn-
mark experienced a wind force 4, which is moderate. The noise level at
these low frequencies is generally believed to be governed by the
passage of major weather fronts over the open ocean. Therefore, it
should not be unexpected to find the higher microseismic noise levels
at the Finnmark array, since this array is located closer to the coast
than the NORESS array.

For the frequency range above 2 Hz, the noise level at the Finnmark
site appears to be 3-5 dB below that of NORESS. A possible explanation
here is that the noise in this band is lower at the northern site
because of a lower population density and also lower level of traffic
and industrial activities, compared to the NORESS site. These noise
levels must also be rated as low relative to year-round averages for
NORESS, as investigated by Fyen (1987).

Figs. VII.4.4a and 4b each show ten uncorrected spectra, taken hourly
between 00.00 GMT and 10.00 GMT of day 315, for the Finnmark and
NORESS arrays, respectively. Each single spectrum represents an
average of 17 spectra for the vertical sensors of A0, the C- and
D-rings. The NORESS spectra show the well-established (Fyen, 1986a,b;
1987) difference between night-time and day-time noise characteristics

(particularly around 6 Hz). The Finnmark data are generally below those of the NORESS site for frequencies above 2 Hz. The two or three curves with the higher noise power in Fig. VII.4.4a represent cases of high frequency noise bursts at the Finnmark site during daytime. These bursts are visually confirmed by careful inspection of the seismograms. A more comprehensive study is needed to clarify the origin of this noise. There is so far, however, no indication of constant noise sources like power plants and sawmills.

It should be emphasized again that in order to establish reliable estimates of ambient noise levels at the new array site, studies like those undertaken by Fyen (1986a,b; 1987) for NORESS are needed. The material analyzed so far, however, indicates that in the range of primary interest to regional seismic verification (i.e., above 2 Hz), the noise level at the new Finnmark array site is generally somewhat lower than the NORESS noise level.

### Noise suppression by beamforming

The NORESS array has proved very proficient in the enhancement by beamforming of the SNR, yielding gains that are often of the order of or even in excess of $\sqrt{N}$ (N being the number of sensors used in the beamforming). It has been shown that this success is largely due to the highly effective noise suppression that can be obtained by selecting appropriate sub-geometries for the various signal frequencies. As a first check on the new array's capabilities in this regard, noise suppression curves were computed and compared with corresponding results from NORESS.

In Fig. VII.4.5a, the noise suppression in the frequency range 0-20 Hz
for vertical beamforming (no shifts introduced) is shown for three
one-minute intervals taken hourly at 00.00, 01.00 and 02.00 GMT on day
315. The sub-geometry used is that of A0, the B- and C-ring instru-
ments (13 sensors). The dots in this figure represent average values
for NORESS that are taken from Fyen (1986c). The $\sqrt{N}$ level is at about
-11 dB, and the general impression left from this figure is that the
new array is as effective in suppressing noise as NORESS, for this
sub-geometry. For another sub-geometry, comprising the sensors of A0,
the C- and D-rings, corresponding results are given in Fig. VII.4.5b.
Again, we see that the noise suppression capability is comparable to
or maybe even better than the average performance of NORESS. This
strongly suggests that the spatial characteristics (e.g., correlation
lengths vs. frequency) of the noise field are very similar to those
found at NORESS. It has previously been established (Korhonen et al,
1987) that the NORESS and FINESA arrays exhibit strong similarities in
this regard.

**Analysis of data from two regional events located at the Finnmark
array**

As examples of regional events recorded on the Finnmark array, we pre-
sent the records for two presumed mining explosions in the Kola penin-
sula of the USSR.

The C-ring seismograms for the first event are shown in Fig. VII.4.6.
The event occurred at 67.6°N, 34.0°E (according to the University of
Helsinki bulletin), at an epicentral distance of 408 km and an azimuth
of 117.9°. The phases Pn, Pg, Sn and Lg can be clearly identified by
visual inspection. These phases were subjected to wide-band slowness

analysis, with results given in Figs. VII.4.7 and VII.4.8. We see that
the phase velocities derived are in the expected range for these pha-
ses and that deviations from the "true" azimuth are within 6-7°.

Data for the second event are shown in Fig. VII.4.9. This event is
located at 68.1°N, 33.2°E, at an epicentral distance of 349 km and an
azimuth of 113.7°. Besides the phases identified for the first event,
we now also see a clearly developed Rg phase. It is of particular
interest to note the difference between the two events in this regard,
particularly since they are separated by not more than about 60 km.
The occurrence of Rg waves in the records for events of epicentral
distances of the order of 350 km also sharply contrasts what we have
found at NORESS, where Rg waves are never observed beyond 100 km
distance. The results of the wide-band slowness analysis of the phases
Pn, Pg, Lg and Rg for this event are shown in Figs. VII.4.10 and
VII.4.11. Again we see that the phase velocities are reasonable, and
the azimuths deviate by not more than 5° from the "true" value.

### Regional event detection

An initial study has been made comparing the regional event detection
performance of the two arrays in Norway. A two-week period (Oct 31 -
Nov 18, 1987) was selected for this purpose, and analysis of RONAPP
processing results for the two arrays was conducted. For both arrays,
the beam deployments and thresholds were identical, and the same as
those used for the past two years in regular NORESS operation.

Fig. VII.4.12 shows a map displaying all regional events located by
NORESS during this time period, whereas Fig. VII.4.13 gives a similar
map for the Finnmark array. We recall that in order for one array to

locate a regional event, at least two phases (P and Lg) from that array must be detected and associated.

Comparing these two figures is quite instructive, and probably gives a reliable impression of what can be expected during long-term operation. The actual number of located events is similar for the two arrays (NORESS 152, Finnmark 117). However, there is almost no overlap of the two populations; in fact only 8 events were located by both arrays. The large majority of located events are within 500 km of the respective arrays, and represent in most cases presumed local explosions of low magnitude ($M_L < 1.5$). Sites where such explosions are clustered can be easily identified on the plots. It is noteworthy in particular that the Finnmark array detects and locates a large number of mining explosions in the Kola peninsula.

Fig. VII.4.14 shows a map of all events of estimated $M_L > 2.0$ located by at least one array. In those cases when both arrays located the same event, the location by the closest array was chosen. Events with at least one confirming phase (P or Lg) from the other array are encircled. Details pertaining to the figure are given in Table VII.4.1.

Compared to the previous figures, it is clear that relaxing the criterion for "common" events to requiring only one confirming phase from the other array significantly increases the overlap of the populations. The majority of events in Fig. VII.4.14 are thus detected by both arrays. It is particularly interesting to observe the good performance for the event cluster near 65°N 40°E, which is at a considerable distance from both arrays (700 and 1500 km, respectively). These events were in the magnitude range 2.5-2.7 and the locations have been independently confirmed by the Finnish network.

In almost all cases of confirming detections by one phase only, this corresponded to a P phase (Table VII.4.1). This result is somewhat surprising in view of earlier P and Lg detection studies for NORESS and may not be representative. Further assessment of the joint detection and location potential of the two arrays will require a more extensive data base, and will be the subject of further study.

S. Mykkeltveit
F. Ringdal
J. Fyen
T. Kværna

## References

Fyen, J. (1986a): NORESS noise spectral studies, preliminary report. Semiannual Technical Summary, 1 Oct 1985 - 31 Mar 1986, NORSAR Sci. Rep. No. 2-85/86, Kjeller, Norway.

Fyen, J. (1986b): NORESS noise spectral studies - noise level characteristics. Semiannual Technical Summary, 1 Apr 1986 - 30 Sept 1986, NORSAR Sci. Rep. No. 1-86/87, Kjeller, Norway.

Fyen, J. (1986c): NORESS noise spectral studies - beam suppression. Semiannual Technical Summary, 1 Apr 1986 - 30 Sept 1986, NORSAR Sci. Rep. No. 1-86/87, Kjeller, Norway.

Fyen, J. (1987): NORESS noise spectral studies. Noise level characteristics. Semiannual Technical Summary, 1 Oct 1986 - 31 Mar 1987, NORSAR Sci. Rep. No. 2-86/87, Kjeller, Norway.

Korhonen, H., S. Pirhonen, F. Ringdal, S. Mykkeltveit, T. Kværna, P.W. Larsen and R. Paulsen (1987): The Finesa array and preliminary results of data analysis. Univ. of Helsinki, Inst. of Seismology, Report S-16.

| Reference Array | | NORESS | Finnmark |
|---|---|---|---|
| Total no. of events located by reference array | | 152 | 117 |
| No. of events $M_L \geqslant 2.0$ | | 31 | 42 |
| No. of events $M_L \geqslant 2.0$ located by the reference array, detected or not detected by the other array. | Both P and Lg | 8 | 8 |
| | P only | 14 | 12 |
| | Lg only | 1 | 1 |
| | Not detected | 8 | 21 |

Table VII.4.1 Statistics of detected and located regional events for the two arrays in Norway during a two-week test period.

REGIONAL ARRAYS IN FENNOSCANDIA



LATITUDE (DEG N)

LONGITUDE (DEG E)
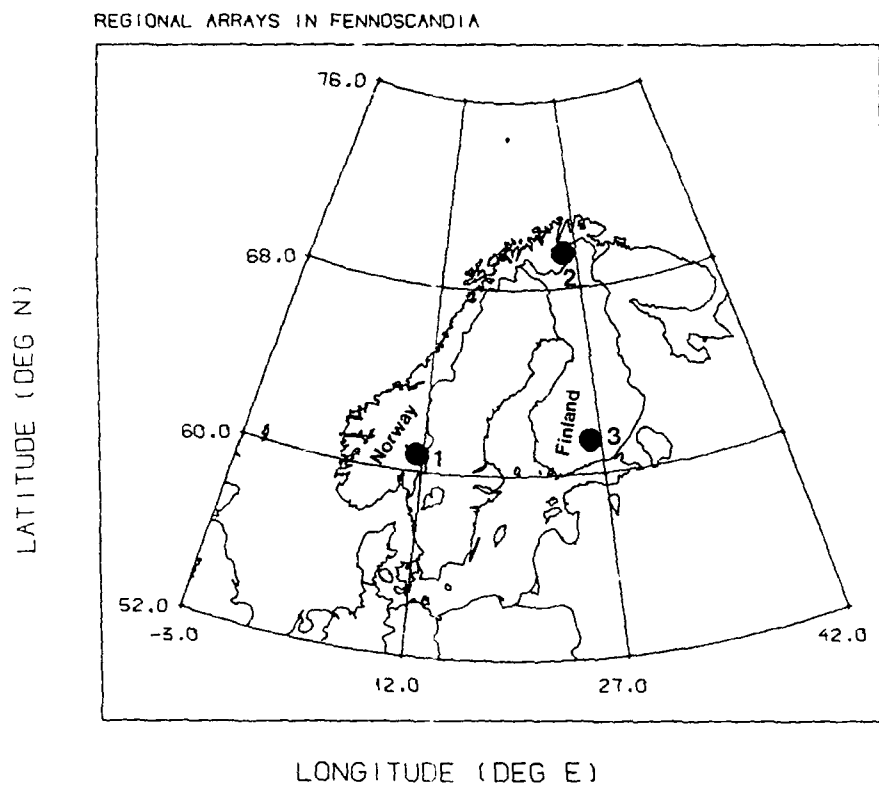
87/11/25  11.42  NORSAR

Fig. VII.4.1   The figure shows the network of three regional arrays in
              Fennoscandia.   1: The NORESS array in southern Norway;
              2: The new array in Finnmark, northern Norway; and
              3: The FINESA array in Finland.
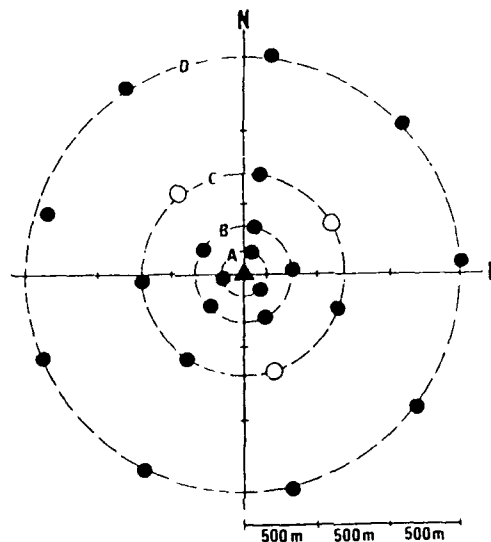
LEGEND:

● VERTICAL SHORT PERIOD

○ 3-COMPONENT SHORT PERIOD

▲ 3-COMPONENT BROAD BAND
AND 3-COMPONENT SHORT PERIOD

Fig. VII.4.2   The geometry of the NORESS array. The geometry of the
new Finnmark array comes very close to being identical
to that of NORESS; deviations between corresponding ele-
ment positions are of the order of some tens of meters.
The channel assignments (vertical only vs. three-
component, short period vs. broadband) are identical for
the two arrays. The short period instrument at the
center of the array is denoted A0.

FINMARK NOISE



11/20/81 10:24:49          FREQUENCY
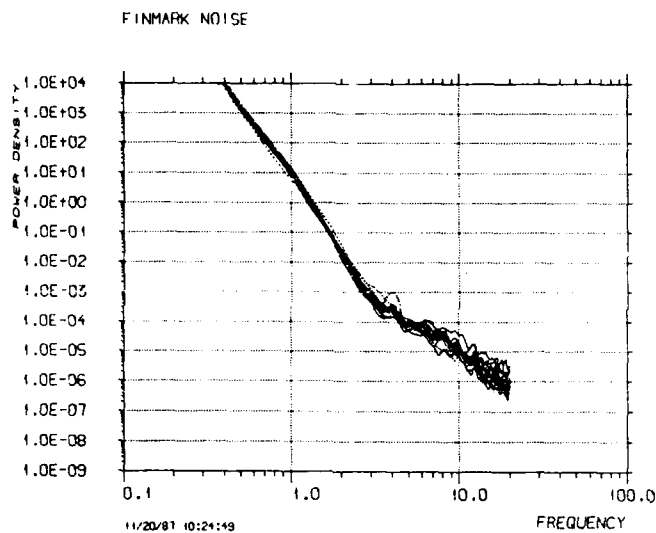
Fig. VII.4.3a Noise spectra corrected for system response for the
Finnmark array for 17 vertical channels at AO, the C-
and D-rings. The spectra are base don one minute of data
at 00.00 GMT on day 315. The power density is in $nm^2/Hz$.

NORESS NOISE



11/24/81 09:31:56          FREQUENCY
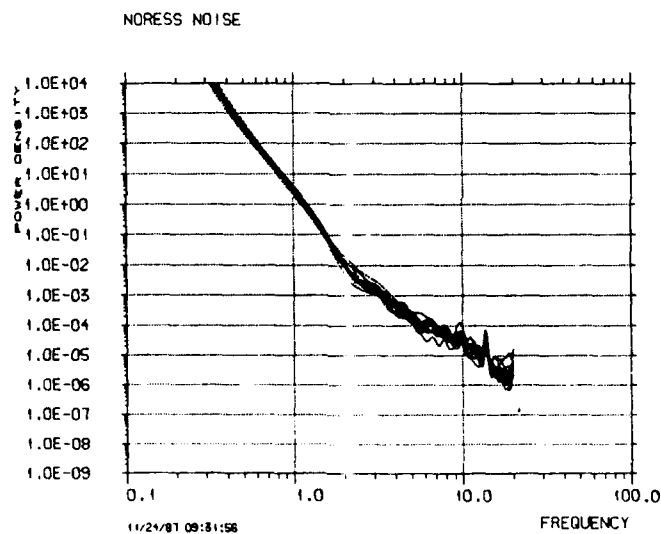
Fig. VII.4.3b Same as Fig. VII.4.3a, but for NORESS data taken at
00.15 GMT on day 315.

FINNMARK AVERAGE NOISE 00-10
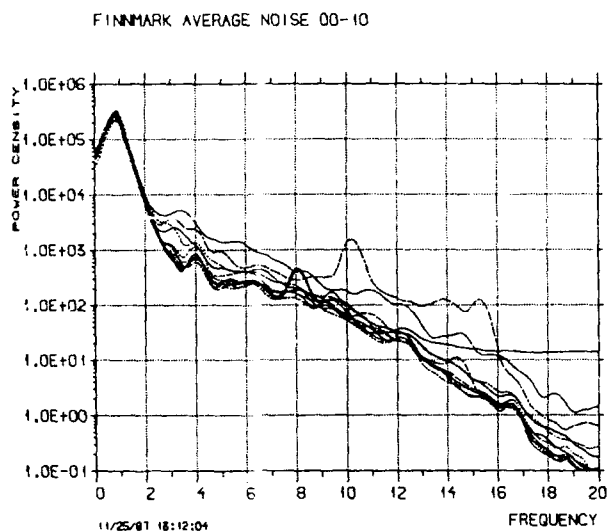


Fig. VII.4.4a  Uncorrected noise spectra for the Finnmark array for ten
one-minute intervals taken hourly between 00.00 and
10.00 GMT on day 315. Each spectrum represents an
average of the 17 vertical sensors of A0, the C- and
D-rings.

NORESS AVERAGE NOISE 00-10
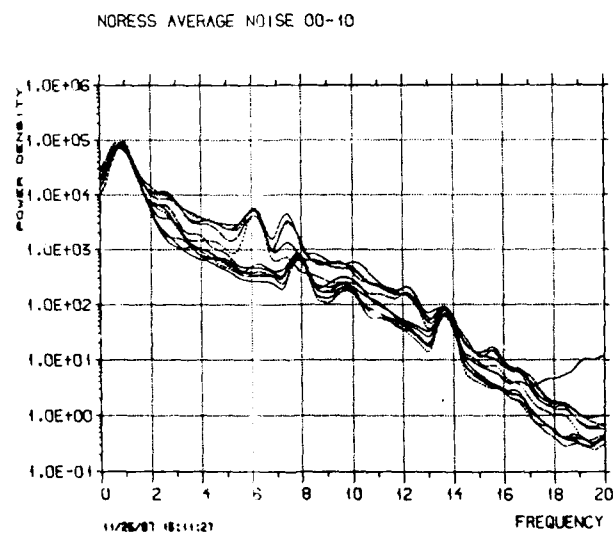


Fig. VII.4.4b  Same as Fig. VII.4.4a, but for NORESS data taken hourly
between 00.00 and 10.00 GMT on day 315.

FINNMARK CRING BEAM SUPPRESSION
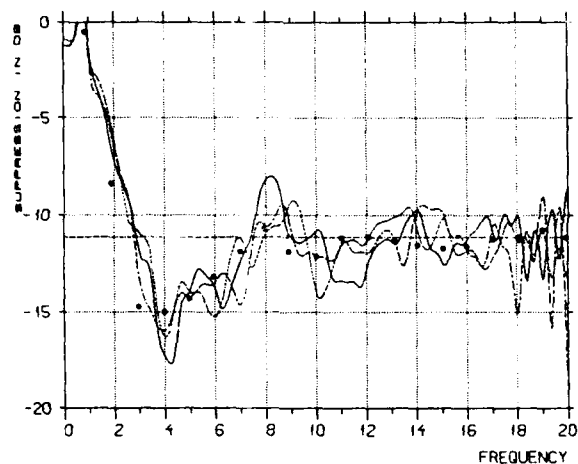


Fig. VII.4.5a Finnmark array noise suppression by beamforming for the sub-
geometry comprising the AO, B- and C-ring sensors. To produce
these curves, a vertical beam is formed and the spectrum for
this beam is divided by the average of the single sensor
spectra. The three curves result from one minute of data
taken hourly at 00.00, 01.00 and 02.00 GMT on day 315. The
dots represent typical NORESS noise suppression values for
this sub-geometry. The horizontal line at -11.1 dB represents
√N suppression for 13 sensors.

FINNMARK TELEV BEAM SUPPRESSION
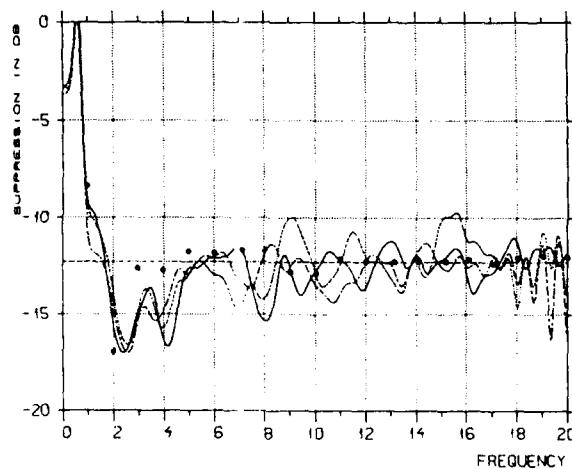


Fig. VII.4.5b Same as Fig. VII.4.5a, but for the sub-geometry comprising
the sensors of AO, the C- and D-rings. The horizontal line at
-12.3 dB represents √N suppression for 17 sensors.

Fig. VII.4.6  Finnmark array data for a presumed mining explosion at
67.6°N, 34.0°E. The plot shows data for the vertical
instruments of the (-ring.

*Wide-band slowness analysis*

*Contours in decibels below maximum peak*

**Pn**

Horizontal slowness Sy (sec/km)

Horizontal slowness Sx (sec/km)

Time 1987/317:12 40 39.170
Interval    3.0 sec

Channels:

| | |
|---|---|
| A0Z | C4Z |
| A1Z | C5Z |
| A2Z | C6Z |
| A3Z | C7Z |
| B1Z | D1Z |
| B2Z | D2Z |
| B3Z | D3Z |
| B4Z | D4Z |
| B5Z | D5Z |
| C1Z | D6Z |
| C2Z | D7Z |
| C3Z | D8Z |
| | D9Z |

BAND   6.0- 8.0 Hz
VEL:    7.38 km/s   AZ: 123.07 deg.   REL.PWR:  0.66   PWR:   73.7 dB

11/26/87 14:06:18

*Wide-band slowness analysis*

*Contours in decibels below maximum peak*

**Pg**

Horizontal slowness Sy (sec/km)

Horizontal slowness Sx (sec/km)

Time 1987/317:12 40 46.970
Interval    3.0 sec

Channels:

| | |
|---|---|
| A0Z | C4Z |
| A1Z | C5Z |
| A2Z | C6Z |
| A3Z | C7Z |
| B1Z | D1Z |
| B2Z | D2Z |
| B3Z | D3Z |
| B4Z | D4Z |
| B5Z | D5Z |
| C1Z | D6Z |
| C2Z | D7Z |
| C3Z | D8Z |
| | D9Z |

BAND   2.0- 4.0 Hz
VEL:    7.22 km/s   AZ: 117.33 deg.   REL.PWR:  0.71   PWR:   66.1 dB

11/26/87 14:29:64

Fig. VII.4.7   Wide-band slowness spectra for the Pn phase (top) and Pg
phase (bottom) for the event in Fig. VII.4.6.

*Wide—band slowness analysis*

*Contours in decibels below maximum peak*

**Sn**

Time 1987/317:12 41 20.970
Interval   3.0 sec

Channels:

| | |
|---|---|
| A0Z | C4Z |
| A1Z | C5Z |
| A2Z | C6Z |
| A3Z | C7Z |
| B1Z | D1Z |
| B2Z | D2Z |
| B3Z | D3Z |
| B4Z | D4Z |
| B5Z | D5Z |
| C1Z | D6Z |
| C2Z | D7Z |
| C3Z | D8Z |
| | D9Z |

BAND   3.5– 5.5 Hz
VEL:   4.02 km/s  AZ: 124.62 deg.  REL.PWR:  0.31  PWR:  63.3 dB

11/26/87  8:43:47

*Wide—band slowness analysis*

*Contours in decibels below maximum peak*

**Lg**

Time 1987/317:12 41 33.970
Interval   3.0 sec

Channels:

| | |
|---|---|
| A0Z | C4Z |
| A1Z | C5Z |
| A2Z | C6Z |
| A3Z | C7Z |
| B1Z | D1Z |
| B2Z | D2Z |
| B3Z | D3Z |
| B4Z | D4Z |
| B5Z | D5Z |
| C1Z | D6Z |
| C2Z | D7Z |
| C3Z | D8Z |
| | D9Z |

BAND   3.0– 5.0 Hz
VEL:   4.22 km/s  AZ: 119.10 deg.  REL.PWR·  0.37  PWR:  73.9 dB

11/26/87  14:34:65

Fig. VII.4.8   Wide-band slowness spectra for the Sn phase (top) and Lg
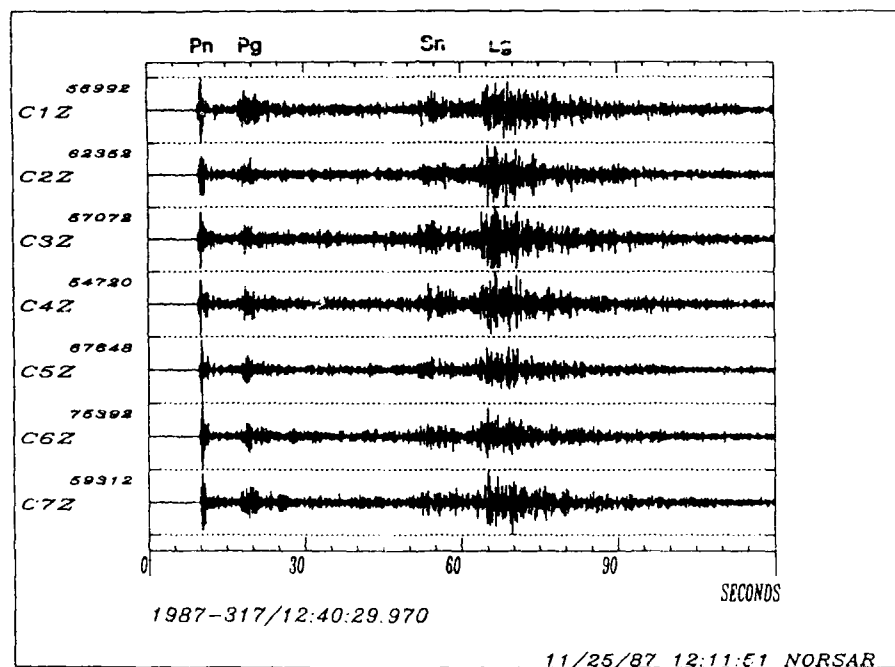phase (bottom) for the event in Fig. VII.4.6.

Fig. VII.4.9 Finnmark array data for a presumed mining explosion at 68.1°N, 33.2°E. The plot shows data for the vertical instruments of the C-ring.
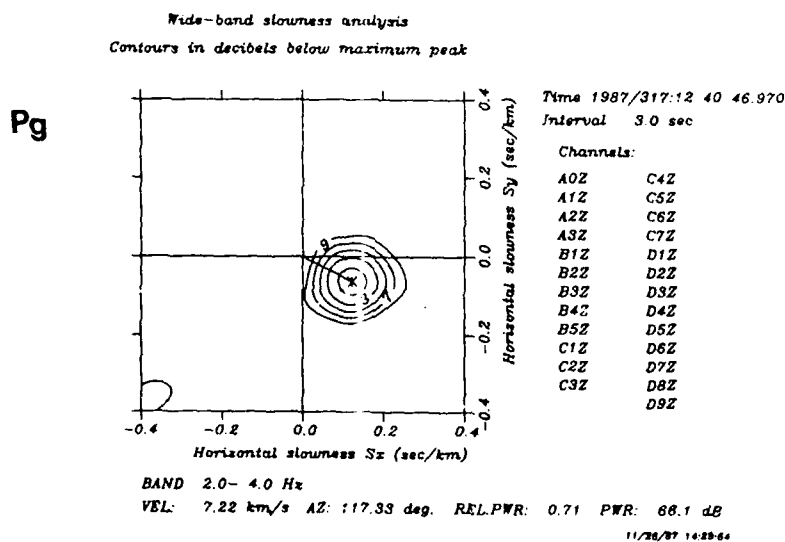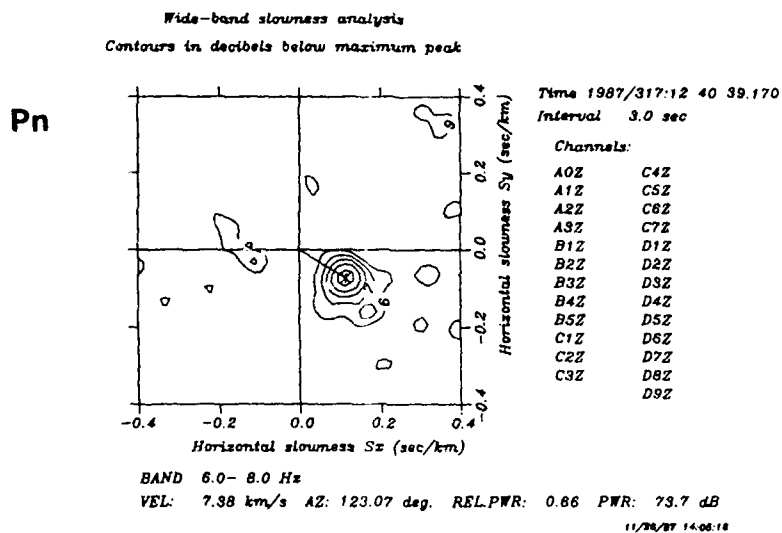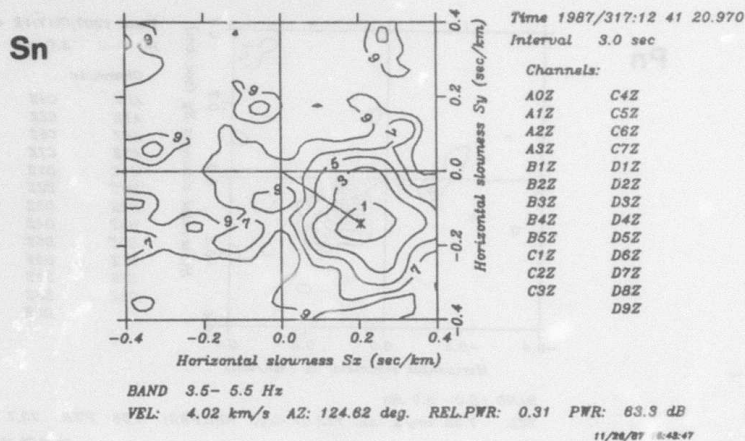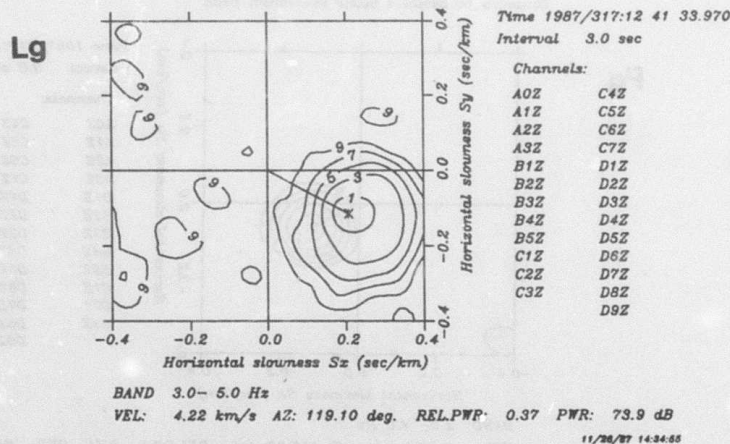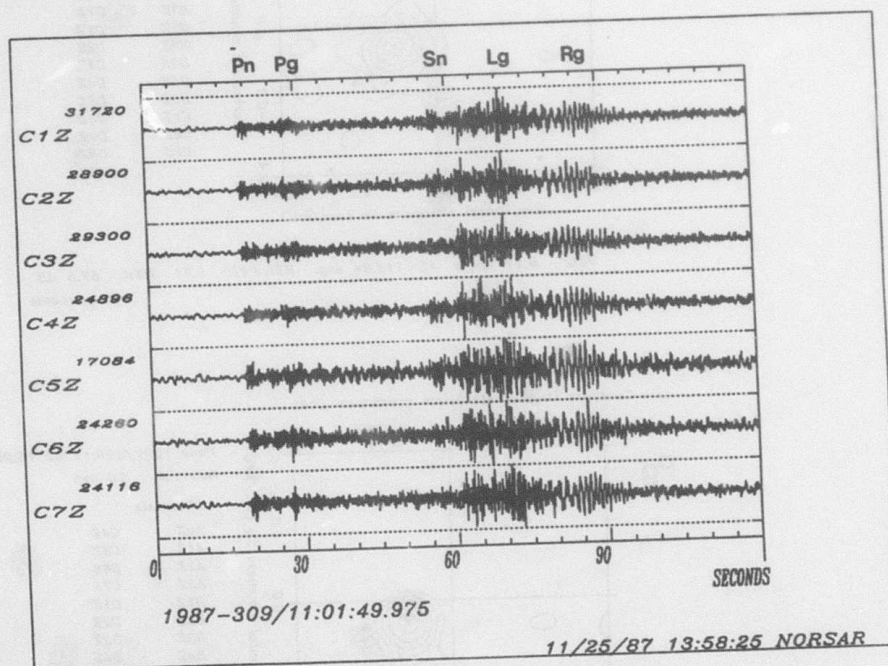
Wide-band slowness analysis

Contours in decibels below maximum peak

**Pn**



Time 1987/309:11 02 07 975
Interval   3.0 sec

Channels:

| | |
|---|---|
| A0Z | C4Z |
| A1Z | C5Z |
| A2Z | C6Z |
| A3Z | C7Z |
| B1Z | D1Z |
| B2Z | D2Z |
| B3Z | D3Z |
| B4Z | D4Z |
| B5Z | D5Z |
| C1Z | D6Z |
| C2Z | D7Z |
| C3Z | D8Z |
| | D9Z |

BAND  5.0- 7.0 Hz

VEL:   8.17 km/s  AZ  118.64 deg.  REL.PWR:  0.71  PWR:  57.5 dB

11/28/87 18-05-28

Wide-band slowness analysis

Contours in decibels below maximum peak

**Pg**



Time 1987/309:11 02 15.975
Interval   3.0 sec

Channels:

| | |
|---|---|
| A0Z | C4Z |
| A1Z | C5Z |
| A2Z | C6Z |
| A3Z | C7Z |
| B1Z | D1Z |
| B2Z | D2Z |
| B3Z | D3Z |
| B4Z | D4Z |
| B5Z | D5Z |
| C1Z | D6Z |
| C2Z | D7Z |
| C3Z | D8Z |
| | D9Z |

BAND  4.0- 6.0 Hz

VEL:   7.69 km/s  AZ  118.70 deg.  REL.PWR:  0.83  PWR:  58.4 dB

11/28/87 18-12-44
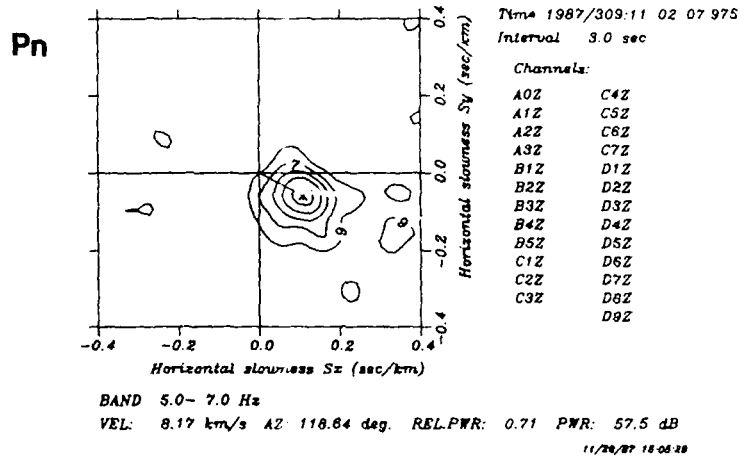
Fig. VII.4.10 Wide-band slowness spectra for the Pn phase (top) and Pg phase (bottom) for the event in Fig. VII.4.9.

**Wide-band slowness analysis**

**Contours in decibels below maximum peak**

**Lg**

Time 1987/309:11 02 58.475
Interval  4.0 sec

Channels:

| | |
|---|---|
| A0Z | C4Z |
| A1Z | C5Z |
| A2Z | C6Z |
| A3Z | C7Z |
| B1Z | D1Z |
| B2Z | D2Z |
| B3Z | D3Z |
| B4Z | D4Z |
| B5Z | D5Z |
| C1Z | D6Z |
| C2Z | D7Z |
| C3Z | D8Z |
| | D9Z |

Horizontal slowness Sx (sec/km)

BAND  2.0- 4.0 Hz
VEL:  4.03 km/s  AZ: 115.03 deg.  REL.PWR:  0.68  PWR:  68.6 dB

**Wide-band slowness analysis**

**Contours in decibels below maximum peak**

**Rg**

Time 1987/309:11 03 08.975
Interval 10.0 sec

Channels:

| | |
|---|---|
| A0Z | C4Z |
| A1Z | C5Z |
| A2Z | C6Z |
| A3Z | C7Z |
| B1Z | D1Z |
| B2Z | D2Z |
| B3Z | D3Z |
| B4Z | D4Z |
| B5Z | D5Z |
| C1Z | D6Z |
| C2Z | D7Z |
| C3Z | D8Z |
| | D9Z |

Horizontal slowness Sx (sec/km)

BAND  0.9- 1.0 Hz
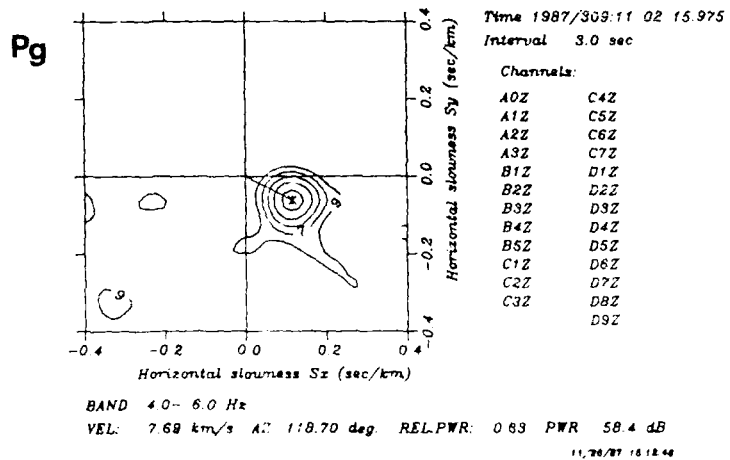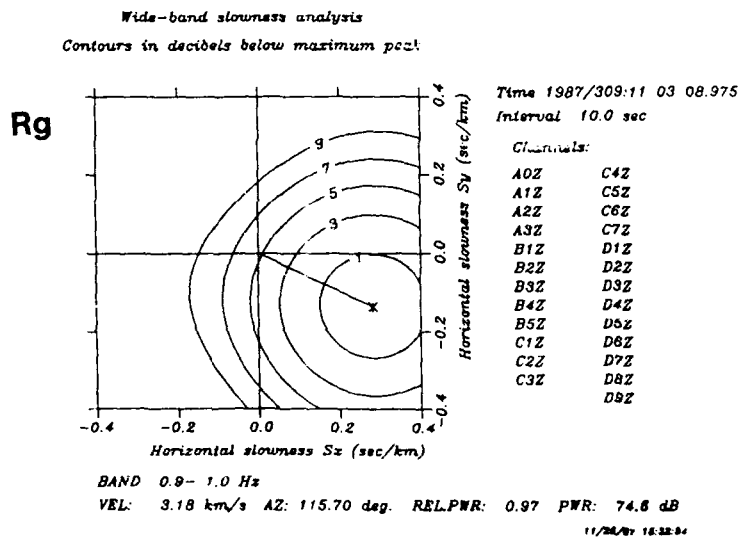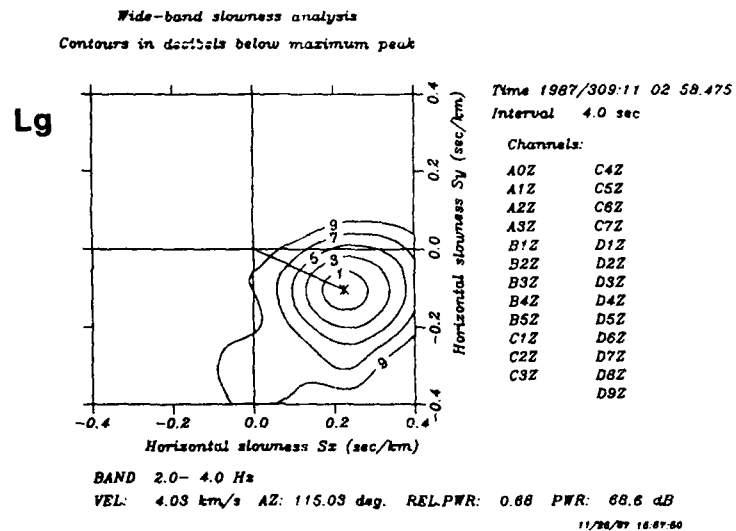VEL:  3.18 km/s  AZ: 115.70 deg.  REL.PWR:  0.97  PWR:  74.6 dB
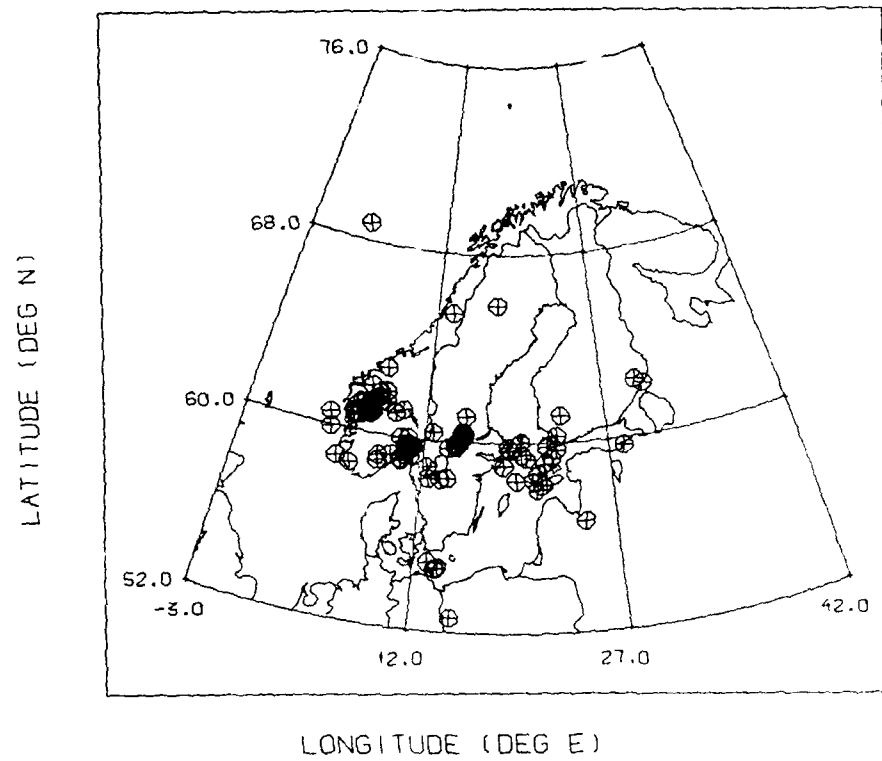
Fig. VII.4.11 Wide-band slowness spectra for the Lg phase (top) and Rg phase (bottom) for the event in Fig. VII.4.9.
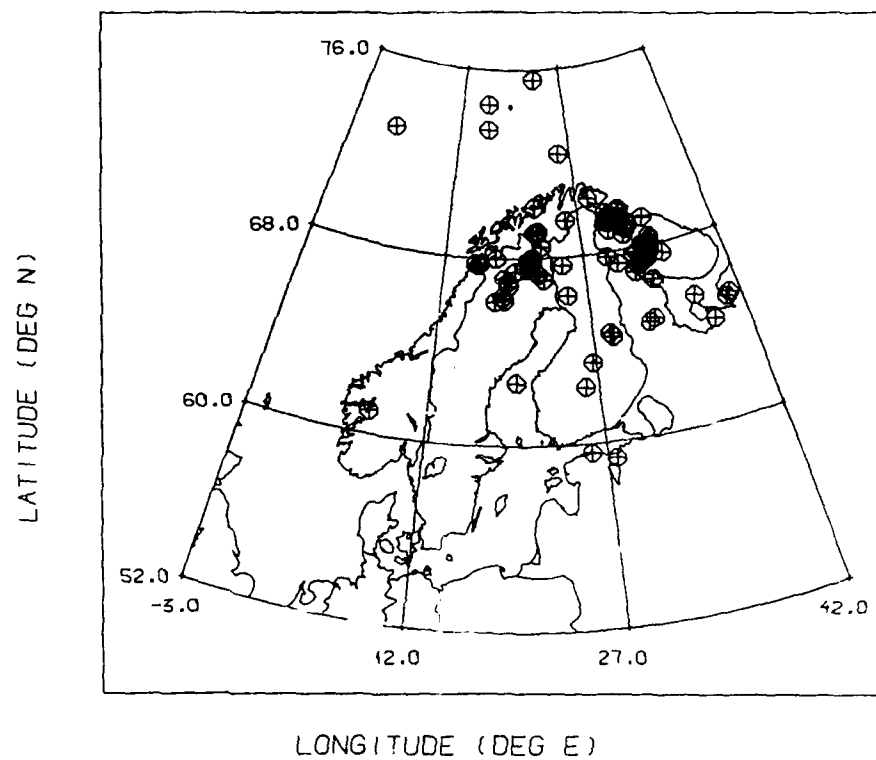
Fig. VII.4.12 Regional events located by the NORESS array during a
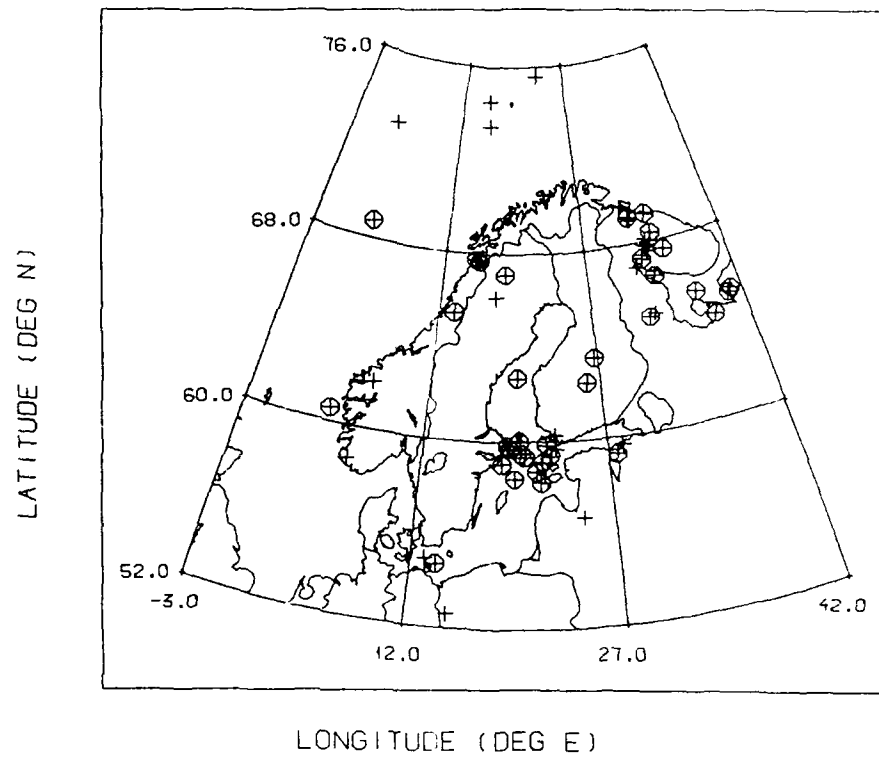two-week test period.

LONGITUDE (DEG E)

87/11/24 14 15 NORSAR

Fig. VII.4.13 Regional events located by the Finnmark array during a
two-week test period.

87/11/25  12.43  NORSAR

Fig. VII.4.14 Regional events of $M_L$ > 2.0 located by at least one of
the two arrays in Norway during a two-week test period.
Events with at least one confirming phase from the other
array are encircled.

## VII.5    Magnitudes of Large Semipalatinsk Explosions using P Coda and Lg Measurements at NORSAR

The objective of this study is to investigate the potential of using NORSAR recordea P coda and Lg waves to obtain stable magnitude estimates of large underground explosions, thereby improving the possibility of obtaining reliable yield estimates from teleseismic recordings.

The NORSAR array (Bungum et al, 1971) has been in operation since 1970. Originally comprising 22 subarrays, with a total of 132 short period vertical seismometers, the array was reduced to 7 subarrays (42 SPZ seismometers) in 1976. In order to obtain consistency over time, this analysis has been restricted to data from these 7 subarrays. With the exception of occasional subarray or instrument outages, this provides for a stable, high quality recording system, making possible reliable comparison of seismic events recorded during the entire time period.

The general characteristics of NORSAR recorded P coda and Lg waves for Semipalatinsk explosions have earlier been studied by Ringdal (1983) and Baumgardt (1985). Ringdal (1983) found by comparing with ISC reported $m_b$ that the use of Lg based magnitudes effectively eliminated the systematic P-wave magnitude differences observed at NORSAR for explosions from the two main test sites within the Semipalatinsk area (Shagan River and Degelen Mountains). Gupta et al (1985) studied NORSAR P and P coda recordings from NTS explosions, and found that P coda measurements provided significantly more precise yields than those based on the initial P. They also obtained promising results in applying P coda measurements to NORSAR recordings from Semipalatinsk explosions.

The propagation path from Semipalatinsk to NORSAR is indicated in Fig. VII.5.1, where also a map of the NORSAR array is shown. In spite of the large epicentral distance (4200 km), the Lg phase can be identified for most explosions of $m_b > 5.0$. However, as shown in the example of Fig. VII.5.2, the Lg amplitude is usually only slightly higher than that of the preceding P coda, and this feature is largely independent of event size.

The data base for this study consists of 72 presumed explosions from the Shagan River area, USSR, covering the time period 1972 to 1987. All such events of ISC $m_b > 5.0$ were included, except for a few cases of NORSAR system outages. The event set is listed in Table VII.5.1, together with ISC or PDE magnitude estimates ($m_b$) as well as parameters estimated in this study. For most of the events, very accurate location estimates have been computed by Marshall et al (1985), and additional such data have been provided by P. Marshall (personal communication). Otherwise, NEIS or NORSAR location estimates are used. In addition, this study has also made use of maximum likelihood $m_b$ magnitudes estimated at Blacknest from ISC data (P. Marshall, personal communication) and $m_b$ (Lg) estimates published by Nuttli (1986).

## Parameter estimation methods

Lg and P coda magnitudes were estimated from NORSAR data for each event using three different methods (for illustration, see Fig. VII.5.2). All three methods were applied to filtered NORSAR SP channels, using a 0.6-3.0 Hz Butterworth bandpass filter. In earlier studies (Ringdal, 1983), this frequency band has been found to retain the main P and Lg energy while suppressing microseismic noise.

The first method pertains to the Lg phase and comprises direct measurement on individual traces of the largest cycle with a period close to 1 Hz, within a group velocity window of 3.25-3.70 km/s. (The

average Lg group velocity is close to 3.5 km/s.) The amplitude (zero
to peak) and the corresponding period were measured and converted to
ground motion $A_{ij}$ (i'th event, j'th channel). The amplitudes were
then corrected for dispersion, geometrical spreading and anelastic
attenuation as described by Nuttli (1986), using parameter values
($Q_0 = 700$, $\xi = 0.4$) derived by Nuttli for the nearby station KON. This
resulted in an Lg magnitude estimate $MLA_{ij}$ for each analyzed trace.

Repeating this process for all center instruments of the 7 operational
NORSAR subarrays (deleting faulty channels) the NORSAR Lg magnitude
MLA was then estimated as:

$$MLA_i = \frac{1}{N} \cdot \sum_{j=1}^{N} MLA_{ij} \qquad (1)$$

where N (N $\leqslant$ 7) is the number of channels.

The second and third methods both comprise automatic RMS measurements
of individual channels and pertain to P coda and Lg magnitudes,
respectively. For the P coda measurement, a time window of 30 seconds
is selected, starting 20 seconds after P onset. The LG window is 2
minutes long, covering the group velocity interval of 3.67 to 3.33
km/s. In addition, a 30 second noise window immediately before P onset
was selected for each processed channel. The estimation procedure
described in the following was applied for each event to all 42
currently operational NORSAR SP channels, except that faulty channels
were deleted.

We denote by $s_{ijk}$ the k'th sample of the filtered trace of event i,
instrument j. We define the log mean square $L_{ij}$ by

$$L_{ij} = \log \left[ \frac{1}{K} \cdot \sum_{k=1}^{K} s^2_{ijk} \right] \tag{2}$$

where K is the number of samples in the selected time window. The quantity $L_i$ is defined as

$$L_i = \frac{1}{M} \cdot \sum_{j=1}^{M} L_{ij} \tag{3}$$

where M($\leq 42$) is the number of operative channels.

We denote $L_i^N$, $L_i^C$ and $L_i^L$ the values of $L_i$ when computed over the noise window (30 seconds, K = 600), P coda window (30 seconds, K = 600) and Lg window (120 seconds, K = 2400), respectively.

The NORSAR P coda RMS magnitudes ($MCR_i$) and Lg RMS magnitudes ($MLR_i$) are then estimated by correcting for noise and adjusting to standard scales as follows:

$$MCR_i = 0.5 \cdot \log\left[\exp(L_i^C) - \exp(L_i^N)\right] + B_C \tag{4}$$

$$MLR_i = 0.5 \cdot \log\left[\exp(L_i^L) - \exp(L_i^N)\right] + B_L \tag{5}$$

The constants $B_C$ and $B_L$ are determined by the constraints:

$$\sum(MCR_i - MBMLE_i) = 0 \qquad\qquad (6)$$

$$\sum(MLR_i - MBLG_i) = 0 \qquad\qquad (7)$$

where $MBLG_i$ is the Lg magnitude given by Nuttli (1986) of the i'th event, $MBMLE_i$ is the maximum likelihood $m_b$ estimate discussed earlier and the sums are taken over all common events.

We also computed uncorrected P coda and Lg magnitudes for purpose of comparison. These were obtained by deleting the noise term in (4) and (5).

## Data analysis

The three estimation methods described above were applied to the events in the data set of Table VII.5.1. The procedure to compensate for background noise level had negligible effect on the RMS P coda magnitudes, since the SNR in these cases was consistently high. However, for some of the smaller events ($m_b$(ISC) < 5.6), the effect on RMS Lg was significant, and the resulting estimates must be considered more uncertain than for the large explosions. This is illustrated in Figs. VII.5.3 and VII.5.4, which show, respectively, the uncorrected and corrected RMS Lg estimates plotted against the NORSAR amplitude based Lg magnitudes.

Table VII.5.2 gives a list of standard deviation of magnitude differences for all combinations of sources. We note that the NORSAR P coda magnitude correlate well with ISC maximum likelihood $m_b$ ($\sigma$ = 0.06), as is also seen from the plot in Fig. VII.5.5. In fact, the

correlation is about as good as between the two ISC-based measurements.

It has earlier been noted by many authors that P coda provides much more stable $m_b$ estimates than the initial P phase, which is subject to strong focussing or defocussing along its ray path. Such effects are to a large extent averaged out in the P coda by various scattering mechanisms. Nevertheless, our analysis has shown that P coda amplitudes across NORSAR are positively correlated with initial P amplitude patterns. Thus, not all of the P focussing/defocussing effects are eliminated, and, by reciprocity, focussing at the source would be expected to significantly affect P coda magnitudes, especially over a larger epicentral area than considered in this paper.

From Table VII.5.2 we also note that the various Lg based measures show surprisingly little correlation with each other, although the RMS noise correction explains much of the scatter between the two Lg estimates based on NORSAR data. Fig. VII.5.6 shows NORSAR RMS Lg versus Nuttli (1986) $m_b$ (Lg) for common events. Even at high magnitudes, where NORSAR noise corrections are insignificant, there is a large scatter. The reasons for this lack of consistency need to be further investigated, but it must be noted that the NORSAR measurements have the advantage of being based on a system stable over time, and with high quality digital recording.

Comparing the Lg based measurements to the ISC maximum likelihood $m_b$, it appears that the NORSAR RMS Lg shows best correlation ($\sigma = 0.092$). Fig. VII.5.7 compares these two magnitude measures, whereas Fig. VII.5.8 shows NORSAR P coda versus NORSAR RMS Lg magnitudes. Comparing these two figures, it is evident that Fig. VII.5.8 has a slightly larger scatter ($\sigma = 0.101$) and, moreover, apparently could be split into two subpopulations with parallel trends.

Figs. VII.5.9 and VII.5.10 show that this is no coincidence. On Fig.
VII.5.9, the NORSAR P coda - RMS Lg magnitude differences are plotted
as a function of event location (Marshall et al (1985) and NEIS data).
The P coda - Lg statistics are clearly region dependent within the
Shagan River area; in particular the northeast part show consistently
low P coda magnitudes, whereas the southwest part shows P coda magni-
tudes consistently higher than those based on Lg. Fig. VII.5.10 shows
that the same trend is apparent when comparing ISC maximum likelihood
$m_b$ to NORSAR RMS Lg magnitudes. It is clear that application of
regional corrections would improve the mutual consistency of these
magnitudes.

Marshall et al (1985) found that explosions in the northeast and
southwest portions of the Shagan River area produce distinctly dif-
ferent P waveforms when recorded at the UK seismological array sta-
tions, suggesting that the Shagan River site can be subdivided into
two test areas characterized by different geophysical properties. Our
results support this suggestion. Our data show an average bias $m_b(P)$ -
$m_b(Lg)$ of $-0.059 \pm 0.014$ for NE Shagan, and $0.112 \pm 0.009$ for SW
Shagan. Thus, if we attempt to explain this anomaly as resulting from
the systematic differences in P recordings only, we obtain a relative
$m_b(P)$ bias of about 0.17 $m_b$ units between the two areas. On the other
hand, the possibility of an $m_b(Lg)$ bias cannot be ruled out either.

Fig. VII.5.11 illustrates the relative occurrence of large Semipala-
tinsk explosions after 1976 as a function of NORSAR RMS Lg magnitudes.
The plot, which has a nominal vertical scaling, has been obtained by
adding Gaussian density functions with standard deviations of 0.015
magnitude units centered at each observed magnitude value. The three
clear peaks on this plot might indicate different yield categories. It
is interesting to note that the highest magnitude group includes
explosions from both the southwest and the northeast areas of Shagan
River, whereas similar plots based on P-wave magnitudes would place
all of the largest events in the southwest area. The rightmost peak of

the diagram (magnitude 6.06) would correspond to a yield between 150 and 200 kilotons TNT if Nuttli's (1986) formulae are used. With the inherent uncertainty in the absolute calibration level, this is clearly not inconsistent with the 150 kiloton upper limit of the Threshold Test Ban Treaty.

In conclusion, NORSAR based P coda and Lg magnitudes appear to provide magnitude estimates of large Semipalatinsk explosions comparable in stability to those of a world-wide network. There are indications that the Lg based measurements avoid some of the bias inherent in P-based magnitudes. It would furthermore be reasonable to expect that such measurements based on network averaging would provide even better stability. In conjunction with calibration data to obtain accurate absolute reference to yield, such data would appear to provide for very reliable monitoring of a threshold treaty.

F. Ringdal
B.K. Hokland

### References

Baumgardt, D.R. (1985): Comparative analysis of teleseismic P coda and Lg waves from underground explosions in Eurasia. Bull. Seism. Soc. Am. 75, 1413-1433.

Gupta, I.N., R.R. Blandford, R.A. Wagner, J.A. Burnetti and T.W. McElfresh (1985): Use of P coda for determination of yield of nuclear explosions. Geophys. J.R. astr. Soc., 83, 2, 541-554.

Marshall, P.D., T.C. Bache and R.C. Lilwall (1985): Body wave magnitudes and locations of Soviet underground explosions at the Semipalatinsk Test Site. AWRE Report No. O 16/84, AWRE, MOD(PE), Aldermaston, Berksh., UK.

Nuttli, O.W. (1986): Lg magnitudes of selected East Kazakhstan under-
   ground explosions. Bull. Seism. Soc. Am. 76, 1241-1251.

Ringdal, F. (1983): Magnitudes from P coda and Lg using NORSAR data,
   in NORSAR Semiannual Technical Summary 1 Oct 82 - 31 Mar 83,
   NORSAR Sci. Rep. No. 2-82/83, NTNF/NORSAR, Kjeller, Norway.

| ORIGIN DATE | ORIGIN TIME | MB | *** LG(AMP) *** MLA | N | STD | *** LG(RMS) *** MLR | N | STD | *** PCODA **** MCR | N | STD |
|---|---|---|---|---|---|---|---|---|---|---|---|
| 11/02/72 | 01.26.57.7 | 6.1 | 6.132 | 7 | 0.040 | 6.121 | 42 | 0.069 | 6.207 | 42 | 0.058 |
| 12/10/72 | 04.27.07.7 | 6.0 | 6.157 | 7 | 0.066 | 6.120 | 42 | 0.068 | 6.013 | 42 | 0.079 |
| 07/23/73 | 01.22.57.8 | 6.1 | 6.185 | 7 | 0.082 | 6.199 | 41 | 0.078 | 6.286 | 41 | 0.060 |
| 12/14/73 | 07.46.57.0 | 5.8 | 5.951 | 7 | 0.087 | 5.876 | 42 | 0.063 | 5.826 | 39 | 0.074 |
| 10/16/74 | 06.32.57.5 | 5.5 | 5.455 | 7 | 0.086 | 5.413 | 42 | 0.062 | 5.596 | 42 | 0.065 |
| 12/27/74 | 05.15.55.8 | 5.6 | 5.849 | 7 | 0.054 | 5.711 | 42 | 0.060 | 5.512 | 42 | 0.093 |
| 04/27/75 | 05.36.57.3 | 5.6 | 5.677 | 7 | 0.060 | 5.550 | 42 | 0.054 | 5.732 | 42 | 0.072 |
| 10/29/75 | 04.46.57.5 | 5.8 | 5.755 | 7 | 0.100 | 5.632 | 42 | 0.062 | 5.733 | 42 | 0.057 |
| 12/25/75 | 05.16.57.0 | 5.7 | 5.817 | 7 | 0.053 | 5.804 | 42 | 0.067 | 0.000 | 0 | 0.000 |
| 04/21/76 | 05.02.57.4 | 5.3 | 0.000 | 0 | 0.000 | 0.000 | 0 | 0.000 | 5.226 | 42 | 0.062 |
| 06/09/76 | 03.02.57.6 | 5.3 | 5.462 | 7 | 0.091 | 5.203 | 42 | 0.056 | 5.126 | 42 | 0.093 |
| 07/04/76 | 02.56.57.7 | 5.8 | 5.831 | 7 | 0.036 | 5.813 | 42 | 0.063 | 5.909 | 42 | 0.075 |
| 08/28/76 | 02.56.57.5 | 5.8 | 5.762 | 7 | 0.085 | 5.737 | 41 | 0.069 | 5.761 | 41 | 0.063 |
| 05/29/77 | 02.56.57.8 | 5.8 | 5.788 | 7 | 0.066 | 5.669 | 39 | 0.061 | 5.796 | 41 | 0.057 |
| 06/29/77 | 03.06.58.0 | 5.3 | 5.274 | 7 | 0.021 | 5.070 | 39 | 0.054 | 5.279 | 40 | 0.072 |
| 09/05/77 | 03.02.57.8 | 5.8 | 5.953 | 7 | 0.075 | 5.891 | 39 | 0.067 | 5.789 | 40 | 0.072 |
| 10/29/77 | 03.07.02.9 | 5.6 | 5.889 | 7 | 0.083 | 5.784 | 39 | 0.061 | 5.768 | 41 | 0.070 |
| 06/11/78 | 02.56.57.7 | 5.9 | 5.824 | 7 | 0.066 | 5.752 | 39 | 0.059 | 5.918 | 39 | 0.072 |
| 07/05/78 | 02.46.57.3 | 5.8 | 5.823 | 7 | 0.086 | 5.789 | 39 | 0.057 | 5.877 | 39 | 0.066 |
| 08/29/78 | 02.37.06.5 | 5.9 | 6.005 | 7 | 0.060 | 6.005 | 39 | 0.057 | 5.914 | 39 | 0.090 |
| 09/15/78 | 02.36.57.3 | 6.0 | 5.948 | 7 | 0.093 | 5.906 | 38 | 0.059 | 5.979 | 41 | 0.077 |
| 11/04/78 | 05.05.57.5 | 5.6 | 5.906 | 7 | 0.039 | 5.691 | 39 | 0.061 | 5.631 | 41 | 0.069 |
| 11/29/78 | 04.33.02.9 | 6.0 | 5.982 | 7 | 0.086 | 5.969 | 39 | 0.067 | 6.004 | 41 | 0.070 |
| 06/23/79 | 02.56.57.6 | 6.2 | 6.088 | 4 | 0.084 | 6.065 | 21 | 0.070 | 6.174 | 23 | 0.057 |
| 07/07/79 | 03.46.57.4 | 5.8 | 5.996 | 7 | 0.091 | 5.967 | 39 | 0.074 | 5.850 | 41 | 0.071 |
| 08/04/79 | 03.56.57.2 | 6.1 | 6.105 | 7 | 0.032 | 6.098 | 39 | 0.062 | 6.170 | 41 | 0.076 |
| 10/28/79 | 03.16.56.9 | 6.0 | 6.060 | 6 | 0.056 | 6.033 | 39 | 0.063 | 5.936 | 41 | 0.085 |
| 12/02/79 | 04.36.57.5 | 6.0 | 5.962 | 5 | 0.046 | 5.903 | 33 | 0.067 | 6.074 | 35 | 0.050 |
| 06/29/80 | 02.32.57.7 | 5.7 | 5.722 | 4 | 0.073 | 5.676 | 29 | 0.094 | 5.721 | 25 | 0.042 |
| 09/14/80 | 02.42.39.3 | 6.2 | 0.000 | 0 | 0.000 | 0.000 | 0 | 0.000 | 6.222 | 36 | 0.049 |
| 10/12/80 | 03.34.14.1 | 5.9 | 5.946 | 6 | 0.043 | 5.912 | 39 | 0.061 | 5.840 | 41 | 0.089 |
| 12/14/80 | 03.47.06.6 | 5.9 | 5.887 | 5 | 0.075 | 5.911 | 39 | 0.045 | 5.965 | 41 | 0.070 |
| 12/27/80 | 04.09.08.2 | 5.9 | 5.948 | 5 | 0.040 | 5.908 | 39 | 0.076 | 5.949 | 41 | 0.069 |
| 03/29/81 | 04.03.50.0 | 5.6 | 5.719 | 5 | 0.052 | 5.521 | 39 | 0.053 | 5.519 | 41 | 0.070 |
| 04/22/81 | 01.17.11.4 | 6.0 | 5.945 | 5 | 0.060 | 5.888 | 33 | 0.046 | 5.991 | 35 | 0.065 |
| 05/27/81 | 03.58.12.1 | 5.5 | 5.576 | 4 | 0.020 | 5.442 | 27 | 0.061 | 5.320 | 29 | 0.098 |
| 09/13/81 | 02.17.18.2 | 6.1 | 6.115 | 6 | 0.081 | 6.092 | 34 | 0.076 | 6.129 | 35 | 0.071 |
| 10/18/81 | 03.57.02.6 | 6.1 | 5.951 | 7 | 0.072 | 5.976 | 39 | 0.057 | 6.069 | 35 | 0.065 |
| 11/29/81 | 03.35.08.7 | 5.7 | 5.789 | 5 | 0.078 | 5.566 | 33 | 0.062 | 5.693 | 35 | 0.071 |
| 12/27/81 | 03.43.14.1 | 6.2 | 6.046 | 6 | 0.040 | 6.056 | 39 | 0.074 | 6.183 | 41 | 0.065 |
| 04/25/82 | 03.23.05.4 | 6.1 | 6.074 | 6 | 0.072 | 6.056 | 39 | 0.077 | 6.111 | 39 | 0.071 |
| 07/04/82 | 01.17.14.4 | 6.1 | 0.000 | 0 | 0.000 | 0.000 | 0 | 0.000 | 6.078 | 32 | 0.089 |
| 08/31/82 | 01.31.00.5 | 5.3 | 0.000 | 0 | 0.000 | 0.000 | 0 | 0.000 | 5.356 | 39 | 0.065 |
| 12/05/82 | 03.37.12.6 | 6.1 | 5.989 | 6 | 0.088 | 5.968 | 37 | 0.078 | 6.076 | 36 | 0.060 |
| 12/26/82 | 03.35.14.1 | 5.7 | 5.834 | 5 | 0.065 | 5.653 | 39 | 0.061 | 5.731 | 29 | 0.061 |
| 06/12/83 | 02.36.43.5 | 6.1 | 6.051 | 5 | 0.077 | 6.070 | 24 | 0.071 | 6.132 | 24 | 0.072 |
| 10/06/83 | 01.47.06.5 | 6.0 | 5.917 | 4 | 0.021 | 5.876 | 18 | 0.054 | 6.034 | 18 | 0.068 |
| 10/26/83 | 01.55.04.8 | 6.1 | 5.996 | 6 | 0.076 | 5.903 | 32 | 0.055 | 6.097 | 32 | 0.065 |
| 11/20/83 | 03.27.04.4 | 5.5 | 0.000 | 0 | 0.000 | 0.000 | 0 | 0.000 | 5.481 | 32 | 0.071 |

Table VII.5.1   List of events used in this study. The table includes
date, origin time, $m_b$(ISC/PDE) as well as NORSAR based
measurements discussed in the text and standard
deviations across NORSAR. Zero entries indicate either
no NORSAR data available or SNR too low for reliable
measurement.

| ORIGIN DATE | ORIGIN TIME | MB | *** LG(AMP) *** | | | *** LG(RMS) *** | | | *** PCODA **** | | |
|---|---|---|---|---|---|---|---|---|---|---|---|
| | | | MLA | N | STD | MLR | N | STD | MCR | N | STD |
| 02/19/84 | 03.57.03.4 | 5.9 | 5.764 | 5 | 0.053 | 5.724 | 27 | 0.051 | 5.889 | 27 | 0.057 |
| 03/07/84 | 02.39.06.4 | 5.7 | 5.775 | 5 | 0.075 | 5.696 | 27 | 0.058 | 5.632 | 27 | 0.073 |
| 03/29/84 | 05.19.08.2 | 5.9 | 5.905 | 5 | 0.035 | 5.897 | 27 | 0.057 | 5.889 | 27 | 0.071 |
| 04/25/84 | 01.09.03.5 | 6.0 | 5.905 | 6 | 0.072 | 5.862 | 33 | 0.066 | 5.972 | 33 | 0.071 |
| 05/26/84 | 03.13.12.4 | 6.0 | 6.075 | 6 | 0.063 | 6.064 | 33 | 0.064 | 5.965 | 33 | 0.115 |
| 07/14/84 | 01.09.10.5 | 6.2 | 6.089 | 6 | 0.073 | 6.043 | 33 | 0.074 | 6.148 | 31 | 0.088 |
| 10/27/84 | 01.50.10.6 | 6.2 | 6.101 | 6 | 0.077 | 6.075 | 32 | 0.067 | 6.254 | 32 | 0.073 |
| 12/02/84 | 03.19.06.3 | 5.8 | 5.973 | 5 | 0.141 | 5.864 | 27 | 0.076 | 5.747 | 25 | 0.081 |
| 12/16/84 | 03.55.02.7 | 6.1 | 6.055 | 5 | 0.093 | 6.030 | 27 | 0.066 | 6.113 | 27 | 0.068 |
| 12/28/84 | 03.50.10.7 | 6.0 | 6.009 | 6 | 0.057 | 5.978 | 33 | 0.073 | 6.147 | 33 | 0.073 |
| 02/10/85 | 03.27.07.6 | 5.9 | 5.898 | 7 | 0.070 | 5.791 | 38 | 0.069 | 5.947 | 39 | 0.068 |
| 04/25/85 | 00.57.06.5 | 5.9 | 5.979 | 5 | 0.078 | 5.850 | 27 | 0.065 | 5.936 | 29 | 0.069 |
| 06/15/85 | 00.57.00.7 | 6.0 | 6.024 | 5 | 0.075 | 5.966 | 28 | 0.062 | 6.099 | 28 | 0.069 |
| 06/30/85 | 02.39.02.7 | 6.0 | 5.983 | 4 | 0.068 | 5.917 | 28 | 0.059 | 6.058 | 28 | 0.065 |
| 07/20/85 | 00.53.14.5 | 5.9 | 5.884 | 7 | 0.076 | 5.855 | 36 | 0.071 | 5.912 | 36 | 0.068 |
| 03/12/87 | 01.57.17.0 | 5.4 | 5.385 | 6 | 0.081 | 5.223 | 31 | 0.059 | 5.437 | 33 | 0.068 |
| 04/03/87 | 01.17.08.0 | 6.2 | 6.062 | 6 | 0.079 | 6.048 | 31 | 0.070 | 6.245 | 32 | 0.052 |
| 04/17/87 | 01.03.04.0 | 6.0 | 5.928 | 6 | 0.072 | 5.895 | 31 | 0.069 | 6.077 | 32 | 0.060 |
| 06/20/87 | 00.53.04.0 | 6.1 | 5.992 | 7 | 0.117 | 5.962 | 34 | 0.070 | 6.124 | 37 | 0.092 |
| 08/02/87 | 00.58.08.0 | 5.9 | 5.945 | 6 | 0.103 | 5.866 | 30 | 0.074 | 5.885 | 30 | 0.074 |
| 11/15/87 | 03.31.08.0 | 6.0 | 6.024 | 7 | 0.088 | 5.959 | 34 | 0.063 | 6.098 | 36 | 0.058 |
| 12/13/87 | 03.21.08.0 | 6.0 | 6.094 | 6 | 0.088 | 6.066 | 29 | 0.080 | 6.081 | 30 | 0.066 |
| 12/27/87 | 03.05.08.0 | 6.0 | 6.109 | 6 | 0.106 | 6.032 | 30 | 0.083 | 6.211 | 30 | 0.052 |

```
AVERAGE STANDARD DEVIATIONS:            0.070              0.064              0.069
STANDARD DEVIATION OF MEAN VALUES:      0.028              0.011              0.012
```

Table VII.5.1   (cont.)

|          | ISC/PDE | ISC(M-L) | MB(LG) | PCODA | LG(RMS) | LG(AMP) |
|----------|---------|----------|--------|-------|---------|---------|
| ISC/PDE  | 0.000   | 0.066    | 0.119  | 0.068 | 0.093   | 0.109   |
| ISC(M-L) | 0.066   | 0.000    | 0.120  | 0.060 | 0.092   | 0.136   |
| MB(LG)   | 0.119   | 0.120    | 0 000  | 0.127 | 0.116   | 0.135   |
| PCODA    | 0.068   | 0.060    | 0.127  | 0.000 | 0.101   | 0.130   |
| LG(RMS)  | 0.093   | 0.092    | 0.116  | 0.101 | 0.000   | 0.065   |
| LG(AMP)  | 0.109   | 0.136    | 0.135  | 0.130 | 0.065   | 0.000   |

Table VII.5.2   Standard deviations of differences between various
magnitude estimates discussed in the text.
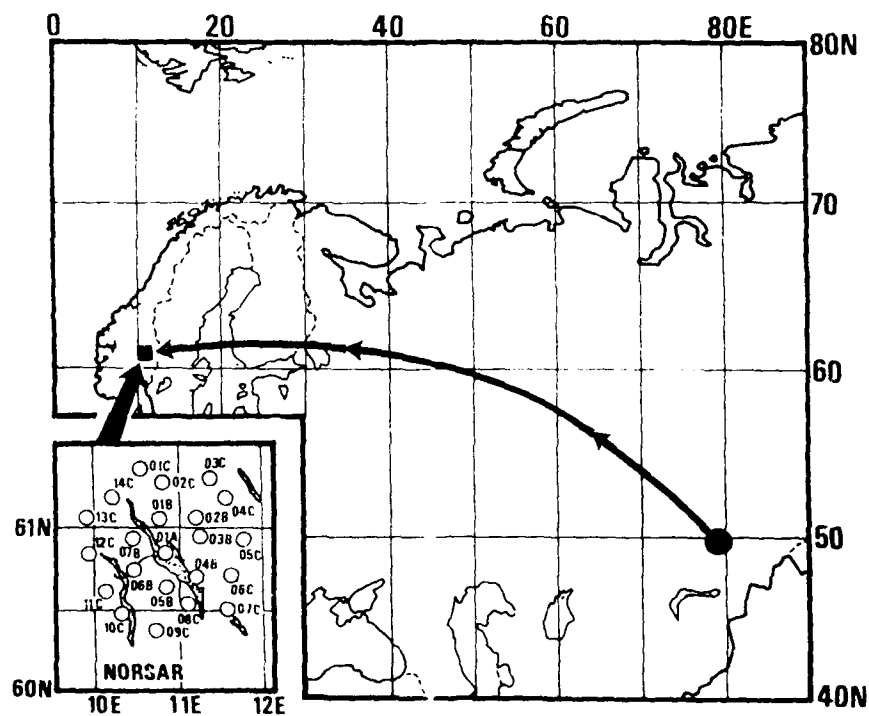
Fig. VII.5.1  Map showing the propagation path from Semipalatinsk to
NORSAR (distance approximately 4200 km). The original
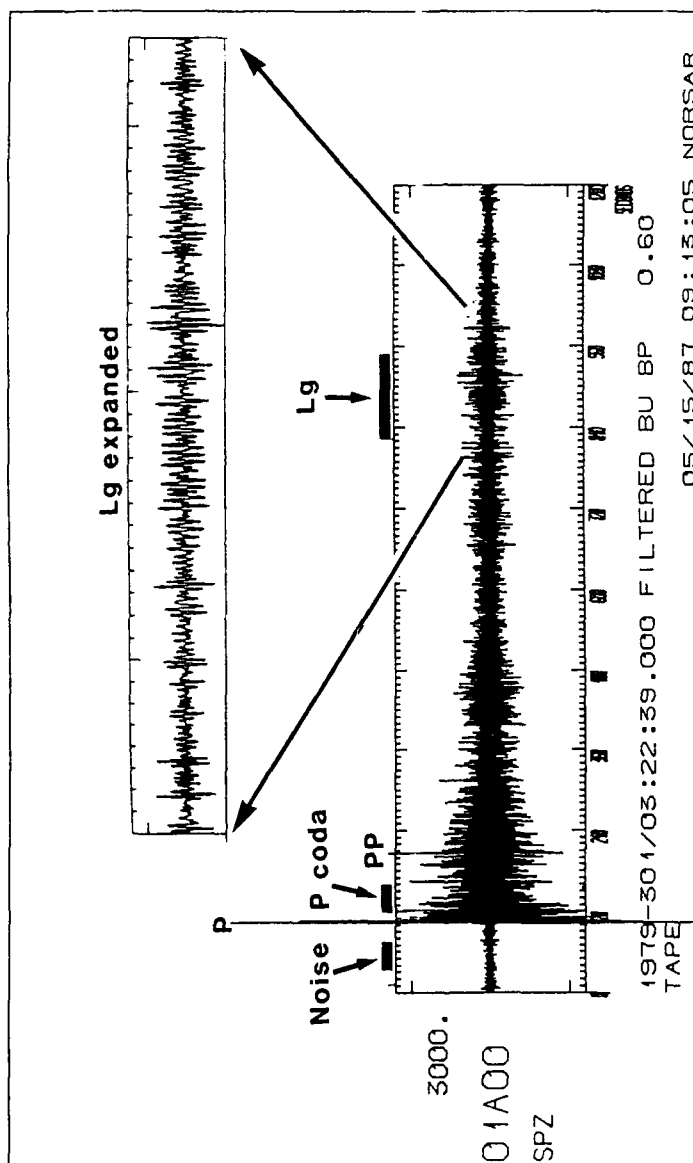NORSAR array configuration is also displayed.

Fig. VII.5.2  Example of a typical NORSAR-recording of a Semipalatinsk explosion (instrument 01A00). The plot covers 20 minutes of data filtered in the passband 0.6-3.0 Hz. The time windows used for RMS Lg, RMS P coda and RMS noise measurements as described in the text are indicated. An expanded plot is shown of the portion of the trace used for NORSAR Lg amplitude.
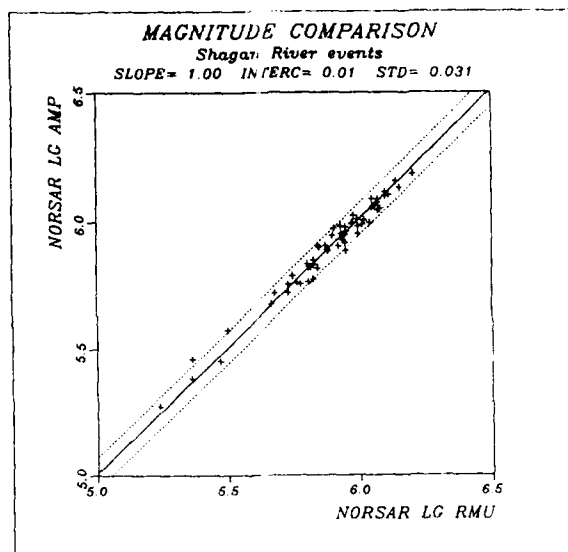
Fig. VII.5.3  Plot of amplitude based NORSAR Lg magnitudes versus
NORSAR RMS Lg magnitudes. In this plot no noise correc-
tion has been applied. The slope has been restricted to
1.00, and the dotted lines correspond to plus/minus two
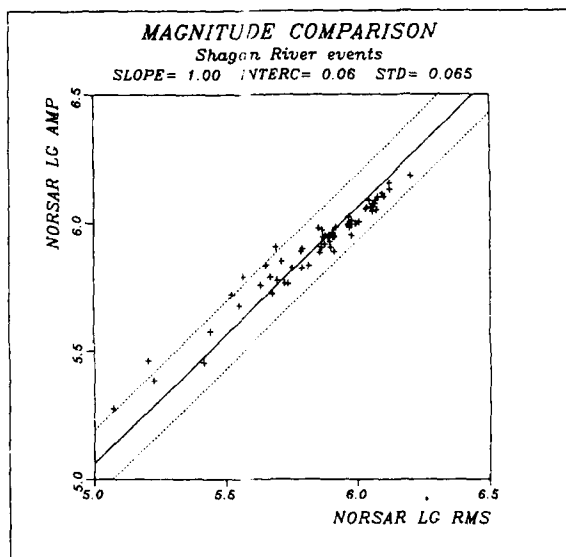standard deviations.



Fig. VII.5.4  Same as Fig. VII.5.3, except that the NORSAR RMS Lg
magnitudes have been corrected for noise as discussed
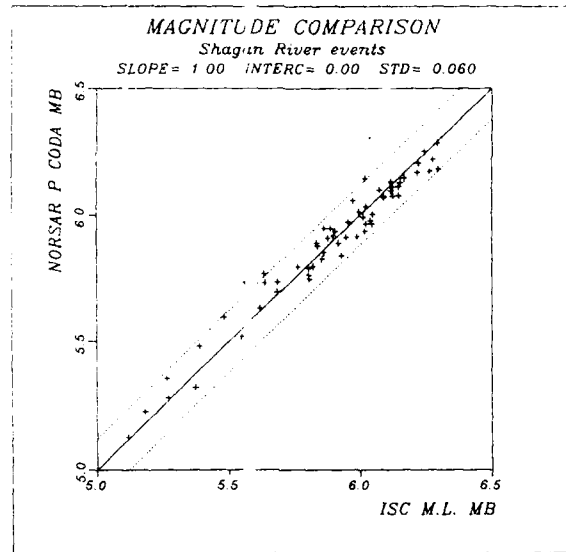in the text. Note the effect of this at low magnitudes.

**Fig. VII.5.5** Plot of NORSAR P coda magnitudes versus ISC maximum likelihood $m_b$. (Slope restricted to 1.00; dotted lines correspond to plus/minus two standard deviations.)
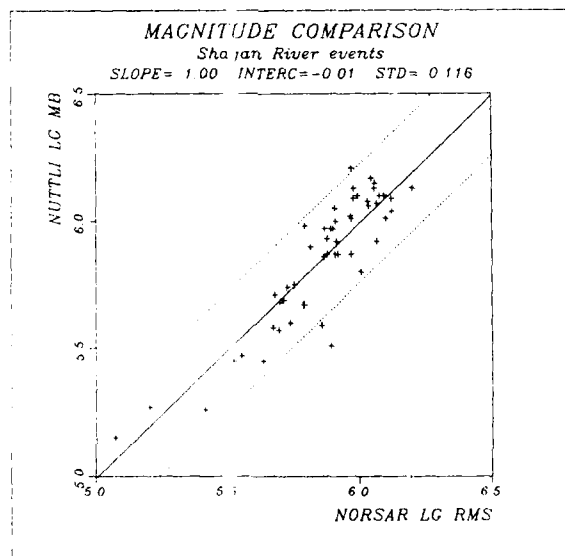


**Fig. VII.5.6** Plot of Nuttli (198 ) $m_b$ (Lg) versus NORSAR Lg RMS magnitudes. The slo e and dotted lines are defined as in Fig. VII.5.5. No e the significant scatter even at high magnitudes.
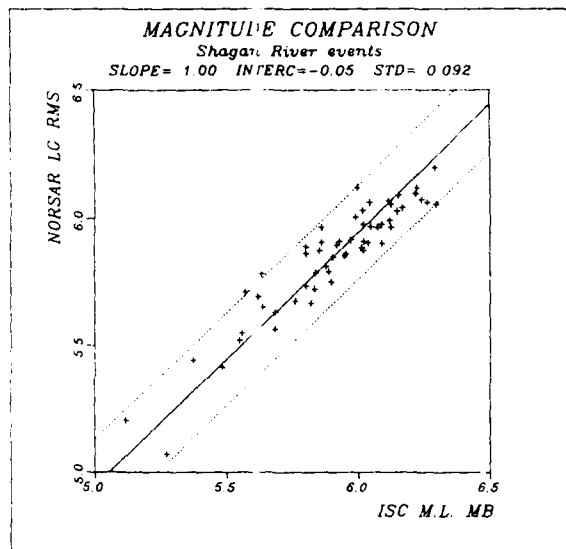
**MAGNITUDE COMPARISON**
Shagan River events
SLOPE= 1.00  INTERC=-0.05  STD= 0.092

Fig. VII.5.7  Plot of ISC maximum likelihood $m_b$ versus NORSAR Lg RMS magnitudes. The slope and dotted lines are defined as in Fig. VII.5.5.



**MAGNITUDE COMPARISON**
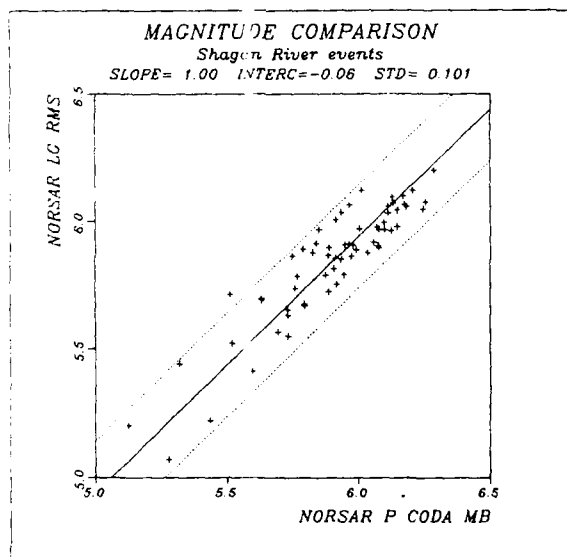Shagan River events
SLOPE= 1.00  INTERC=-0.06  STD= 0.101

Fig. VII.5.8  Plot of NORSAR RMS P coda $m_b$ versus NORSAR RMS Lg magnitudes. The slope and dotted lines are defined as in Fig. VII.5.5.
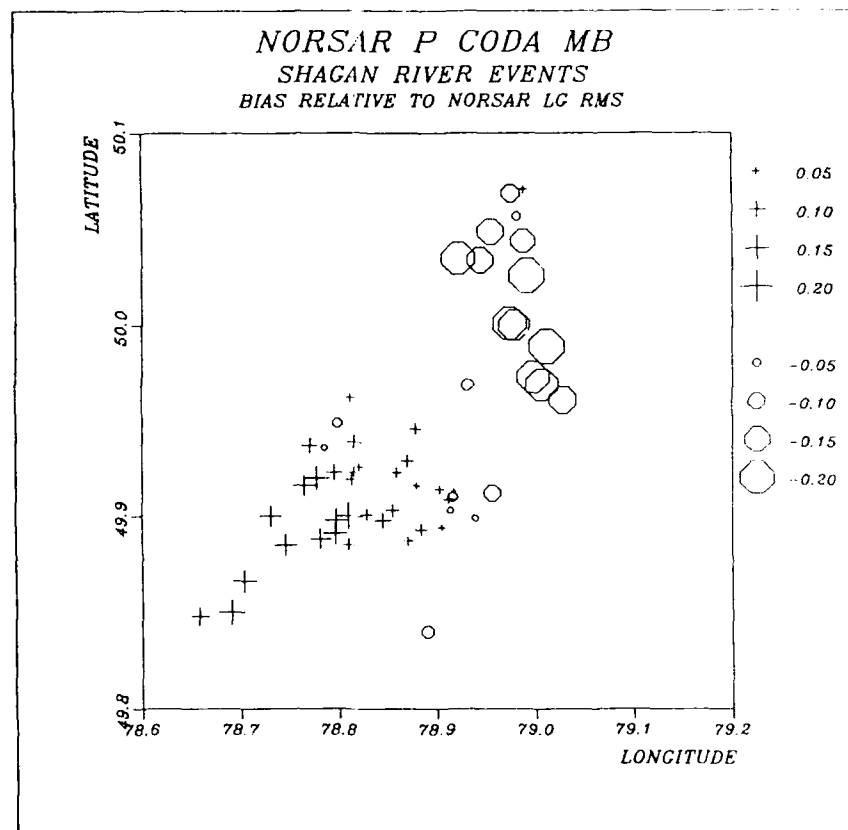
Fig. VII.5.9   Plot of magnitude residuals (NORSAR P coda minus NORSAR
Lg RMS magnitudes) as a function of event location for
events of $m_b \geq 5.60$. Plusses and circles correspond to
residuals greater or less than the average, respec-
tively, with symbol size proportional to the deviation.
Location estimates are those of Marshall et al (1985)
where available, otherwise NEIS estimates have been
used. Note the systematic variation within the Shagan
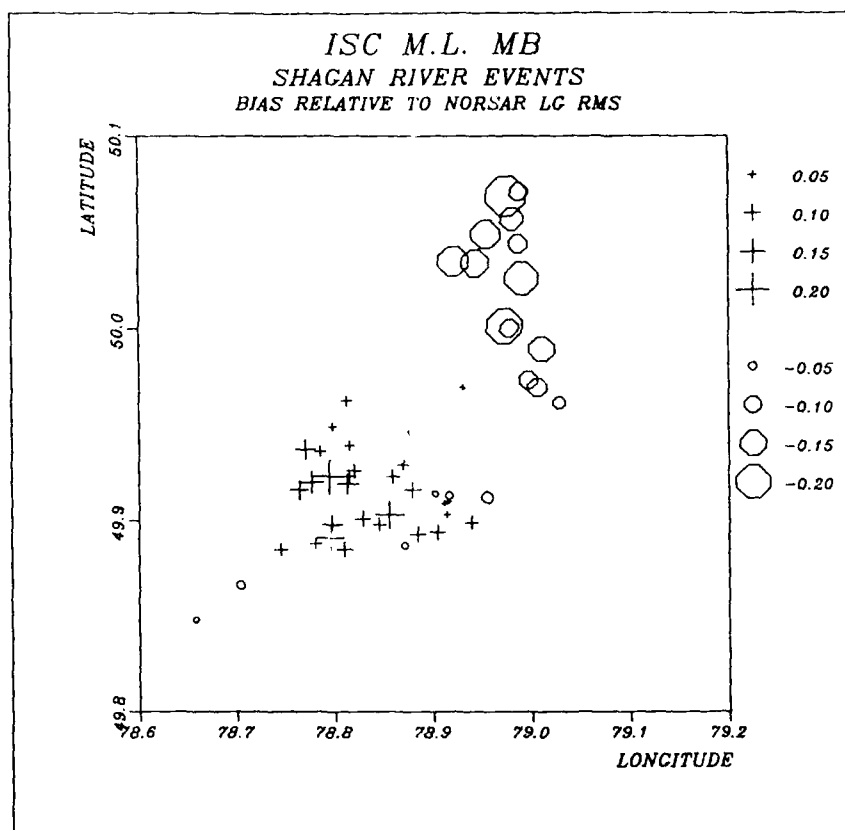River area.

Fig. VII.5.10 Same as Fig. VII.5.9, except that the residual
corresponds to ISC maximum likelihood $m_b$ minus NORSAR
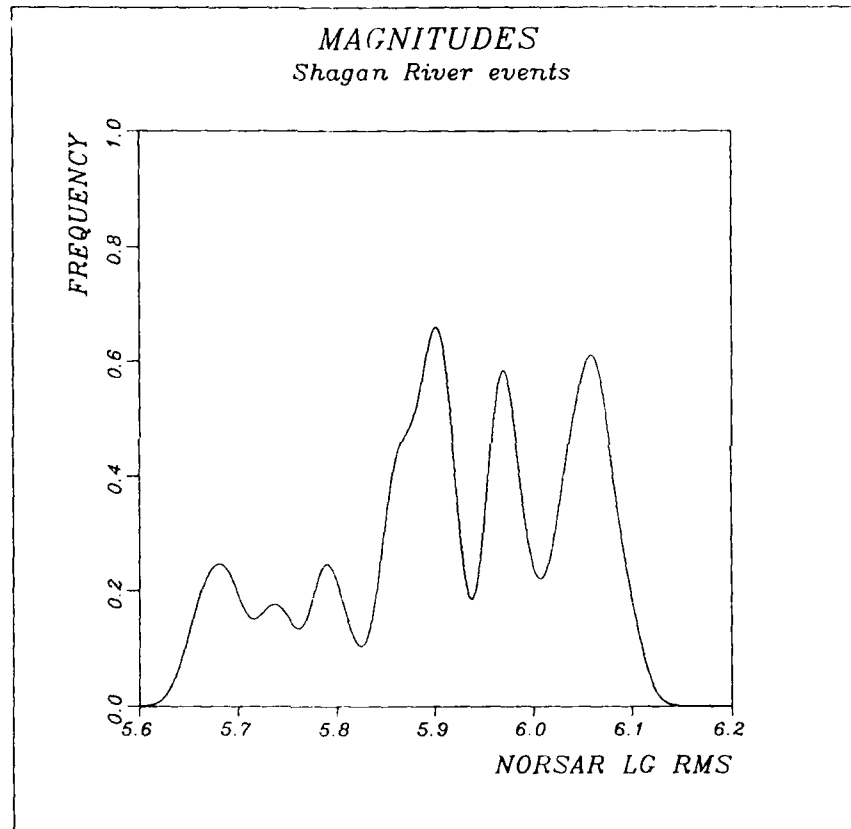Lg RMS magnitudes. Note the similarities with Fig.
VII.5.9.

Fig. VII.5.11 Relative frequency of occurrence of large Shagan River
explosions after 1976, based on estimated NORSAR Lg RMS
magnitudes. The figure has been generated by adding
Gaussian probability density functions with standard
deviations of 0.015 centered at each magnitude value.
Note the three distinct peaks in the diagram.

VII.6    Towards an optimum beam deployment for NORESS;
         experiments with a North Sea / western Norway data base

Several of our previous investigations have addressed the problem of
determining the number and type of beams needed for adequate detection
of signals recorded on NORESS. For example, Kværna and Mykkeltveit
(1986) arrived at a recommendation for an optimum beam deployment for
detection of regional and teleseismic P-waves.

As described in several papers, e.g., Mykkeltveit and Bungum (1984),
automatic determinations of event epicenters using our on-line pro-
cessing package requires detection and identification of both P- and
S-arrivals from each event. This study utilizes data from a fairly
extensive data base of regional events recorded at NORESS, and we
attempt to determine an optimum beam deployment with respect to detec-
tion of all phases from these events.

**Data base and detection processing**

The data base comprises 101 events from the North Sea / western Norway
region with locations as shown in Fig. VII.6.1. These events were
located  by the western Norway network and/or the network operated by
the British Geological Survey. The epicentral distance range from
NORESS is 250 - 1100 km, and the magnitudes are between 1.6 and 4.2.

This event data base comprises well located events for which it is
possible  to accurately define the types of observed phases and to
read their onsets manually, as illustrated in Fig. VII.6.2.

All events were subjected to detection processing by a large beam set
using a new program system developed at NORSAR (Fyen, 1987).  Distri-
buted among 12 different filter bands, this beam set contained 72

steered beams for detection of P-waves, 132 beams for detection of S-waves, 12 incoherent beams made from the vertical channels and 12 incoherent beams made from the horizontal channels. In selecting this beam set we attempted to include all candidates that could conceivably contribute to increasing the detection capability. A description of this beam set is given in section VII.3 of this report (Kværna et al, 1987).

The output from the detection analysis is a report containing parameters such as an identification of the detecting beam, detection time, STA, LTA and STA/LTA (SNR). For all events, the detection reports were divided into Pn, Pg, Sn and Lg detections. Table VII.6.1 shows an example of a report where the different detections are identified.

The essence of the following is a strategy for determination of a beam set that meets certain performance criteria and at the same time contains the lowest possible number of beams, selected from the set of 228 beams described above.

## Analysis procedure

In the work presented in section VII.3 of this report (Kværna et al, 1987), we attempted to infer the STA/LTA (SNR) detection thresholds of the respective beams from noise statistics. For each phase detected in the present investigation, these thresholds were used to create a basis for comparison between the different beams. The procedure for comparing the maximum SNR values can be illustrated by the following example:

i)    Assume that a Pn phase is detected by three different beams,

by beam A, with a maximum SNR of 26.0 dB,

by beam B, with a maximum SNR of 23.5 dB and

by beam C, with a maximum SNR of 22.0 dB.

ii)   Assume that the detection thresholds inferred from noise statistics
are,

for beam A, 12.0 dB

for beam B, 10.0 dB and

for beam C,  6.0 dB

iii)  If we take the detection thresholds to represent
a common basis for comparison, a unified quality measure
of the maximum SNR values will be the number of decibels
exceeding these thresholds.  These quality measures, from now
on referred to as 'the adjusted SNR values', will for the
three beams in this example be:

Adjusted SNR value for beam A:  (26.0 - 12.0) dB = 14.0 dB.

Adjusted SNR value for beam B:  (23.5 - 10.0) dB = 13.5 dB.

Adjusted SNR value for beam C:  (22.0 -  6.0) dB = 16.0 dB.

From this we conclude that beam C is the 'best' beam for detecting
this particular Pn phase.

Rather than progressing in our investigation with the concept of a
'best' beam, we introduce the concept of a 'valid' beam  or 'valid'
detection: The maximum obtainable SNR value of a detection will be
reduced by phenomena like mis-steering of the coherent beams, random
increase in the noise level and lowered data quality on single chan-
nels.  We therefore decided that all detections with adjusted SNR

values within 3 decibels of the best adjusted SNR for the phase, were
to be counted as 'valid' detections. This implies that each detected
phase will have several possible candidates for the 'best' beam.

The 3 decibels acceptance level is chosen rather subjectively,
however, the coherent beam deployment is sufficently dense that signal
losses due to mis-steering are within 3 decibels. In later analyses,
this acceptance level can of course be reduced or increased.

Table VII.6.2 shows the maximum SNR values and corresponding adjusted
SNR values for one of the Pn-phases in this investigation, for all 48
beam types.

### Results

After finding the 'valid' detections for all phases in the data
base of 101 events, we were in a position to evaluate which beams
should be included in the optimum deployment. Tables VII.6.(3a-3d)
show the 'valid' detections for all Pn, Pg, Sn and Lg-phases,
respectively.

When considering the Pn phase in Table VII.6.3a, we found that beam
number 10 had the maximum number of 'valid' entries, 60 out of a total
number of 98. From this we concluded that this beam should obviously
be included in the final beam deployment. An interesting observation
was that many of the Pn phases from the North Sea / western Norway
region had dominant signal frequencies above 10 Hz.

Beam number 6 had the highest number of 'valid' detections for the Pg
phase, see Table VII.6.3b. For the Sn phase, (Table VII.6.3c), beam
number 45 or 46 was an obvious candidate. Beam number 46 had 66 'va-
lid' entries, which is about 80% of the total number of Sn detections.

Like the Pn phase, the Sn phases from this region contain much energy at high frequencies.

For the Lg phase (Table VII.6.3d) no specific beam is an obvious candidate for inclusion in the recommended beam deployment. Beam 42, however, exhibits the highest number of 'valid' entries.

In order to find the optimum beam deployment, we attempted to group the beams together in various ways. We required that all (or almost all) detected phases should be represented by at least one 'valid' beam in the final deployment. First, we attempted to do the grouping for each phase type individually.

For the Pn-phase, the number of 'valid' entries for the various beams are given in the last column of Table VII.6.3a. We first select the beam with the highest number of 'valid' entries, in this case beam number 10, and that beam handles 60 of the detected Pn-phases. Next, beam number 6 accommodates 22 of the remaining 38 beams, and so on. By iteration, we ended up with a priority list of beams as given in Table VII.6.4a.

From this we can infer that 8 beams are required to cover all Pn phases, but 5 beams alone cover 96% of the 'valid' entries. Note that, e.g., beam 10 (10.0 - 16.0 P) includes eight coherent beams with different steering delays. The actual azimuth range for this data base is 180-360 degrees, so it is sufficient to distribute about 4 coherent P-beams in each filter band to span this area. If we in addition accept that it is sufficient to cover 96% of the valid detections, the optimum beam deployment for detecting Pn-phases from this specific region will contain 16 coherent P-beams and one incoherent beam made from the vertical channels. If we require the coherent beam deployment to span all azimuth directions (symmetrically), about 32 coherent P-beams must be included.

The beam priority lists for the Pg, Sn and Lg phases are given
in Tables VII.6.4b-d, respectively.

An interesting observation is the large number of beams required
to cover the Pg detections. From Tables VII.6.4a-d we can infer the
beam deployment required for optimum detection under the given
requirements, when treating the phases individually; see Table
VII.6.5.

When recommending specific beam deployments, it is important to
keep in mind the implications on computational load for the
on-line processor. This load is primarily determined by the
total number of traces that must be bandpass filtered, and the
number of beams that are created.

For processing the data with the deployment of Table VII.6.5,
178 single channels must be filtered, and 55 beams must be formed,
each of which is subjected to STA/LTA-type detection processing.

These numbers can be considerably reduced if we apply an algorithm
where all phases are treated at the same time. We first include
the most obvious beam candidates (beams no. 46, no. 10, no. 42 and
no. 6), and then start the interative sorting procedure. The results
from this procedure are given in Table VII.6.6. Compared to the num-
bers in Table VII.6.5, the size of the beam deployment is reduced
by 30-40%.

As a final experiment, we decided to exclude the coherent S-beams
from the analysis. The results are given in Table VII.6.7.
Compared to the results given in Table VII.6.6, the number of beams to
be formed were marginally reduced, but the number of traces to be
filtered were increased due to including more incoherent beams made
from the vertical channels.

## Conclusion

For detection of Pn-phases from the North Sea / western Norway region,
the high frequency coherent P-beams will contribute significantly to
an optimized beam deployment. For the more low frequency Pg phase,
the coherent P-beam filtered between 3.5 and 5.5 Hz seem to do best.

Including incoherent beams made from the horizontal channels, will
improve the detectability of Sn significantly. We also found that the
Sn phase in most cases had dominant frequencies around 10 Hz.

Like Pg, the Lg phase had maximum SNR in the range 1.5-4.5 Hz. Inco-
herent beams made from both the horizontal and vertical channels must
be included for optimum detection of the Lg phase.

A tool for determining the optimum beam deployment has been developed.
To validate the method and find a beam deployment that adequately
covers also other relevant regions, we plan to perform similar studies
for events from other areas, like the western USSR.

In our future work, then, we want to test whether the symmetric beam
deployment inferred from the North Sea/western Norway data base is
sufficient for optimum detection of events from other regions, or
if other beam types have to be added to the beam deployment.

T. Kværna
S. Kibsgaard
S. Mykkeltveit
F. Ringdal

References

Fyen, J. (1987): Improvements and modifications.
    Semiannual Technical Summary, 1 October - 31 March 1987,
    NORSAR Sci. Rep. No. 2-86/87, Kjeller, Norway.

Kværna, T. and S. Mykkeltveit (1986):  Optimum beam deployment for
    NORESS P-wave detection.  Semiannual Technical Summary, 1 April -
    30 September 1986, NORSAR Sci. Rep. No. 1-86/87, Kjeller, Norway.

Kværna, T., S. Kibsgaard and F. Ringdal (1987): False alarm
    statistics and threshold determination for regional event detection,
    Semiannual Technical Summary, 1 April - 30 September 1987,
    NORSAR Sci. Rep. No. 1-87/88, Kjeller, Norway.

Mykkeltveit, S. and H. Bungum (1984):  Processing of regional
    events using data from small-aperture arrays, Bull. Seism. Soc.
    Am. 74, 2313-2333.

Manually read arrival times:

Pn: 14.11.56.4  Pg: 14.12.05.5  Sn: 14:12.39.0  Lg: 14.12.51.1

Detection results for steered P-beams.

Time interval subjected to detection processing:

017:14.09.46.0 - 14.13.46.0

| Beam | Detection interval | STA | LTA | SNR | #detections |
|------|-------------------|-----|-----|-----|-------------|
| ***> Pn | | | | | |
| I0906 | 017:14.11.56.6 - 12.03.9 | 827.01 | 18.52 | 44.661 | 1 |
| H0807 | 017:14.11.56.9 - 12.06.4 | 647.98 | 12.91 | 50.173 | 4 |
| J1006 | 017:14.11.56.9 - 12.04.9 | 543.86 | 11.58 | 46.969 | 9 |
| E0505 | 017:14.11.57.1 - 12.03.4 | 318.56 | 26.33 | 12.099 | 2 |
| F0607 | 017:14.11.57.1 - 12.03.4 | 454.06 | 26.09 | 17.406 | 5 |
| G0707 | 017:14.11.57.1 - 12.03.6 | 793.77 | 30.41 | 26.106 | 5 |
| D0408 | 017:14.11.57.4 - 12.03.4 | 263.52 | 23.11 | 11.403 | 9 |
| C0308 | 017:14.11.57.6 - 12.03.1 | 279.83 | 30.10 | 9.297 | 13 |
| B0201 | 017:14.11.58.4 - 11.58.9 | 112.92 | 27.44 | 4.116 | 1 |
| ***> Pg | | | | | |
| H0803 | 017:14.12.05.4 - 12.11.9 | 234.43 | 41.59 | 5.637 | 16 |
| F0607 | 017:14.12.06.1 - 12.10.6 | 812.29 | 90.77 | 8.949 | 8 |
| E0505 | 017:14.12.06.1 - 12.09.1 | 520.37 | 76.49 | 6.803 | 15 |
| G0707 | 017:14.12.06.6 - 12.12.9 | 749.01 | 132.91 | 5.635 | 4 |
| J1002 | 017:14.12.07.6 - 12.08.1 | 128.03 | 30.39 | 4.213 | 8 |
| D0408 | 017:14.12.08.1 - 12.08.9 | 345.48 | 74.75 | 4.622 | 11 |
| F0602 | 017:14.12.13.6 - 12.13.9 | 138.17 | 34.16 | 4.045 | 1 |
| ***> Sn | | | | | |
| H0805 | 017:14.12.40.1 - 12.42.1 | 318.42 | 77.59 | 4.104 | 2 |
| D0402 | 017:14.12.40.4 - 12.40.9 | 231.42 | 55.96 | 4.136 | 2 |
| G0702 | 017:14.12.40.4 - 12.41.4 | 516.81 | 98.40 | 5.252 | 3 |
| C0302 | 017:14.12.40.4 - 12.40.9 | 253.58 | 57.01 | 4.448 | 2 |
| ***> Lg | | | | | |
| F0603 | 017:14.12.51.9 - 12.54.1 | 735.74 | 103.15 | 7.065 | 1 |
| E0502 | 017:14.12.52.1 - 12.54.1 | 662.00 | 78.63 | 8.419 | 12 |
| D0405 | 017:14.12.52.6 - 12.54.4 | 464.31 | 83.58 | 5.555 | 2 |
| C0302 | 017:14.12.53.1 - 12.59.6 | 449.74 | 78.16 | 5.754 | 3 |
| H0806 | 017:14.12.53.4 - 12.53.9 | 474.39 | 112.32 | 4.223 | 1 |
| F0602 | 017:14.12.55.9 - 12.56.6 | 538.07 | 95.86 | 5.613 | 2 |
| B0201 | 017:14.12.57.4 - 12.57.6 | 305.59 | 73.26 | 4.171 | 2 |
| D0402 | 017:14.12.58.1 - 12.58.6 | 497.49 | 116.50 | 4.270 | 1 |

Table VII.6.1 The detection report shown in this table is the output
from detection analysis of the event displayed in Fig.
VII.6.2. We have here only given the results from pro-
cessing the 3-minute time interval containing the Pn,
Pg, Sn and Lg phases, with the 72 coherent beams with P-
wave velocities.  The beam types are identified from the
first character of the beam name.  The last two digits
of the beam name identify the coherent beam with maximum
SNR within that beam type.  In the experiment outlined
in this paper, we give results for each coherent beam
type rather than for individual coherent beams. The last
column of the detection report gives the number  of
detections for the beam type within the detection
interval, i.e., the time interval for which the  SNR
values exceed the threshold.

Distance: 400.9 km.
Azimuth : 229.0 degrees
ML      :   2.7

| Beam no. | Beam type | SNR in dB | | Adjusted SNR in dB |
|---|---|---|---|---|
| 1 | 1.0 − 3.0 P | 0.00 | / | 0.00 |
| 2 | 1.5 − 3.5 P | 12.30 | / | 1.29 |
| 3 | 2.0 − 4.0 P: | 19.37 | / | 6.67 |
| 4 | 2.5 − 4.5 P: | 21.14 | / | 8.74 |
| 5 | 3.0 − 5.0 P: | 21.66 | / | 10.25 |
| 6 | 3.5 − 5.5 P: | 24.82 | / | 13.91 |
| 7 | 5.0 − 7.0 P: | 28.34 | / | 16.63 |
| 8 | 6.5 − 8.5 P: | 34.01 | / * | 22.51 |
| 9 | 8.0 − 16.0 P: | 33.00 | / * | 24.60 |
| 10 | 10.0 − 16.0 P: | 33.44 | / * | 24.94 |
| 11 | 1.0 − 2.0 P: | 0.00 | / | 0.00 |
| 12 | 2.0 − 3.0 P: | 0.00 | / | 0.00 |
| 13 | 1.0 − 3.0 S: | 0.00 | / | 0.00 |
| 14 | 1.5 − 3.5 S: | 0.00 | / | 0.00 |
| 15 | 2.0 − 4.0 S: | 0.00 | / | 0.00 |
| 16 | 2.5 − 4.5 S: | 0.00 | / | 0.00 |
| 17 | 3.0 − 5.0 S: | 15.56 | / | 3.26 |
| 18 | 3.5 − 5.5 S: | 19.41 | / | 7.41 |
| 19 | 5.0 − 7.0 S: | 20.82 | / | 8.12 |
| 20 | 6.5 − 8.5 S: | 26.52 | / | 14.72 |
| 21 | 8.0 − 16.0 S: | 28.17 | / | 19.17 |
| 22 | 10.0 − 16.0 S: | 31.88 | / * | 22.88 |
| 23 | 1.0 − 2.0 S: | 0.00 | / | 0.00 |
| 24 | 2.0 − 3.0 S: | 0.00 | / | 0.00 |
| 25 | 1.0 − 3.0 V: | 0.00 | / | 0.00 |
| 26 | 1.5 − 3.5 V: | 7.24 | / | 0.64 |
| 27 | 2.0 − 4.0 V: | 0.00 | / | 0.00 |
| 28 | 2.5 − 4.5 V: | 0.00 | / | 0.00 |
| 29 | 3.0 − 5.0 V: | 11.43 | / | 4.22 |
| 30 | 3.5 − 5.5 V: | 14.12 | / | 7.32 |
| 31 | 5.0 − 7.0 V: | 18.69 | / | 13.99 |
| 32 | 6.5 − 8.5 V: | 23.17 | / | 18.67 |
| 33 | 8.0 − 16.0 V: | 26.63 | / * | 22.63 |
| 34 | 10.0 − 16.0 V: | 27.94 | / * | 23.94 |
| 35 | 1.0 − 2.0 V: | 0.00 | / | 0.00 |
| 36 | 2.0 − 3.0 V: | 7.60 | / | 0.00 |
| 37 | 1.0 − 3.0 H: | 0.00 | / | 0.00 |
| 38 | 1.5 − 3.5 H: | 0.00 | / | 0.00 |
| 39 | 2.0 − 4.0 H: | 0.00 | / | 0.00 |
| 40 | 2.5 − 4.5 H: | 0.00 | / | 0.00 |
| 41 | 3.0 − 5.0 H: | 0.00 | / | 0.00 |
| 42 | 3.5 − 5.5 H: | 17.13 | / | 11.84 |
| 43 | 5.0 − 7.0 H: | 15.46 | / | 10.36 |
| 44 | 6.5 − 8.5 H: | 19.34 | / | 14.54 |
| 45 | 8.0 − 16.0 H: | 20.00 | / | 16.30 |
| 46 | 10.0 − 16.0 H: | 20.82 | / | 17.12 |
| 47 | 1.0 − 2.0 H: | 0.00 | / | 0.00 |
| 48 | 2.0 − 3.0 H: | 0.00 | / | 0.00 |

Table VII.6.2 This table gives the maximum SNR values and the corresponding adjusted SNR values for the Pn phase shown in Fig. VII.6.2. The beam types with the characters 'P' or 'S' are coherent beams with P- or S-wave velocities. The character 'V' indicates incoherent beams made from the vertical channels, whereas 'H' indicates incoherent beams made from the horizontal channels. The beam types with a star ( * ) in the column for adjusted SNR are 'valid' beams, i.e., within 3 decibels of the beam type of highest SNR. Beam types with the value 0.0 have not detected the phase.
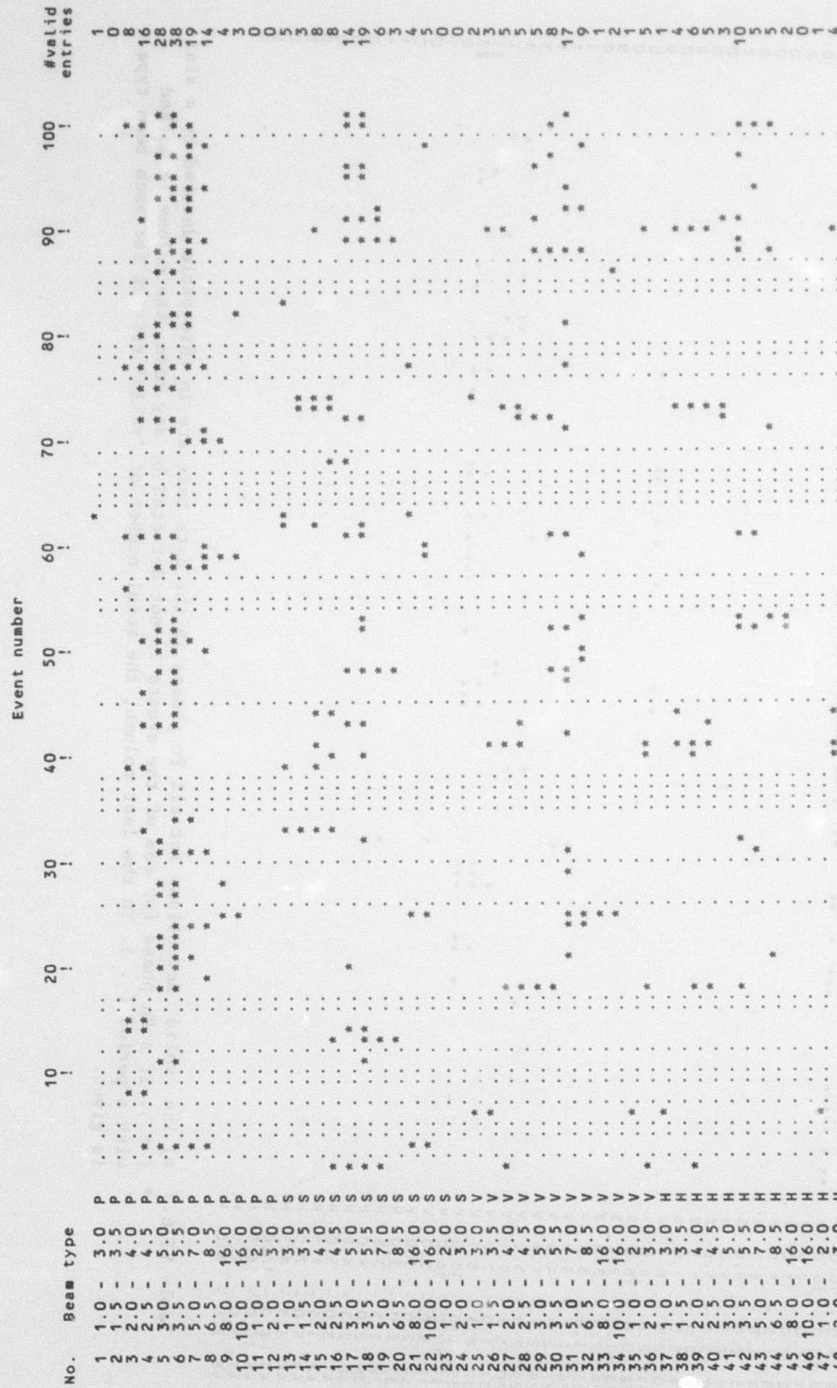
Event number

No. Beam type

#valid entries

Table VII6.3   a) The 'valid' detections for all Pn phases in the data base are in this table denoted by a star ( * ). If a Pn phase for one of the events is not detected by any beam, the coloum is marked with a period ( . ). In the last column, the total number of 'valid' entries for each beam type is given.

Event number

#valid
entries

Table VII.6.3  b) This table shows the 'valid' detections for all Pg phases in the data base.

#valid
entries

Event number

No.   Beam type
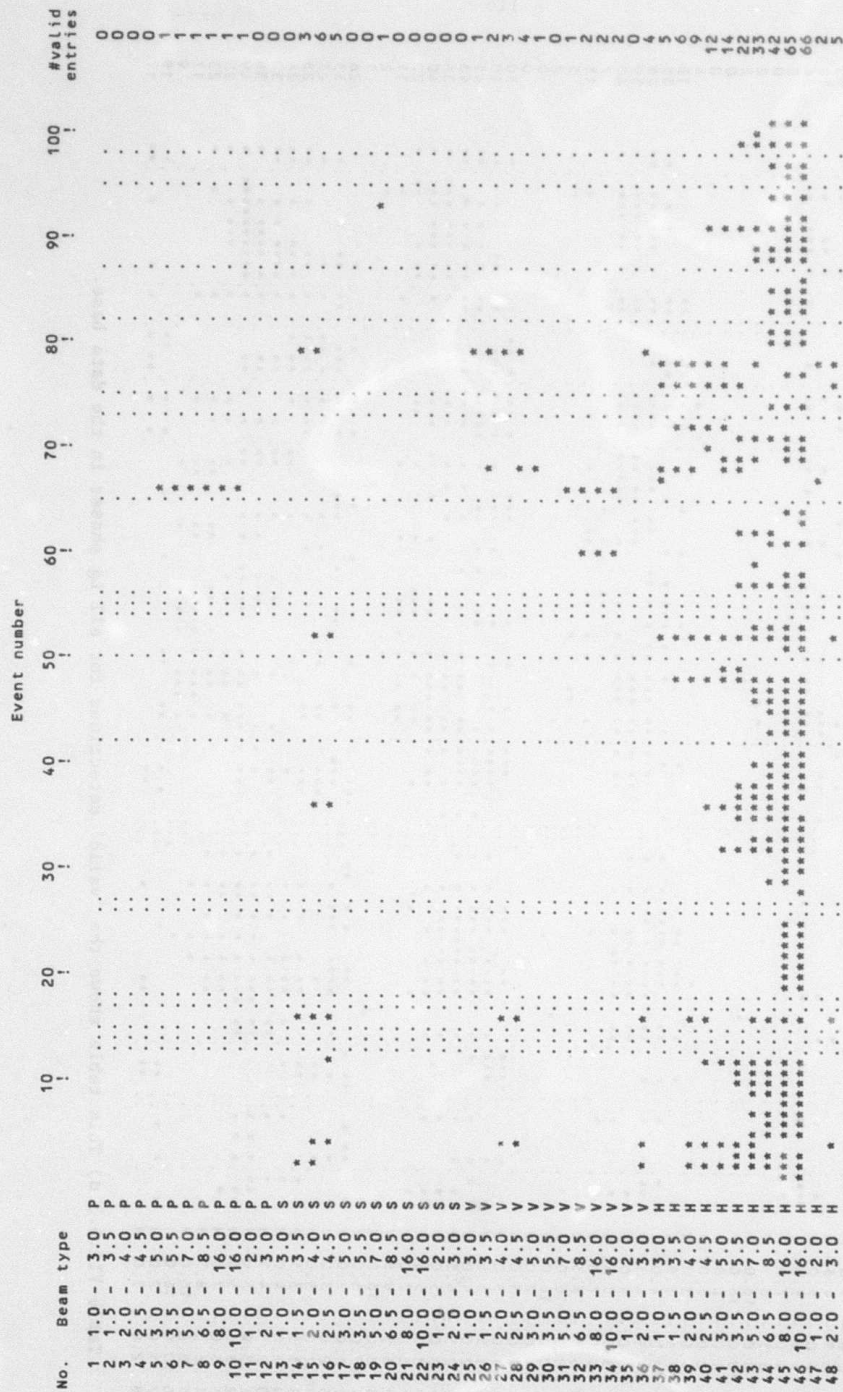
Table VII.6.3 c)  This table shows the 'valid' detections for all Sn phases in the data base.

Event number

#valid entries

No.   Beam type
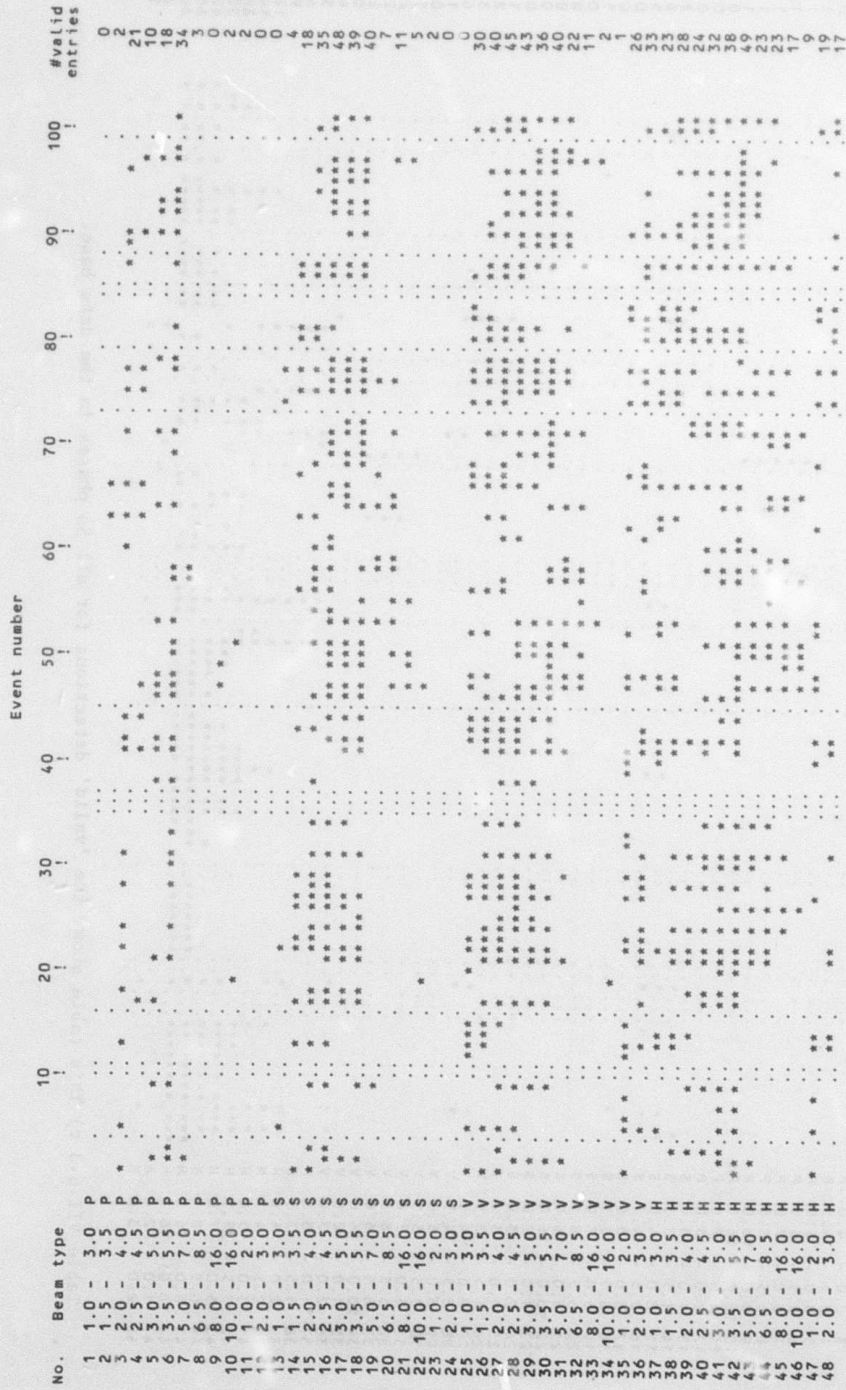
Table VII.6.3 d) This table shows the 'valid' detections for all Lg phases in the data base.

a)

| Beam 10 | 10.0 - 16.0 P | : | 60 entries | |
|---|---|---|---|---|
| Beam 6 | 3.5 - 5.5 P | : | 22 entries | |
| Beam 7 | 5.0 - 7.0 P | : | 5 entries | 96% |
| Beam 9 | 8.0 - 16.0 P | : | 4 entries | |
| Beam 22 | 10.0 - 16.0 V | : | 3 entries | |

---

| Beam 4 | 2.5 - 4.5 P | : | 2 entries | |
|---|---|---|---|---|
| Beam 5 | 3.0 - 5.0 P | : | 1 entry | 4% |
| Beam 27 | 2.0 - 4.0 V | : | 1 entry | |

Total number of detected Pn-phases : 98

b)

| Beam 6 | 3.5 - 5.5 P | : | 38 entries | |
|---|---|---|---|---|
| Beam 4 | 2.5 - 4.5 P | : | 8 entries | |
| Beam 16 | 2.5 - 4.5 S | : | 6 entries | |
| Beam 8 | 6.5 - 8.5 P | : | 4 entries | |
| Beam 31 | 5.0 - 7.0 V | : | 4 entries | 97% |
| Beam 13 | 1.0 - 3.0 S | : | 3 entries | |
| Beam 25 | 1.5 - 3.5 V | : | 3 entries | |
| Beam 18 | 2.5 - 5.5 S | : | 2 entries | |

| Beam 3 | 2.0 - 4.0 P | : | 1 entry | 3% |
|---|---|---|---|---|
| Beam 20 | 6.5 - 8.5 V | : | 1 entry | |

Total number of detected Pg-phases : 70

c)

| Beam 46 | 10.0 - 16.0 H | : | 66 entries | |
|---|---|---|---|---|
| Beam 41 | 3.5 - 5.5 H | : | 7 entries | |
| Beam 43 | 5.0 - 7.0 H | : | 3 entries | 96% |
| Beam 32 | 6.5 - 8.5 V | : | 2 entries | |
| Beam 14 | 1.5 - 3.5 S | : | 1 entry | |

| Beam 19 | 5.0 - 7.0 S | : | 1 entry | |
|---|---|---|---|---|
| Beam 37 | 1.0 - 3.0 H | : | 1 entry | 4% |
| Beam 44 | 6.5 - 8.5 H | : | 1 entry | |

Total number of detected Sn-phases : 82

d)

| Beam 42 | 3.5 - 5.5 H | : | 49 entries | |
|---|---|---|---|---|
| Beam 25 | 1.0 - 3.0 V | : | 19 entries | |
| Beam 35 | 1.0 - 2.0 V | : | 7 entries | 96% |
| Beam 16 | 2.5 - 4.5 S | : | 6 entries | |
| Beam 27 | 2.0 - 4.0 V | : | 3 entries | |

| Beam 20 | 6.5 - 8.5 S | : | 2 entries | 4% |
|---|---|---|---|---|
| Beam 37 | 10.0 - 16.0 P | : | 1 entry | |

Total number of detected Lg-phases : 87

Table VII.6.4 (a-d) In these tables we give the beam priority lists for detection of Pn, Pg, Sn and Lg phases that result from applying the iterative procedure to each phase type individually.

|  |  |  |  | Number of traces to be filtered | Number of beams to be formed |
|---|---|---|---|---|---|
| Beam 46 | 10.0 - 16.0 H | : | | 8 | 1 |
| Beam 10 | 10.0 - 16.0 P | : | | 4 | 4 |
| Beam 42 | 3.5 - 5.5 H | : | | 8 | 1 |
| Beam 5 | 3.5 - 5.5 P | : | | 4 | 4 |
| Beam 41 | 3.5 - 5.5 H | : | | 8 | 1 |
| Beam 35 | 1.0 - 2.0 V | : | | 17 | 1 |
| Beam 16 | 2.5 - 4.5 S | : | | 6 | 0 |
| Beam 7 | 5.0 - 7.0 P | : | | 4 | 4 |
| Beam 9 | 8.0 - 16.0 P | : | | 4 | 4 |
| Beam 8 | 6.5 - 8.5 P | : | | 4 | 4 |
| Beam 31 | 5.0 - 7.0 V | : | | 22 | 1 |
| Beam 22 | 10.0 - 16.0 V | : | | 22 | 1 |
| Beam 13 | 1.0 - 3.0 S | : | | 6 | 6 |
| Beam 25 | 1.5 - 3.5 V | : | | 17 | 1 |
| Beam 43 | 5.0 - 7.0 H | : | | 8 | 1 |
| Beam 18 | 2.5 - 5.5 S | : | | 6 | 6 |
| Beam 32 | 6.5 - 8.5 V | : | | 22 | 1 |
| Beam 14 | 1.5 - 3.5 S | : | | 8 | 8 |

|  |  | | 178 | 55 |
|---|---|---|---|---|
| Symmetric deployment | : | | 222 | 99 |

Table VII.6.5 From the results produced by the iterative procedure
with each phase type treated individually, the beam
deployment given in this table was inferred. For each
phase type, this beam deployment cover 96% of the 'va-
lid' detections. We have also given the number of tra-
ces to be filtered and the number of beams to be formed.
To cover the North Sea / western Norway region 178 tra-
ces must be filtered and 55 beams formed. To span all
azimuth directions by the coherent beam deployment the
numbers will be 222 and 99, respectively. Note that for
incoherent beamforming, each individual trace must be
filtered prior to the beamforming.

|  |  |  | Number of traces to be filtered | Number of beams to be formed |
|---|---|---|---|---|
| Beam 46 | 10.0 - 16.0 H | : | 8 | 1 |
| Beam 10 | 10.0 - 16.0 P | : | 4 | 4 |
| Beam 42 | 3.5 - 5.5 H | : | 8 | 1 |
| Beam 6 | 3.5 - 5.5 P | : | 4 | 4 |
| Beam 25 | 1.0 - 3.0 V | : | 17 | 1 |
| Beam 4 | 2.5 - 4.5 P | : | 4 | 4 |
| Beam 8 | 6.5 - 8.5 P | : | 4 | 4 |
| Beam 39 | 2.0 - 4.0 H | : | 8 | 1 |
| Beam 35 | 1.0 - 2.0 V | : | 17 | 1 |
| Beam 18 | 3.5 - 5.5 S | : | 6 | 6 |
| Beam 31 | 5.0 - 7.0 V | : | 22 | 1 |
| Beam 22 | 10.0 - 16.0 V | : | 22 | 1 |
| Beam 7 | 5.0 - 7.0 P | : | 4 | 4 |
|  |  |  | 128 | 33 |
| Symmetric deployment |  | : | 154 | 59 |

Table VII.6.6 The beam deployment of this table was produced by the iterative procedure when treating all phases at the same time, after first having required that beam nos. 46, 10, 42 and 6 should be included in the final deployment. Compared to the results presented in Table VII.6.5, the volume of the beam deployment is considerably reduced.

|  |  |  | Number of traces to be filtered | Number of beams to be formed |
|---|---|---|---|---|
| Beam 46 | 10.0 - 16.0 H | : | 8 | 1 |
| Beam 10 | 10.0 - 16.0 P | : | 4 | 4 |
| Beam 42 | 3.5 - 5.5 H | : | 8 | 1 |
| Beam 6 | 3.5 - 5.5 P | : | 4 | 4 |
| Beam 25 | 1.0 - 3.0 V | : | 17 | 1 |
| Beam 4 | 2.5 - 4.5 P | : | 4 | 4 |
| Beam 8 | 6.5 - 8.5 P | : | 4 | 4 |
| Beam 39 | 2.0 - 4.0 H | : | 8 | 1 |
| Beam 35 | 1.0 - 2.0 V | : | 17 | 1 |
| Beam 31 | 5.0 - 7.0 V | : | 22 | 1 |
| Beam 22 | 10.0 - 16.0 V | : | 22 | 1 |
| Beam 7 | 5.0 - 7.0 P | : | 4 | 4 |
| Beam 9 | 8.0 - 16.0 P | : | 4 | 4 |
| Beam 29 | 3.0 - 5.0 V | : | 22 | 1 |
|  |  |  | 148 | 32 |
| Symmetric deployment | | : | 172 | 56 |

Table VII.6.7 The procedure for finding the results given in this table, is essentially the same as outlined for Table VII.6.6. The only difference is that we have not allowed any S-beams to be included in the final beam deployment.
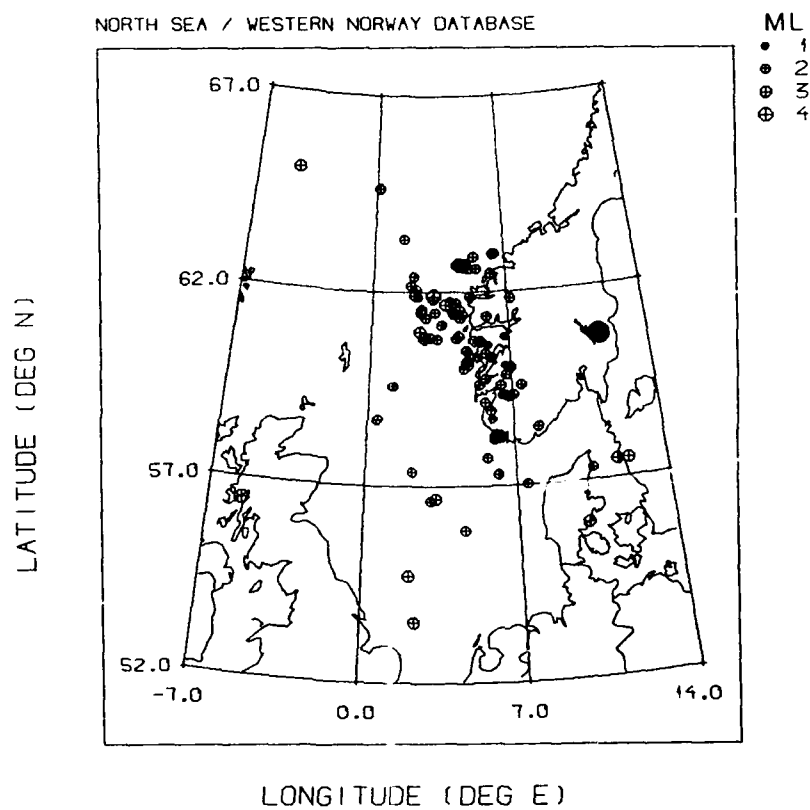
Fig. VII.6.1 The figure shows the locations of the 101 events in the
North Sea / western Norway data base. The loaction of
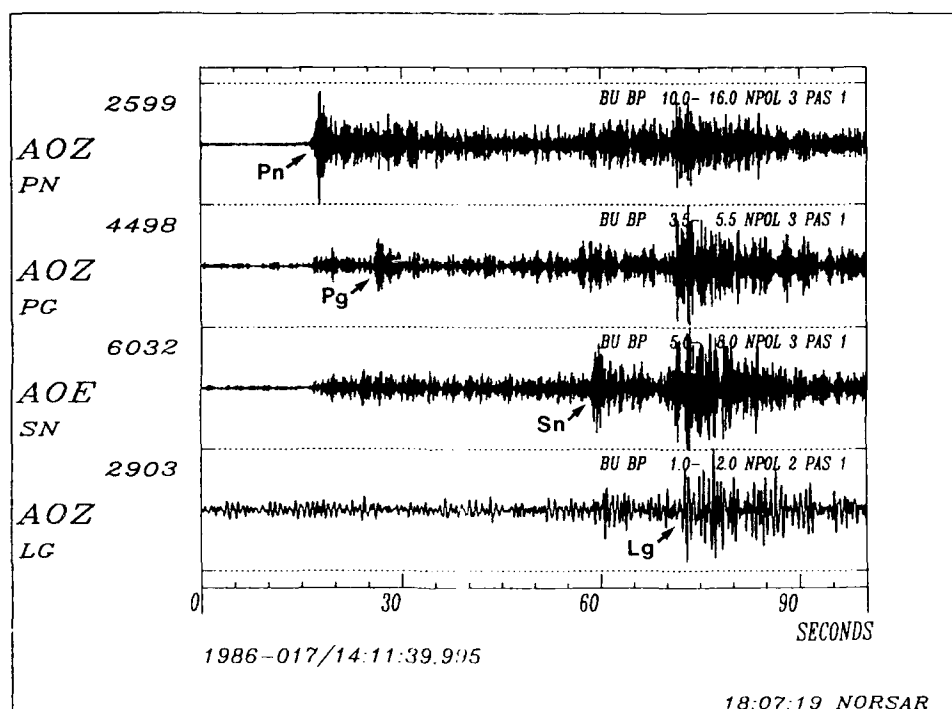the NORESS array is indicated by a filled circle.

Fig. VII.6.2 To identify the different regional phases and pick their arrival times, several filters were applied to both the vertical and horizontal components. This figure shows filtered NORESS recordings from an event in southwestern Norway. The distance from NORESS is about 400 km and the local magnitude is 2.7.

## VII.7    Local geology of the regional array sites in Norway

Information on local geological conditions at the NORESS and Finnmark
array sites is available from various sources. In this contribution,
we have attempted to compile information that is considered relevant
from the seismological viewpoint. In particular, such information may
be used to provide tentative explanations of certain observed features
in the seismograms.

### Local geology of the NORESS site

The NORESS site is located within the Precambrian (also referred to
as pre-Eocambrian) rock complexes of southeastern Norway. Maps showing
the local geology of the siting area have not yet been published.
However, geologists of the Norwegian Geological Survey have conducted
surveys in the area and have made available to us hand-colored maps of
the local surface geology. These maps show that three different rock
types are present at the array site, namely: (1) granite, (2) gabbro
and (3) rhyolite. The information in these maps is transcribed onto
the array configuration map of Fig. VII.7.1.

Johnson and Olheft (1984) and Bott (1982) give the following typical
values for density and P-wave velocities (at a pressure of 0.3 Kbar,
corresponding to a depth of 1 km) for these rock types:

|  | Density $(g/cm^3)$ | Velocity (km/s) |
|---|---|---|
| Granite | 2.66 | 5.91 |
| Gabbro | 2.99 | 6.74 |
| Rhyolite | 2.60 | - |

One should keep in mind that these values represent averages over a
large number of samples from various geological environments. Wwe
think, however, that these values could be used, with due care, for

the site considered here. For instance, such values can be used to estimate reflection coefficients of possible subsurface interfaces.

The possible existence of such interfaces beneath the array can be inferred from data from a reflection seismic survey that was carried out in 1983. Reflection data were collected along the profiling line shown in Fig. VII.7.1. The length of the line was approximately 2500 m and charges of 1.4 kg of explosives were fired in 8 m deep boreholes spaced at 40 m intervals along the profile. Each shot was recorded on a spread of 24 geophones at 20 m intervals, with a constant distance of 120 m between the shot and the nearest geophone. The data were recorded using NORSAR's reflection profiling instrumentation (Texas Instruments DFS-V). A sampling rate of 2 ms was chosen, and the analog filters had cutoffs at 8 and 256 Hz. The recording interval was 20 s for each shot. The field work and subsequent processing of the data was organized and carried out by NORSAR personnel, notably Håvar Gjøystdal, Paul W. Larsen and Ottar A. Sandvin.

The data were subjected to conventional CDP-stacking with a 10 m interval between consecutive traces in the stacked section, giving a 6-fold coverage (except at the ends of the profile). The section shown in Fig. VII.7.2 resulted from this processing and shows the data filtered in the 100-250 Hz band. The section covers a two-way travel time (TWT) of 0.0-1.0 s.

Several interesting features can be observed in the section of Fig. VII.7.2. First of all, we see a dipping interface that appears to intersect the surface near the southern end of the profile. The TWT of 0.37 s observed at the northern end of the profile indicates a depth of roughly 1 km at that point, giving a dip of approximately 20°. Based on the available information on the surface geology, we speculate that this horizon represents the interface between the granite

and the gabbro, which is outcropping near the southern end of the pro-
file, see Fig. VII.7.2. The reflection coefficient resulting from den-
sity and velocity changes across a granite/gabbro interface could
become significant and would be of the order of 0.12, using the values
given above.

In addition to this dipping interface, there are at least two clearly
observable events in Fig. VII.7.2. One of these is dipping across the
middle of the section at arr nd 0.5-0.6 s TWT, and the other is an
apparently flat horizon at about 0.8 s TWT. Suffice it here to point
to these arrivals, without going any further into geological interpre-
tations.

The recording interval cf 20 s for each shot made it possible to look
for coherent arrivals from depths even larger than the base of the
crust. Extensive plotting of sections for TWT intervals within the
1.0-20.0 s range only revealed one such arrival that could be traced
over any length of distance and tentatively attributed to a definite
structure at depth. This event is seen at about 5.5 s TWT in the
middle of the section of Fig. VII.7.3. The corresponding depth would
be approximately 18 km.

### Local geology of the Finnmark array site

Only very limited information is yet available on the local geology of
the new regional array site in Finnmark, northern Norway. The Nor-
wegian Geological Survey has published a regional geological map of
the Karasjok, Finnmark area (Skålvoll, 1972). This map shows that all
seismometers of the new array are within an outcropping gabbro for-
mation approximately 4 x 10 km large. This gabbro window is located
within the Karasjok Group, which consists of metamorphic sedimentary
and igenous rocks of age 2000 million years. It is therefore reason-
able to assume the existence of high-density, high-velocity material

at the surface all across the new array. The possible existence of
subsurface layering is, however, unknown at this time.


S. Mykkeltveit


## References

Bott, M.H.P. (1982): The Interior of the Earth: Its Structure,
    Constitution and Evolution. Second Ed., Edward Arnold, London.

Johnson, G.R. and G.R. Olhoeft (1984): Density of rocks and minerals,
    In: CRC Handbook of Physical Properties of Rocks, Vol. III.
    R.S. Carmichael, ed., CRC Press, Boca Raton, Florida.

Skålvoll, H. (1972): Beskrivelse til geologisk kart over Norge
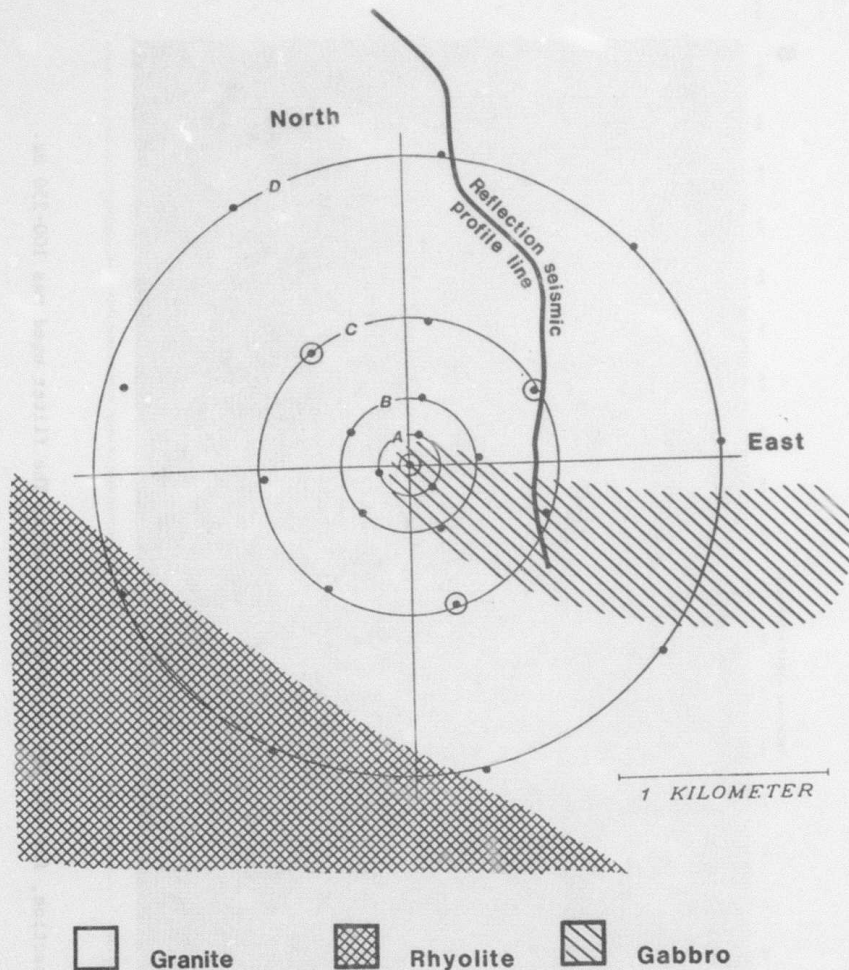    1:250 000, Karasjok. Norges Geologiske Undersøkelse.

Fig. VII.7.1 Configuration and local geology of the NORESS array. The four three-component stations are marked with special symbols. The station at the center of the array is named AO. The surface geology of the site is transcribed from a map provided by the Norwegian Geological Survey. A 60 m deep borehole was drilled at site AO. According to the drilling log, this hole was drilled in gabbro all the way down to its bottom. A reflection seismic survey was conducted with shots and geophones along the line running into the array from the north.
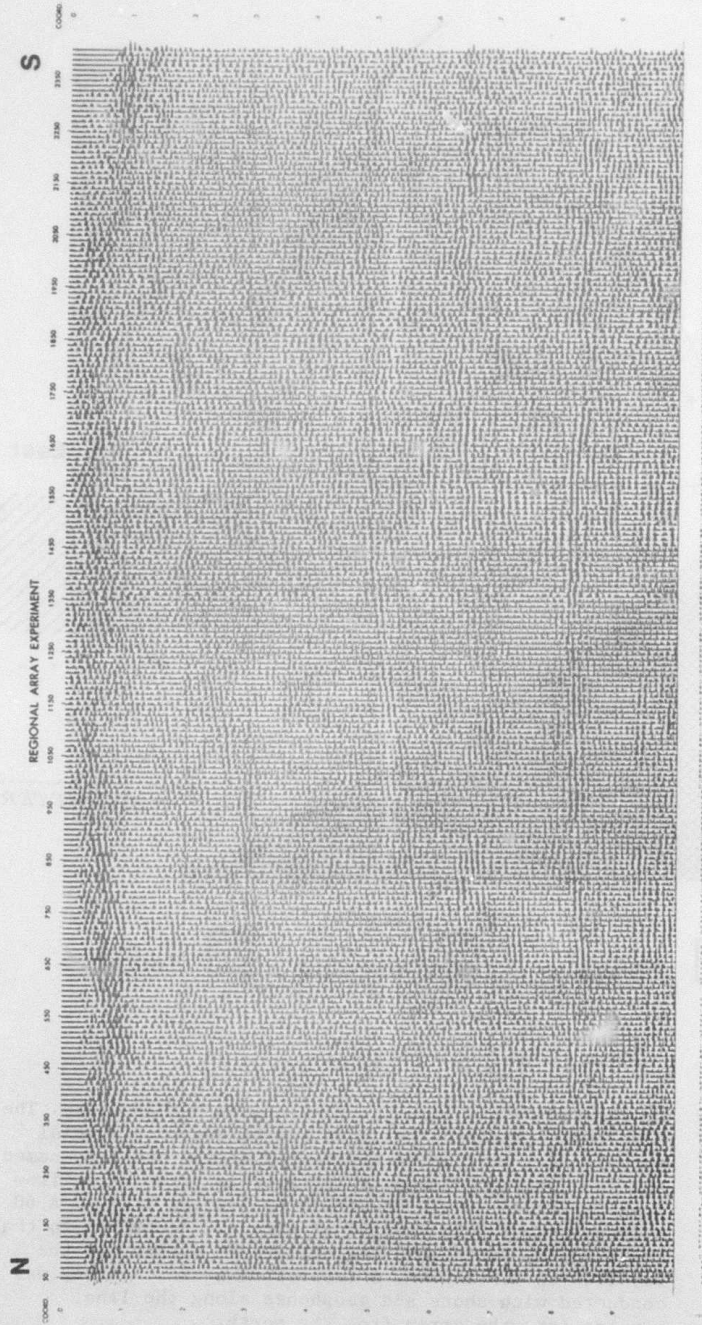
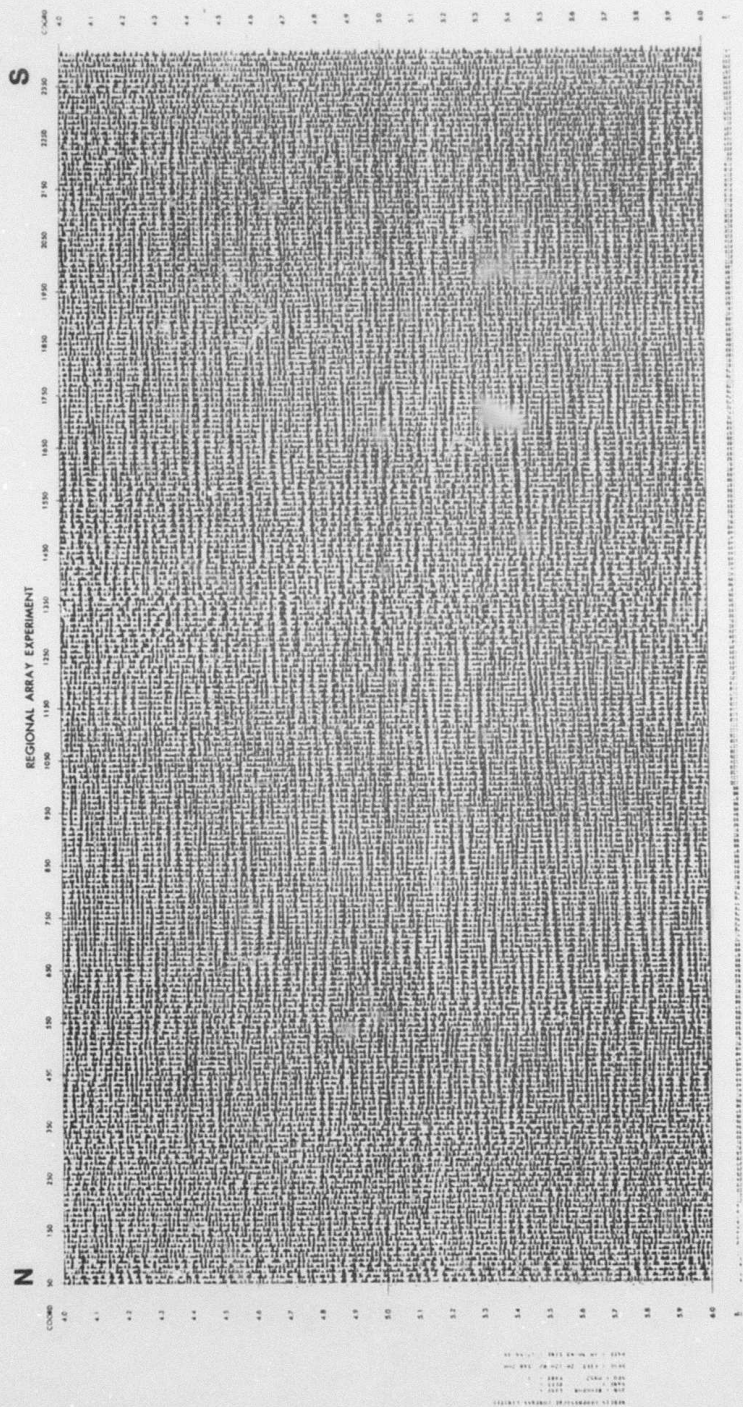Fig. VII.7.2 CDP-stacked section, for the TWT interval 0.0-1.0 s. The filter used was 100-250 Hz.

Fig. VII.7.3  CDP-stacked section, for the TWT interval 4.0-6.0 s. The filter used was 20-120 Hz.